63-3-3

RESULTS OF INDEPENDENT RESEARCH AND DEVELOPMENT STUDIES BY THE DOUGLAS AEROPHYSICS LABORATORY STAFF IN FLUID MECHANICS AND SIMULATION TECHNIQUES FISCAL YEAR 1962

JANUARY 1, 1963 **DOUGLAS REPORT SM-41379**

MISSILE & SPACE SYSTEMS DIVISION
DOUGLAS AIRCRAFT COMPANY, INC.
SANTA MONICA CALIFORNIA

$13.00

(5) 268700

(6) RESULTS OF INDEPENDENT RESEARCH AND DEVELOPMENT STUDIES BY THE DOUGLAS AEROPHYSICS LABORATORY STAFF IN FLUID MECHANICS AND SIMULATION TECHNIQUES FISCAL YEAR 1962,

(7) NA (8) U (9) (See p-iii)

JANUARY 1, 1963

~~DOUGLAS~~ REPORT SM-41379

(14) (10.)

(15) - (19) NA

(20) U. (21) NA

Approved by:

J.S. Murphy
Branch Chief
R&D Aerophysics Laboratories

Prepared by:
Aerophysics Laboratory Staff
(10) Edited by:
W.E. Smith.

(11) 1 Jan 63, (12) 1v. (13) NA

DOUGLAS MISSILE & SPACE SYSTEMS DIVISION

PREFACE

(9) Summary of progress for

This document is a compilation of technical papers written by the Douglas Aerophysics Laboratory staff to summarize progress during fiscal year 1962 (year ending November 30, 1962) in company-funded investigations conducted within the Independent Research and Development Program of the Douglas Aircraft Company.

All of the nine IR&D studies conducted at DAL during FY 1962 are categorized as applied research, as opposed to basic research on the one hand and technically oriented development on the other. Two of the studies directly concern fluid mechanics and seven deal with new techniques for simulating the environment of advanced aerodynamic vehicles, or with specific problems involved in implementing such techniques.

Section I
Experimental Work On Transition At Hypersonic Speeds

R.E. Deem

January 1, 1963

Report Number SM-41379-1

Sales Order: 81260-287
Engineering Work Order: 51900
Job Work Order: 0001

SUMMARY

Boundary layer transition has been successfully detected on conical bodies in hypersonic airstreams. Shadowgraphs and, alternatively, china clay techniques were applied in the DAL Hypersonic Two-Foot Wind Tunnel. Best shadowgraphs are obtained by mounting the film plate at the edge of the free jet adjacent to the model. Eugenol is a suitable wetting agent for detecting transition on china clay coatings in these experiments. Transition measurements by the alternative methods agree, and indicate rather early transition possibly due to surface roughness or an unrealistically high base pressure.

Recent measurements of transition by similar techniques are also reported for a flat plate in supersonic airflow in the DAL Trisonic Four-Foot Wind Tunnel.

TABLE OF CONTENTS

LIST OF ILLUSTRATIONS

1. INTRODUCTION

Knowledge of the location of transition of the boundary layer from laminar to turbulent is important for the analysis of wind tunnel tests of scale models, especially at hypersonic Mach numbers. The DAL staff believes that a capability for detecting transition points is essential to the operational status of a hypersonic wind tunnel. To this end the subject Independent Research and Development (IR&D) investigation of experimental techniques for detection of transition at hypersonic speeds has been initiated and completed during FY 1962. The specific task has been to provide a capability for detecting transition on typical scale models in the DAL Hypersonic Two-Foot Wind Tunnel. This capability has been successfully demonstrated. This final report describes the program and presents the results of the experiments.

The present investigation in the Hypersonic Two-Foot Wind Tunnel is a logical extension of previous work in the DAL Trisonic Four-Foot Wind Tunnel. The previous IR&D investigation, completed in FY 1961, is reported in Reference 1. The purpose of the previous study was not only to develop techniques to detect transition but also to start a library of measured transition points. Transition values are to be measured whenever opportunities arise during various model tests in DAL wind tunnels. A certain amount of such data has been obtained during FY 1962 in the Trisonic Four-Foot Wind Tunnel and, consequently, is included as an appendix to this report.

2. FACILITY

The DAL Hypersonic Two-Foot Wind Tunnel is an intermittent blowdown tunnel with existing provisions for testing in heated air at Mach 6 and 8 and a future capability at Mach 10. Figure 1 shows an air-flow diagram and the major components of the tunnel. A detailed description of the facility is presented in Reference 2.

An important feature of the tunnel that relates to boundary layer transition work is the free-jet test section and model support system. The test section is enclosed by a large plenum chamber, or test cabin, with 30-inch-diameter schlieren windows on the side-walls. Models are usually sting-mounted from a gimbaled strut which can be translated vertically into and out of the free jet.

3. MODELS

Two bodies of revolution were tested for transition during FY 1962. The first is a 5.5%-scale Nike Zeus model without the canard controls, essentially a blunt cone as shown in Figure 2. Detailed descriptions of this model are contained in References 3 and 4. The second model is a blunt cone, 4-degree half angle, configuration N5B1 of the Sprint Model M-149, represented in Figure 3. All tests were at zero angles of attack and yaw.

The surface of each model is somewhat rougher than would be produced by standard practice of steel fabrication. This is because of erosion due to impingement of solid particle contaminants in the airstream during routine testing. It is estimated that the surface finish after several runs is typically on the order of 200 microinches, about the roughness of 200 or 300 grit sandpaper.

4. EXPERIMENTAL APPARATUS AND TECHNIQUES

4.1 Standard Shadowgraph

Shadowgraphs of bodies of revolution in the Trisonic Four-Foot Wind Tunnel produced clear evidence of transition (Reference 1). Consequently, the same apparatus and technique were transferred to the Hypersonic Two-Foot Wind Tunnel for initial tests. This standard shadowgraph arrangement is shown schematically in Figure 4. The spark light source, whose duration is approximately three microseconds, is located as far from the model as practical. The film plate*, 11 by 14 inches, is placed against the outer surface of the opposite window, about 5 feet from the model. The resulting image magnification is approximately 1.33. This arrangement permits only one picture per run.

Shadowgraphs of the Nike Zeus model were obtained with the standard arrangement during several runs at Mach 6 and at Mach 8. Results, typified by Figure 5, are somewhat unsatisfactory. Although the bow shock wave is prominent, the boundary layer is somewhat obscured by background disturbances. Detection of transition at Mach 6 in Figure 5, for example, is considered to be marginally reliable. Shadowgraphs at lower densities associated with Mach 8 tests are still less satisfactory.

4.2 Improved Shadowgraph

Three methods have been tried to improve the shadowgraph quality: reduction of the spark light source duration, elimination of the window nearest the film, and reduction of the separation of the film from the model.

Eddies and flow oscillations within the transition zone and the turbulent boundary layer can be better identified if the duration of the light source is decreased. Consequently, the DAL light source in the standard arrangement, described above, was replaced by a portable AVCO package light source, type LS-020, model 3, whose duration is about 0.3 microsecond. Exposure of the film during tests of the Sprint model was inadequate due to the less intensity and shorter duration of the AVCO light source. Nevertheless, the density gradients (actually the second derivatives of density) were observed to be sharper within the boundary and elsewhere. The corresponding sharpening of the background perturbations prevented any real improvement in transition

* DuPont Cronar Commercial - S, blue sensitive, medium contrast, was used for all shadowgraph experiments.

detection, however. Consequently, the DAL three-microsecond source was reinstalled for subsequent tests.

The next step was to bypass the window between model and film. Although this window is of high-quality glass and has been examined by schlieren optics and found to be relatively free of striations, it is undeniable that some distortion of the shadowgraph image occurs therein. Shadowgraphs of the Sprint model, obtained by mounting the film on the interior window surface, are judged slightly superior to the standard typified by Figure 5.

The ultimate improvement resulted from moving the film still closer to the model. This modification risks damage to the film by the high velocity, hot, free jet of test air. The film would fail to withstand temperatures of about 200°F. By trial during several runs, it was found that the film can be placed as close to the model as the nominal edge of the free jet if the film is protected from the aerodynamic forces by a plate glass cover. Although only medium quality glass was used as a shield, this arrangement has produced the best results of all; for example, see Figure 6. This one shadowgraph illustrates on the upper surface of the Sprint conical model, magnified in the shadowgraph system by a factor of 1.09, the laminar boundary layer, spots of turbulence in the transition zone, and the fully turbulent boundary layer. The boundary layer on the lower surface appears to have separated and reattached in the turbulent state.

4.3 China Clay Technique

As has been demonstrated in the DAL Trisonic Four-Foot Wind Tunnel in 1961 (Reference 1) and subsequently, the china clay technique is a valuable adjunct to the use of the shadowgraph for detecting transition at transonic and supersonic speeds. China clay can be used on practically any portion of any configuration and the technique can be utilized at any time during routine force, pressure, or other tests. It is desirable to attain these same objectives at hypersonic speeds. Consequently, such tests have been performed and results have been compared with shadowgraph data on transition.

Use of the china clay technique is fairly simple and is described in detail in Reference 1. The model is sprayed with a special lacquer in which are suspended particles of china clay. When the lacquer is dry, a volatile oil is sprayed on the model and the run is made. The oil is dried and the white clay is exposed by a turbulent boundary layer, whereas the surface remains wet and dark under a laminar boundary layer (aft of the nose region). Volatile oils in common use at DAL are, in order of increasing drying time, methyl salicylate, isosafrol, and eugenol. The first of these is the most useful at transonic and supersonic speeds.

Methyl salicylate was tried first on the Sprint model at Mach 8 in the DAL Hypersonic Two-Foot Wind Tunnel. The model injection and withdrawal feature of the support system was used to avoid the transient effects of starting and stopping the tunnel. However, methyl salicylate dries much too fast in the hypersonic stream to permit visual control of model withdrawal while laminar regions remain wet. Relatively slow-drying eugenol was tried next and an apparently successful result is illustrated in Figure 7. Transition is indicated about one-half inch forward of the base. The dry (white) region at the blunt nose of the cone results from the locally high shear forces.

5. TRANSITION DATA

Apparently valid transition data have been obtained for the Sprint conical model at Mach 8. Complete transition is detected at 12.3 inches from the model nose by the shadowgraph and at 14 inches by the china clay. These distances yield transition Reynolds numbers of about 4.5 to 5 million, about an order of magnitude less than would be expected on a cold, blunt cone at Mach 8 and Reynolds number 0.4 million per inch. A plausible explanation of this discrepancy is that transition was induced earlier than normal by the roughness of the model surface. Another possibility is that the proximity of the model base in these experiments triggered transition artifically, at a station related more closely to the position of the base than to the running length and growth of the boundary layer, for the following reason. The geometry of the scoop and of the body support system prohibits the establishment around the model of a flow field that is free of extraneous shock waves at Mach 8. Oblique shock waves are observed to impinge on the sting behind the model base. The high pressure field downstream of these oblique shock waves is propagated forward along the sting to the base region, where unrealistically high base pressures have been observed, about the free-stream magnitude. This unrealistically high base pressure could produce the transition herein observed just forward of the base. This explanation is supported by recent, unreported, transition experiments on a longer conical model in the same flow condition in this tunnel, but with the model support system better streamlined to produce lower, more realistic base pressures. At any rate, some confidence can be placed in the ability of the present shadowgraph system, at least, to detect transition because the transition region (alternate regions of laminar and turbulent boundary layer) appears in Figure 6 to be relatively long, over five inches. A large transition region is expected qualitatively based on the results of hypersonic tests at AEDC, Reference 5.

It is concluded that much work remains to be done on experimental detection of transition at hypersonic speeds.

6. APPENDIX. FLAT PLATE TRANSITION MEASUREMENTS IN SUPERSONIC AIRFLOW

Boundary layer transition has been measured on an uninclined, unyawed flat plate at several transonic and supersonic airspeeds during Saturn SA-5 acoustic and pressure tests (S-61) in the DAL Trisonic Four-Foot Wind Tunnel The leading edge of the flat plate model is 0.002 inch thick and

the "under" surface is beveled at 10 degrees. Primarily, transition was detected by means of a coat of china clay lacquer wetted with methyl salicylate. Shadowgraphs were obtained at some test conditions for corroboration. The model and tests are described more fully in Reference 6.

The results of the transition measurements are presented in Figure 8. Although the unit Reynolds numbers vary slightly, the data are plotted together because each point represents essentially the minimum available unit Reynolds number. Generally, the unit Reynolds number for these data increases with the Mach number. This fact allows comparison with the correlated AEDC data of Reference 5. The AEDC data account for variable unit Reynolds number, leading edge thickness, and bevel angle, but apply only at Mach 3. The interpolated value of unit Reynolds number of the DAL data at Mach 3 is about 0.75 million per inch. Therefore, the AEDC point represented in Figure 8 is for this value of unit Reynolds number and for the stated thickness and bevel angle. The AEDC value for transition Reynolds number exceeds the trend of the DAL transition data by a significant amount. No explanation for this disagreement is available.

7. REFERENCES

1. Deem, R. E., Experimental Study of Location of Boundary Layer Transition. Douglas Aircraft Company, Inc., Report SM 41368-4, dated January 15, 1962.

2. Cole, R. M. and G. T. Gibbs, The Hypersonic Two-Foot Tunnel, Description of the Facility and Provisions for Testing. Douglas Aircraft Company Inc., Report SM 41369, dated March 1, 1962.

3. Deem, R. E., Supersonic Force Tests of the Nike Zeus Mainstage Stability Wind Tunnel Model M-64A. Douglas Aerophysics Laboratory Report S-9, dated September 13, 1960.

4. Cole, R. M., A 6-Component Force and Moment Correlation Test of a Douglas DM-15B (Nike Zeus) Missile Mainstage Model M-64 at Mach 6 and 8. Douglas MSSD Research and Development Support Technical Memorandum DM-15B-R/AT-L3291, dated November 23, 1962.

5. Potter, J. L., and J. D. Whitfield, Effects of Unit Reynolds Number, Nose Bluntness, and Roughness on Boundary Layer Transition. AEDC-TR-60-5, dated March, 1960.

6. Deem, R. E., Summary of Test S-61, Investigation of the Static Pressures and the Pressure Fluctuations Within the Turbulent Boundary Layer of the Saturn SA-5 Pressure Model (SVM-14) at Mach Numbers 0.8 to 5.0. Douglas Aerophysics Laboratory Internal Memorandum A270-R/AT-IM250, dated December 18, 1962.

DAL HYPERSONIC TUNNEL DESIGN FEATURES

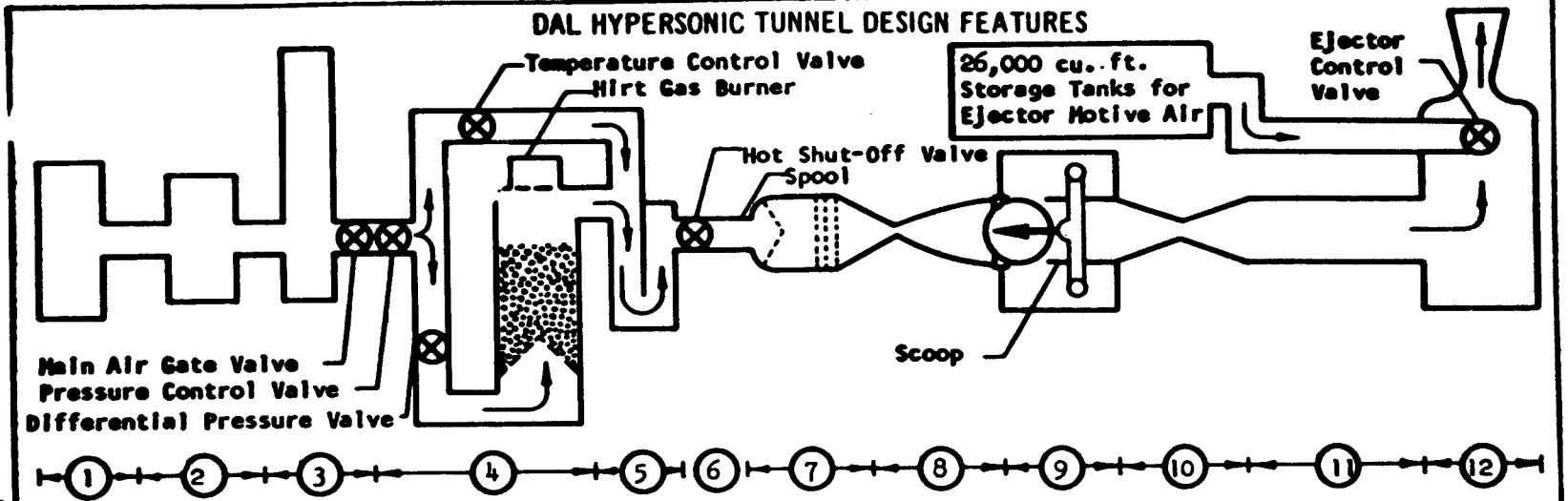

1. **COMPRESSOR** 6 stage Cooper-Bessemer, non-lubricated, reciprocating compressor with interstage cooling. Intake is 1825 cfm at 14.5 psia and 85°F; exhaust at 3500 psia and 100°F.
2. **DRYER** Semi-automatic desiccant Pritchard Hydryer dries air to a dewpoint of -50°F or lower.
3. **AIR STORAGE TANKS** Two vertical cylinders, of 250 ft.^{3} each, store air at 3500 psia and atmospheric temperature.
4. **PEBBLE BED HEATER** Alumina pebble bed heater regenerated by combustion of natural gas.
5. **THERMAL MIXER** Mixes hot air from heater and cold air from storage tanks to obtain desired stream temperature.
6. **HOT SHUT-OFF VALVE** Air-cooled ceramic-lined 12-inch rotovalve, hydraulically actuated between full open and full closed positions.
7. **SPOOL & STILLING CHAMBER** Removable spools to make up for length of nozzles. 25-inch diameter stilling chamber containing perforated cone and three turbulence screens.
8. **NOZZLE** Fixed Mach number, axisymmetric nozzles for Mach 6, 8, and 10. Exit diameter approximately 26 inches.
9. **PLENUM & TEST SECTION** Free jet surrounded by plenum chamber with 30-inch diameter windows on sidewalls. A scoop captures jet. Model support provides ±30° pitch, ±22 inches vertical translation, and ±200° roll.
10. **VARIABLE DIFFUSER** Two-dimensional single-peak type with top and bottom walls movable.
11. **FIXED DIFFUSER** Completes expansion to ejector plenum.
12. **EJECTOR & MUFFLER** One main and four side ejectors reduce exit pressure to 1 to 3 psia, depending on mass flow.

FIGURE 1

NIKE ZEUS CONICAL MODEL

FIGURE 2

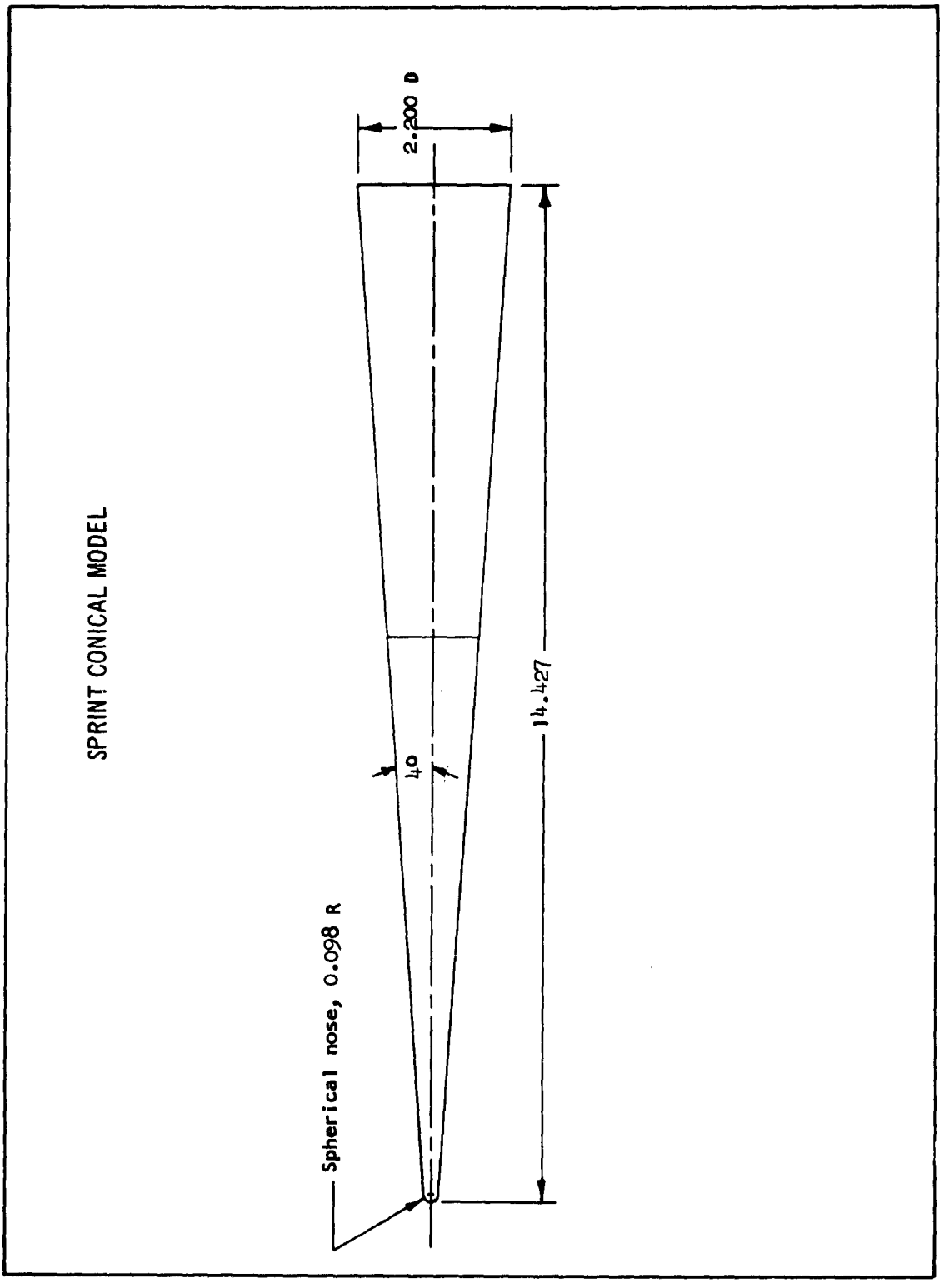

FIGURE 3

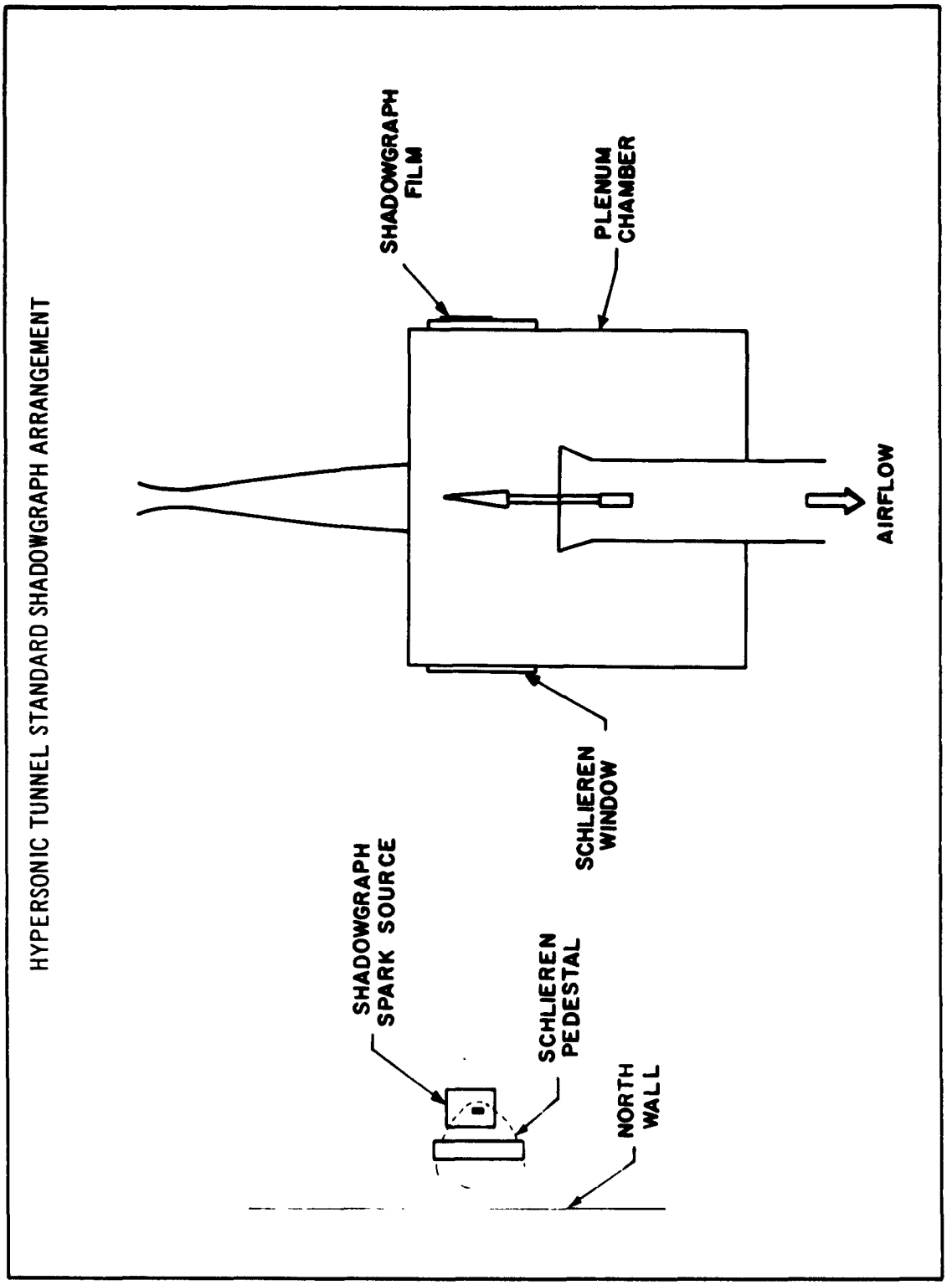
HYPERSONIC TUNNEL STANDARD SHADOWGRAPH ARRANGEMENT
SHADOWGRAPH FILM
PLENUM CHAMBER
AIRFLOW
SCHLIEREN WINDOW
SHADOWGRAPH SPARK SOURCE
SCHLIEREN PEDESTAL
NORTH WALL

FIGURE 4

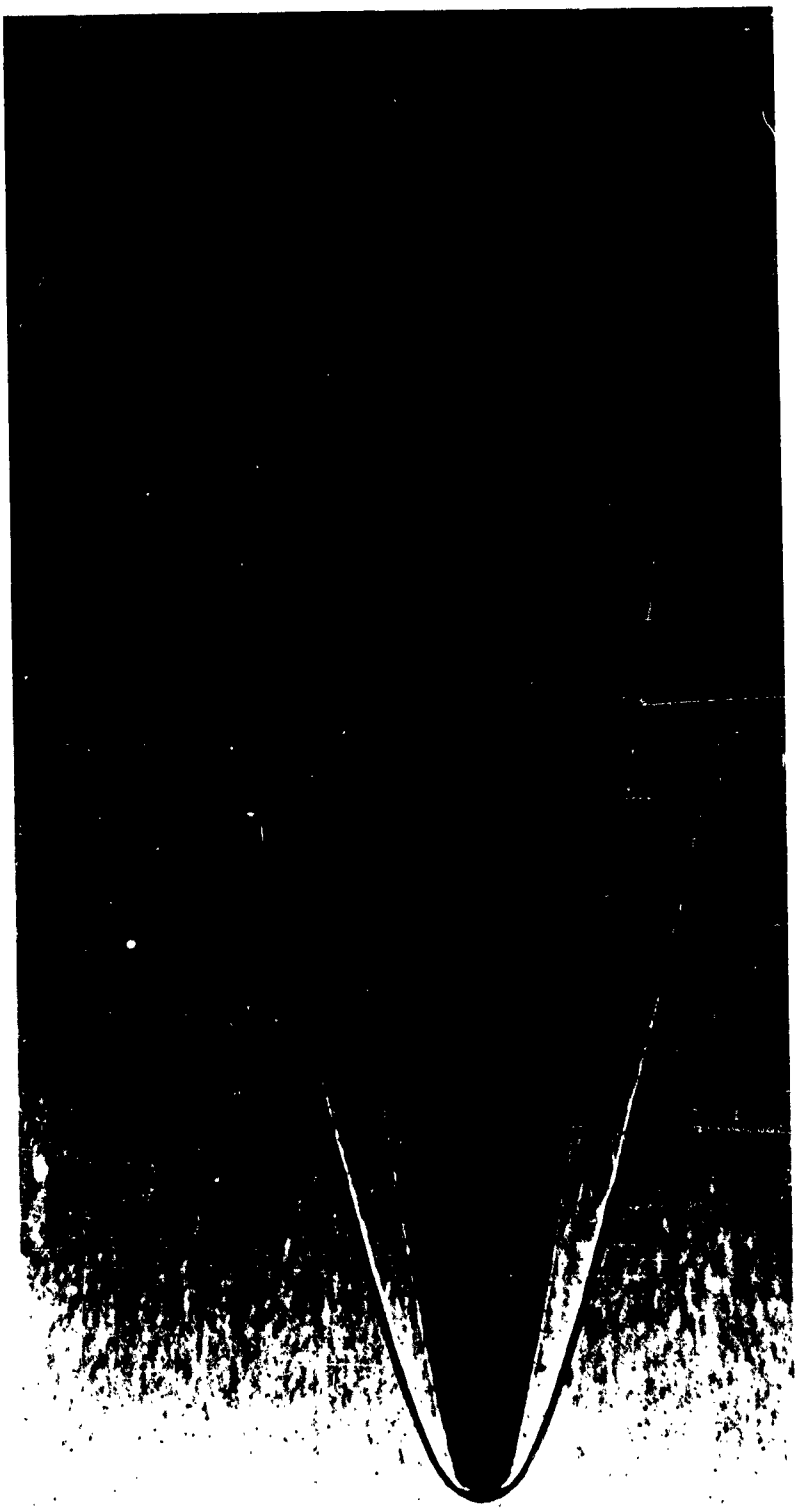

SHADOWGRAPH SHOWING TRANSITION ON THE NIKE ZEUS MODEL AT MACH 6
(UNIT REYNOLDS NUMBER = 0.58 x 10^6/IN.), STANDARD OPTICS,
DAL HYPERSONIC TWO-FOOT WIND TUNNEL.

FIGURE 5

SHADOWGRAPH SHOWING TRANSITION ON THE SPRINT MODEL AT MACH 8
(UNIT REYNOLDS NUMBER = 0.39 x 10^6/IN.), FILM AT EDGE OF FREE JET.

FIGURE 6

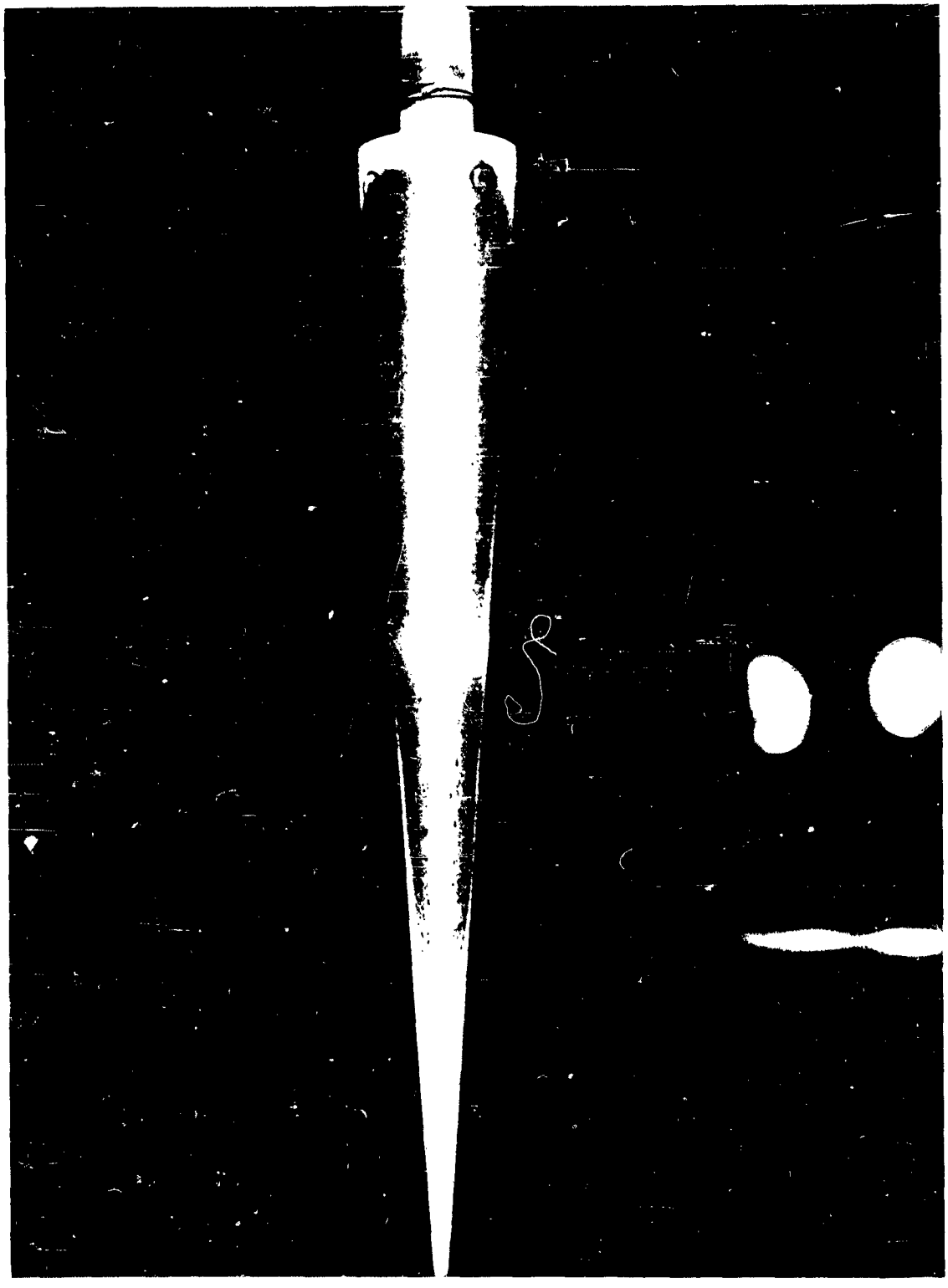

CHINA CLAY COATING SHOWING TRANSITION ON THE SPRINT MODEL AFTER MACH 8 TEST (UNIT REYNOLDS NUMBER = 0.38×10^6/IN.)

FIGURE 7

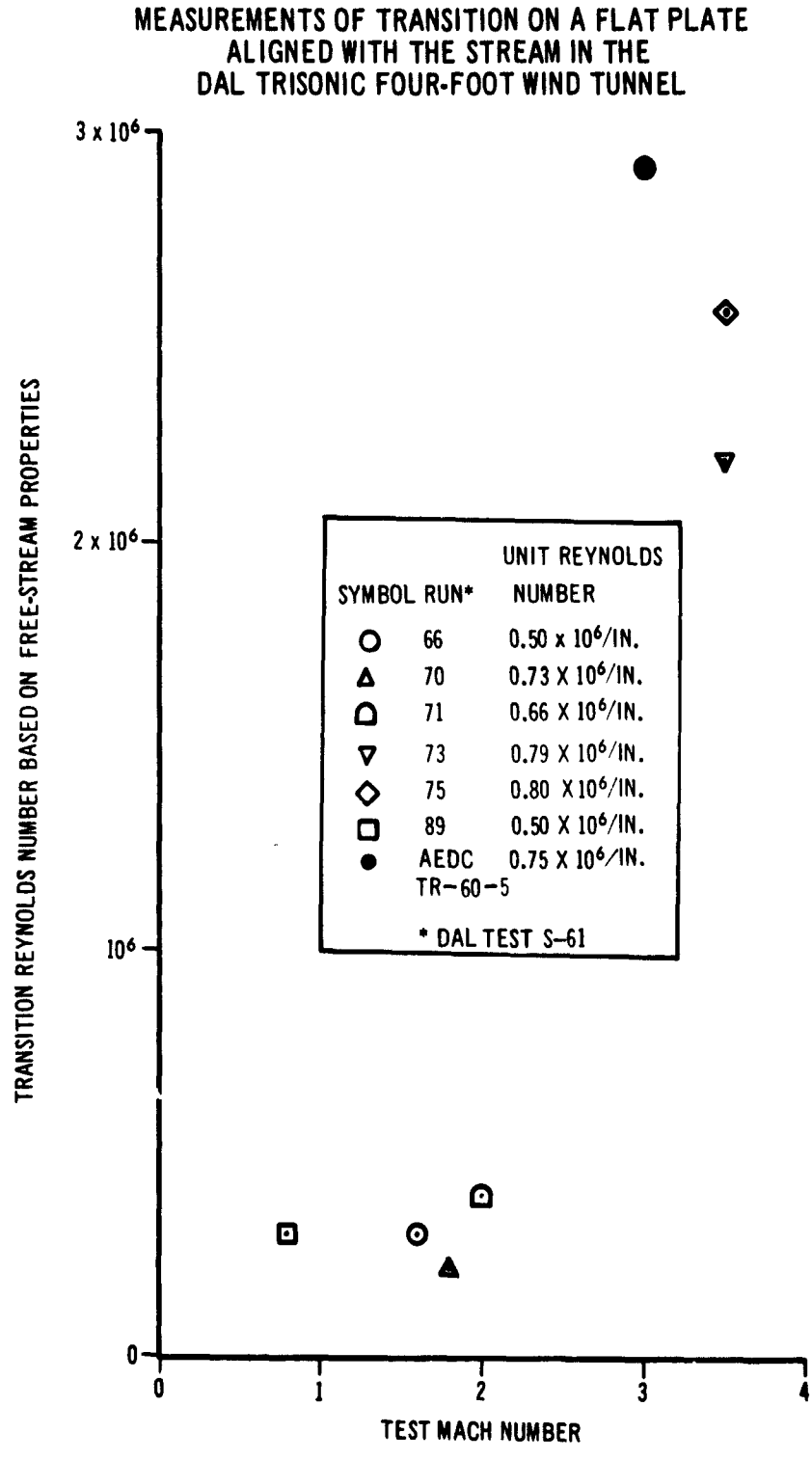
MEASUREMENTS OF TRANSITION ON A FLAT PLATE
ALIGNED WITH THE STREAM IN THE
DAL TRISONIC FOUR-FOOT WIND TUNNEL
TRANSITION REYNOLDS NUMBER BASED ON FREE-STREAM PROPERTIES
3 x 10⁶
2 x 10⁶
10⁶
0
0
1
2
3
4
TEST MACH NUMBER
SYMBOL RUN* UNIT REYNOLDS NUMBER
66 0.50 x 10⁶/IN.
70 0.73 X 10⁶/IN.
71 0.66 X 10⁶/IN.
73 0.79 X 10⁶/IN.
75 0.80 X10⁶/IN.
89 0.50 X 10⁶/IN.
AEDC TR-60-5 0.75 X 10⁶/IN.
* DAL TEST S-61

FIGURE 8

Section 2
Hypersonic Turbulent Heat Transfer

R.E. Deem

January 1, 1963

Report Number SM-41379-2

Sales Order: 81260-287
Engineering Work Order: 51901
Job Work Order: 0001

SUMMARY

Pressure and heat transfer distributions have been measured on a standard model of a hypervelocity ballistic vehicle. The data pertain primarily to a turbulent boundary layer at Mach 8 at zero pitch and at a pitch angle of 20 degrees. Analysis of the data indicates that recovery temperature could not be measured accurately on the model; consequently heat transfer coefficients could not be determined reliably. However, an accurate description of the heat input to the model is afforded in terms of heat transfer rates. Measured heat transfer rates at the stagnation point remain rather inaccurate because of large conduction effects at the model nose. Development of a heat shield has been initiated to alleviate the conduction problem.

TABLE OF CONTENTS

LIST OF TABLES

LIST OF ILLUSTRATIONS

1. INTRODUCTION

An IR&D study has been initiated at DAL during FY 1962 to establish a capability for conducting heat transfer tests in the Hypersonic Two-Foot Wind Tunnel, and to provide model test data which can be compared with data from other facilities. The approach taken is to develop the capability stepwise by alternatively testing a model, analyzing the results, making any system modifications required to improve the data, and then repeating the cycle until the data are satisfactory. However, only the first two steps and part of the third step of one cycle have been accomplished during the present investigation. Heat transfer tests were conducted on the model (HB-2) at Mach 8 during June 4 - 7, 1962; and several runs were subsequently performed to develop a heat shield that would prevent development of an uneven temperature distribution along the model before data are extracted. The tests are identified as H-R6.

This report describes the investigation and presents the results. An account is given of the tunnel, model, instrumentation and program used in conducting the initial heat transfer test, the results are discussed, and a description is given of the steps taken to modify the system.

2. FACILITY

The DAL Hypersonic Two-Foot Wind Tunnel is an intermittent blow-down tunnel with provisions for testing at Mach 6, 8 and 10 with run times of up to 2 minutes. Figure 1 shows an airflow diagram and the major components of the tunnel. A detailed description of the facility is presented in Reference 1.

The feature of the tunnel pertinent to heat transfer tests is the free-jet test section and the model support system. A sting-mounted model is held above or below the jet during the tunnel start. After the airstream has reached a steady state the support strut translates the model into the flow at a rate of 12 inches per second.

3. MODEL

The model tested is a ballistic-type, hypervelocity configuration consisting of a spherical nose, a conical forebody, a cylindrical body, and a flared afterbody. This configuration, designated model HB-2, is currently proposed for adoption by the Wind Tunnel and Model Testing Panel of AGARD as a standard, hypersonic, blunt-body, calibration model. The model specifications have been developed by members of the Supersonic Tunnel Association and are discussed in Reference 2.

The model consists of an outer shell and an inner support, with pressure tubes and thermocouple leads passing between them. An electroformed nickel shell, approximately 0.062-inch thick, forms the external contour. The internal support is a 1.5-inch-diameter dummy balance supported as a cantilever from a two-piece sting. Figure 3 is a photograph of the model installed in the tunnel. A more detailed description of the model is contained in Reference 3.

4. INSTRUMENTATION

A row of 1/32-inch-diameter pressure orifices is located along the bottom centerline of the model and a row of thermocouples is welded to the inside surface of the skin along the top centerline. Locations of the instrumented model stations are given in table 1. Five orifice pressures (6, 7, 8, 13 and 14) are sensed by Pace variable-reluctance, 0.5-psi transducers referenced to vacuum. The others use Statham 15-psi differential transducers referenced to atmospheric pressure. Tunnel stagnation pressure is sensed in the stilling chamber by a 2500-psig transducer. Outputs from the pressure transducers are digitized and recorded by a Central Data Gathering System (CDGS). Chromel-alumel thermocouples made from 30-gage wire (with fiberglass insulation) are used to sense model temperatures. A Douglas TR-1, 250°F reference junction is used as a thermocouple reference. Tunnel stagnation temperature is sensed in two places by individual chromel-alumel thermocouples. One uses a Pace 150°F reference junction and is measured with the CDGS. The other tunnel stagnation temperature and all model temperatures are digitized and recorded on magnetic tape by an Automatic Data Handling System (ADHS).

The ADHS is a multichannel data acquisition and recording unit that is borrowed from the Data and Computing Laboratory of the Research and Development Support Department, Missile & Space Systems Division of the Douglas Aircraft Company. This unit commutates the analog signals, converts them to digital form, and records them on magnetic tape. Each thermocouple signal is recorded every 0.02 second. The CDGS consists of 16 Leeds and Northrup Speedmax potentiometers with attached Giannini shaft digital encoders and an IBM 523 summary card punch. This system is described more fully in Reference 1.

Schlieren and shadowgraph systems are used for visual and photographic monitoring. The schlieren system is a conventional Z-type arrangement of two mirrors, a continuous lamp, and an automatic camera. Shadowgraphs are taken with an 11-by 14-inch film plate mounted just outside one test-section window and a 3-microsecond-duration spark source outside the opposite side of the test section.

5. TEST PROGRAM

The present program utilizes experience gained in previous supersonic heat transfer tests (References 3 and 4); yet an attempt has been made to keep procedures simple and straightforward and to employ a minimum of auxiliary tunnel equipment and modifications.

It is known that, for heat transfer rate measurements, the model should be subjected to a step input of aerodynamic heating just before temperature histories are extracted. This is provided by allowing the model to reach an equilibrium temperature before injecting it into the airstream. Occasionally it is necessary to cool the model to room temperature with an air hose prior to a run. When the model is observed to reach the tunnel centerline a switch is thrown manually which marks time zero on the magnetic tape.

There is normally insufficient run time available for the model temperature to reach equilibrium starting from room temperature. Therefore, just prior to a run whose purpose is to measure recovery temperature, the model is preheated with propane blow torches. Near the end of the run, a manually-initiated event marker signals a two-second edit interval to be used for determining equilibrium temperatures.

A total of 15 runs were made in 8.8 hours of tunnel occupancy. Five of these runs are allotted to establishment of shock-wave-free flow in the test section. Seven are heat transfer runs and three are recovery temperature runs. The Mach number is 8.08 and the stagnation pressure is approximately 1050 psia for all runs. The stagnation temperature is either 1500°R or 1900°R. The model was tested at angles of attack of zero and 20° and at roll angles of zero, 90° and 180°. A summary of the test conditions is given in table 2.

6. DATA

Measured data consist of tunnel stagnation pressure and temperature, model angles of attack and roll, and model pressure and temperature histories. Calculation of free-stream parameters is based on isentropic expansion of real air and on the Sutherland viscosity equation, together with a calibrated Mach number based on the measured total pressure and temperature. Model angles of attack and roll are determined directly from the support system without corrections for deflections due to airload. Model pressures are reduced to coefficient form, $C_p \equiv (p - p_\infty)/q_\infty$, where p is the local pressure, p_∞ is free stream static pressure and q_∞ is free stream dynamic pressure. Tunnel parameters, model angles, and model pressure coefficients are calculated on an IBM 1620 computer and results tabulated on an IBM 407 accounting machine.

Model temperature histories and tunnel total temperature are recorded on magnetic tape, edited, and reduced to heat transfer rates, coefficients, and equilibrium temperatures on an IBM 7090 computer and results tabulated on an IBM 1403 printer. This reduction process is based on the transient temperature method and is described in detail in References 4 and 5. Briefly, the reduction process consists of fitting a least-squares parabola through 49 consecutive temperatures

measured at 0.02-second intervals during a heat transfer run and calculating the slope at the midpoint. Heat transfer rate is then equal to the product of the slope, the model skin density, specific heat, and thickness. Model equilibrium temperature is averaged over approximately two seconds during a recovery temperature run and the value divided by tunnel total temperature. This ratio is multiplied by the total temperature during a heat transfer run and is assumed to be the recovery temperature. The heat transfer coefficient is equal to the heat transfer rate divided by the difference between recovery and model temperatures.

The measured pressure coefficients are listed in table 3. Heat transfer rates, measured at 0.5 second after time zero, are listed in table 4. Some of these data are plotted. Figure 4 shows the pressure distribution at zero angle of attack (runs 6, 7, 8 and 9). Figure 5 shows the heat transfer distribution to the windward centerline at 20 degrees angle of attack (runs 10 and 15). Note that the heat transfer data are plotted as ratios of heat transfer rate to the heat transfer rate at thermocouple 1 (stagnation point). Figure 6 is a schlieren picture taken during run 7.

7. DISCUSSION

One of the purposes of the investigation is to establish the capability at DAL for conducting heat transfer tests. To this end it must be established that the technique developed to obtain the data produces results within satisfactory tolerances.

The technique used to obtain model pressures has been established as valid by many tests over many years. It has been calculated that at least 50% of the pressure coefficients of each run are determined with a tolerance not exceeding $\Delta C_p = \pm .009$. This agrees closely with the pressure coefficient accuracy reported in Reference 3. It may be noted also that the measured pressure data plotted in Figure 4 agree substantially with the theoretical Newtonian pressure distribution.

The technique used to obtain heat transfer data is the prime concern of the investigation. Three items, all affecting accuracy, have been studied: the magnitude of the heat input with the model initially at room temperature, the accuracy of assuming equilibrium temperatures are equal to recovery temperatures, and the ability of the model support system to generate a step function of heat input.

The magnitudes of measured heat transfer rates, as presented in table 4, clearly indicate that rates of change of temperature with time are sufficient to minimize data errors due to the accuracy of the temperature-measuring equipment. The temperature rate (in degrees F per second) is approximately three times the heat transfer rate (in Btu/sec ft^2). Thus, for an average heat transfer rate of 5 Btu/sec ft^2, the model temperature

changes about 15 degrees F during the one-second period the slope is being formed. Random errors in the temperatures when measured with a thermocouple are believed to be on the order of $\pm 3^{\circ}$F. This should have only a small effect on the accuracy of the calculated slope since the slope is based on a least-squares curve fit.

The initial concern over whether or not the preheated model would reach equilibrium during the blowdown is unfounded. Within engineering accuracy, the model temperature does not change during the last two seconds of a recovery temperature run. However, the measured equilibrium temperatures are not nearly close enough to estimated recovery temperatures to be useful in deriving recovery temperatures. For example, the highest measured equilibrium temperature at the stagnation point is 90% of the tunnel stilling chamber air temperature. Other points on the model body likewise experience low values of equilibrium temperature. Apparently, the heat losses from the model due to radiation and conduction cause these low equilibrium temperatures. Consequently, the calculated heat transfer coefficients are invalid. In an attempt to circumvent this problem, the heat transfer rates (which are not affected by recovery temperatures) have been divided by the measured stagnation point heat transfer rate and the ratio analyzed. This seems to be a satisfactory way of establishing the distribution of heat input to the body. The distribution shown in Figure 5 appears to be quite valid.

The ability of the model support system to approximate a step heat input is assessed by considering the heat transfer rates at the stagnation point. The three heat transfer runs at zero angle of attack (6, 8 and 9) are analyzed by comparing theoretical with measured stagnation point heat transfer rates.

The theory from Fay and Riddell, Reference 6, equation 63, is:

$$q_s = 0.94\,(\rho_w \mu_w)^{0.1}\,(\rho_s \mu_s)^{0.4}\left[1 + (L^{0.52} - 1)\,\frac{h_D}{h_s}\right](h_s - h_w)\sqrt{\left(\frac{du_e}{dx}\right)_s}$$

where ρ is the gas density, μ its coefficient of viscosity, L its Lewis number, h its static enthalpy, h_D its dissociation enthalpy, and $(du_e/dx)_s$ is the local velocity gradient at the edge of the boundary layer in the stagnation region; and where subscripts w and s identify conditions at the model wall temperature and at the edge of the boundary layer in the stagnation region. For Newtonian flow around a sphere of a gas sufficiently cool that real gas effects can be neglected, the above equation becomes

$$q_s = \frac{55.7}{\sqrt{r_o}}\left(\frac{\mu_w}{T_w}\right)^{0.1}\left(\frac{\mu_s}{T_s}\right)^{0.4}(T_s - T_w)\left[p_s\,(p_s - p_\infty)\,T_s\right]^{1/4}$$

where the rate of stagnation heating q_s is in Btu/ft^2 sec, nose radius r_o is in inches, coefficients of viscosity μ are in lb sec/ft^2, temperatures T are in degrees Rankine, and pressures p are in psia.

Using the measured temperature at the model stagnation point and the tunnel total pressure and temperature, the theoretical heat transfer rates are calculated and compared with the measured values. This comparison is shown in figure 7. The results show disagreement by about 10% to 20%.

In an attempt to discover a source of this disagreement, an analysis has been made of the error due to heat conduction at the stagnation point. The computed heat transfer rates do not include a correction for conduction of heat laterally from the stagnation point. The temperature distribution at the model nose at the time heat transfer is measured can be used for the conduction correction in the following manner. An equation of the form

$$T = a + c\theta^2 + d\theta^3 + e\theta^4$$

is fitted to the temperatures T from thermocouples 1, 2, 3, and 4 located at polar angles θ of 0°, 10°, 35°, and 58° respectively. The conduction correction (additive) in polar coordinates is:

$$q_{cond} = \frac{-k\,b}{r_o^2}\left(\frac{d^2T}{d\theta^2} + \text{ctn}\ \theta\ \frac{dT}{d\theta}\right)$$

where k is the thermal conductivity and b is the shell thickness. At the stagnation point, $\theta = 0$, this reduces to

$$q_{cond} = -\frac{2kb}{r_o^2}\ \frac{d^2T}{d\theta^2}$$

Only run 6 has been analyzed in this detail, but by comparing the temperature gradients around the nose on all runs, it appears that the results for run 6 should be typical. The rate of heat transfer from the stagnation point by conduction along the shell is calculated to be 17.9 Btu/sec ft^2, the same magnitude as the uncorrected heat transfer rate* Thus, this conductivity correction fails to improve the correlation of experiment with theory as represented in Figure 7.

The method proposed to circumvent this paradox is to provide a mechanical system which will produce a step input more nearly the ideal function than does the existing model-injection system. The method of providing a step heat input by increasing the injection rate is deemed impractical from a structural point of view. A retractable heat shield system to be combined with model injection is considered worthy of development. This consists of a wedge placed vertically across the nozzle exit with the apex forward and the back and open. The support system injects the model to the tunnel centerline, the model always staying behind the shield. When the model reaches the centerline, the wedge is quickly retracted in a vertical direction.

Several runs have been made in the tunnel to evaluate the effectiveness of such a wedge as a heat shield. Since no shield injection system was available, an attempt was made to fix the shield to the nozzle exit and

*If the temperature measurements at 35° and 58° were ignored, i.e., if the conduction were calculated on the basis of measurements only at zero and 10°, its value would be 11.5 Btu/sec ft^2, still about the magnitude of the uncorrected measurement.

to start the tunnel. All attempts to start the tunnel in this configuration have failed, thus shield effectiveness remains unknown. It is proposed now to start the tunnel empty, then to inject the shield, inject the model, and withdraw the shield. Final development of this system will be accomplished in 1963.

8. REFERENCES

1. Cole, R. M., and G. T. Gibbs, The Hypersonic Two-Foot Tunnel, Description of the Facility and Provisions for Testing, Douglas Aircraft Company Report SM 41369, dated March 1, 1962.

2. Lukasiewicz, J., Standard Ballistic-Type, Hypervelocity Model, ARO Letter Reference No. 30, dated March 1, 1960.

3. Deem, R. E., Pressure and Heat Transfer Distribution Tests on a Standard Ballistic-Type Model HB-2 at Mach 2 to 5 Including the Effects of Shock Impingement, Douglas Aerophysics Laboratory Report S-R6, dated June 29, 1961.

4. Deem, R. E., Pressure and Heat Transfer Tests of the Nike Zeus Jethead Model M126-1A at Mach 4.46, Including Calibration Tests of a Flat Plate and Cylinder, Douglas Aerophysics Laboratory Report S-24, dated April 25, 1962.

5. McCormick, M. A., Heat Transfer Data Reduction (ΔDC Input), Douglas MSSD Research and Development Support Technical Memorandum No. TM-DM15-D/C-L3185, dated August 30, 1962.

6. Fay, J. A., and Riddell, F. R., Theory of Stagnation Point Heat Transfer in Dissociated Air, J. of the Aeronautical Sciences, Vol. 25, No. 2, pp 73-85, February 1958.

TABLE I

PRESSURE ORIFICE AND THERMOCOUPLE LOCATIONS

Axial station, x, nondimensionalized by the model length, L = 18.375 inches	Pressure Orifice Number (180 degrees azimuth)	Thermocouple Number (0 degrees azimuth)
0		1
.0009		2
.0111	1	3
.0288	2	4
.0544		5
.0816	3	6
.1088	4	7
.1360	5	8
.1633	6	9
.3129	7	10
.3809		11
.4490	8	12
.5578		13
.5850	9	14
.6090		15
.6329		16
.6601		17
.6905	10	18
.7243		19
.7586		20
.8231	11	21
.8914		22
.9592	12	23

Note: Pressure orifices 13 and 14 are located on the base at radial positions 81.2% and 60.5% of the base radius and at an azimuth angle of 60 degrees.

TABLE 2

RUN SUMMARY

Model Angle of Attack (Degrees)	Model Angle of Roll (Degrees)	Run Numbers for a Tunnel Stagnation Temperature of	
		1500°R	1900°R
0	0	6, (7), 9	8
20	90	11, (13)	12
	180	10, (14)	15

Note: 1. Run numbers in parentheses are recovery temperature runs; others are heat transfer runs.

2. Model pressures are measured on all runs.

3. The angle of attack of a rolled model is actually its angle of pitch in the tunnel-fixed coordinate system.

TABLE 3

MEASURED PRESSURE COEFFICIENTS $C_p \equiv (p - p_\infty)/q_\infty$

Orifice Number \ Run Number	6	7	8	9	10	11	12	13	14	15
1	1.196	1.209	1.211	1.215	.601	1.061	1.088	1.124	.618	.638
2	.474	.487	.486	.487	.149	.403	.432	.433	.152	.165
3	.277	.350	.303	.282	--	.275	.286	.291	.098	.059
4	.251	.264	.274	.266	.074	.264	.256	.255	.069	.049
5	--	--	--	.148	--	--	.127	.123	.030	.032
6	--	.030	.030	--	--	.023	.025	.024	.004	--
7	--	--	.029	--	--	--	.019	.019	.008	.010
8	--	.017	--	--	--	--	.011	.014	--	--
9	.031	.046	.026	.038	--	--	.021	.027	.020	.022
10	.067	.030	.035	.052	.031	.038	.019	.033	.019	.020
11	.029	.035	.001	.067	.013	.043	.001	.020	-.018	-.001
12	-.034	.000	.020	.042	.011	.034	.034	.033	-.019	-.008
13	.065	.068	.060	.064	.000	-.001	-.001	.000	-.001	.000
14	.063	.066	--	.062	--	-.001	-.002	.002	-.002	-.001

TABLE 4

MEASURED HEAT TRANSFER RATES (Btu/sec ft^2)

at 0.5 second after time zero

Thermocouple Number \ Run Number	6	8	9	10	11	12	15
1	14.180	21.306	19.786	20.229	18.288	27.923	26.734
2	14.124	23.531	16.822	20.014	17.128	21.718	29.068
3	10.022	12.546	14.524	18.701	13.852	21.523	29.963
4	7.825	12.547	6.856	14.914	8.639	14.284	22.820
5	4.106	5.492	4.446	11.301	6.426	8.779	15.724
6	3.514	6.320	4.306	9.845	5.930	7.439	11.902
7	4.268	6.579	5.615	9.688	1.792	7.418	10.418
8	2.307	1.699	15.640	7.289	3.364	4.481	10.019
9	.724	2.581	.962	4.746	.813	1.885	7.157
10	.559	.756	.882	2.401	2.942	.409	4.519
11	.206	.036	-1.342	2.829	- .211	1.677	4.855
12	.396	.311	3.296	3.268	- .564	1.849	4.461
13	1.492	.537	- .021	2.850	1.163	.676	4.815
14	.307	.951	- .014	3.555	.220	1.049	4.457
15	.030	.028	.231	3.221	3.161	.210	4.819
16	.389	.103	- 1.083	4.093	.109	1.272	6.053
17	.246	- .235	2.413	4.752	- .454	2.113	6.649
19	1.883	2.253	.570	5.011	- .225	4.461	8.103
20	1.170	-1.280	1.528	5.919	.912	1.496	6.934
21	.674	1.130	- .329	6.497	.797	.065	9.638
22	- .376	.339	.082	7.646	1.221	1.653	10.493
23	2.150	1.400	.292	7.995	2.633	1.807	10.047

DAL HYPERSONIC TUNNEL DESIGN FEATURES

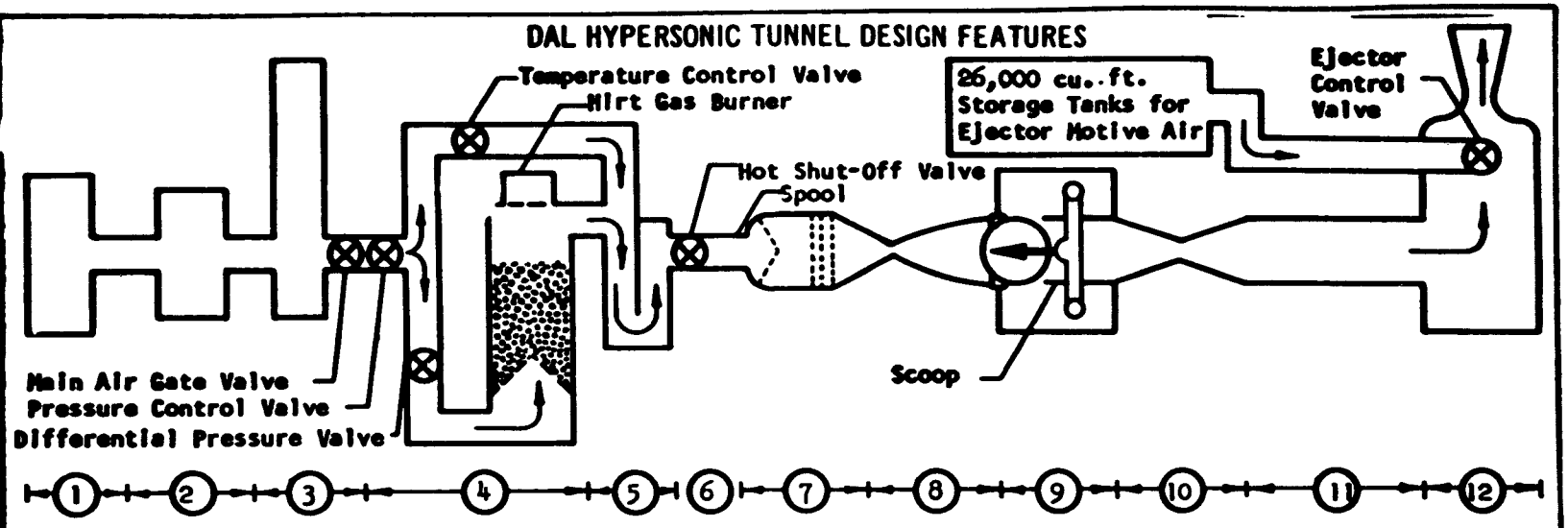

① COMPRESSOR 6 stage Cooper-Bessemer, non-lubricated, reciprocating compressor with interstage cooling. Intake is 1825 cfm at 14.5 psia and 85°F; exhaust at 3500 psia and 100°F.

② DRYER Semi-automatic desiccant Pritchard Hydryer dries air to a dewpoint of -50°F or lower.

③ AIR STORAGE TANKS Two vertical cylinders, of 250 ft.^{3} each, store air at 3500 psia and atmospheric temperature.

④ PEBBLE BED HEATER Alumina pebble bed heater regenerated by combustion of natural gas.

⑤ THERMAL MIXER Mixes hot air from heater and cold air from storage tanks to obtain desired stream temperature.

⑥ HOT SHUT-OFF VALVE Air-cooled ceramic-lined 12-inch rotovalve, hydraulically actuated between full open and full closed positions.

⑦ SPOOL & STILLING CHAMBER Removable spools to make up for length of nozzles. 25-inch diameter stilling chamber containing perforated cone and three turbulence screens.

⑧ NOZZLE Fixed Mach number, axisymmetric nozzles for Mach 6, 8, and 10. Exit diameter approximately 26 inches.

⑨ PLENUM & TEST SECTION Free jet surrounded by plenum chamber with 30-inch diameter windows on sidewalls. A scoop captures jet. Model support provides ±30° pitch, ±22 inches vertical translation, and ±200° roll.

⑩ VARIABLE DIFFUSER Two-dimensional single-peak type with top and bottom walls movable.

⑪ FIXED DIFFUSER Completes expansion to ejector plenum.

⑫ EJECTOR & MUFFLER One main and four side ejectors reduce exit pressure to 1 to 3 psia, depending on mass flow.

FIGURE 1

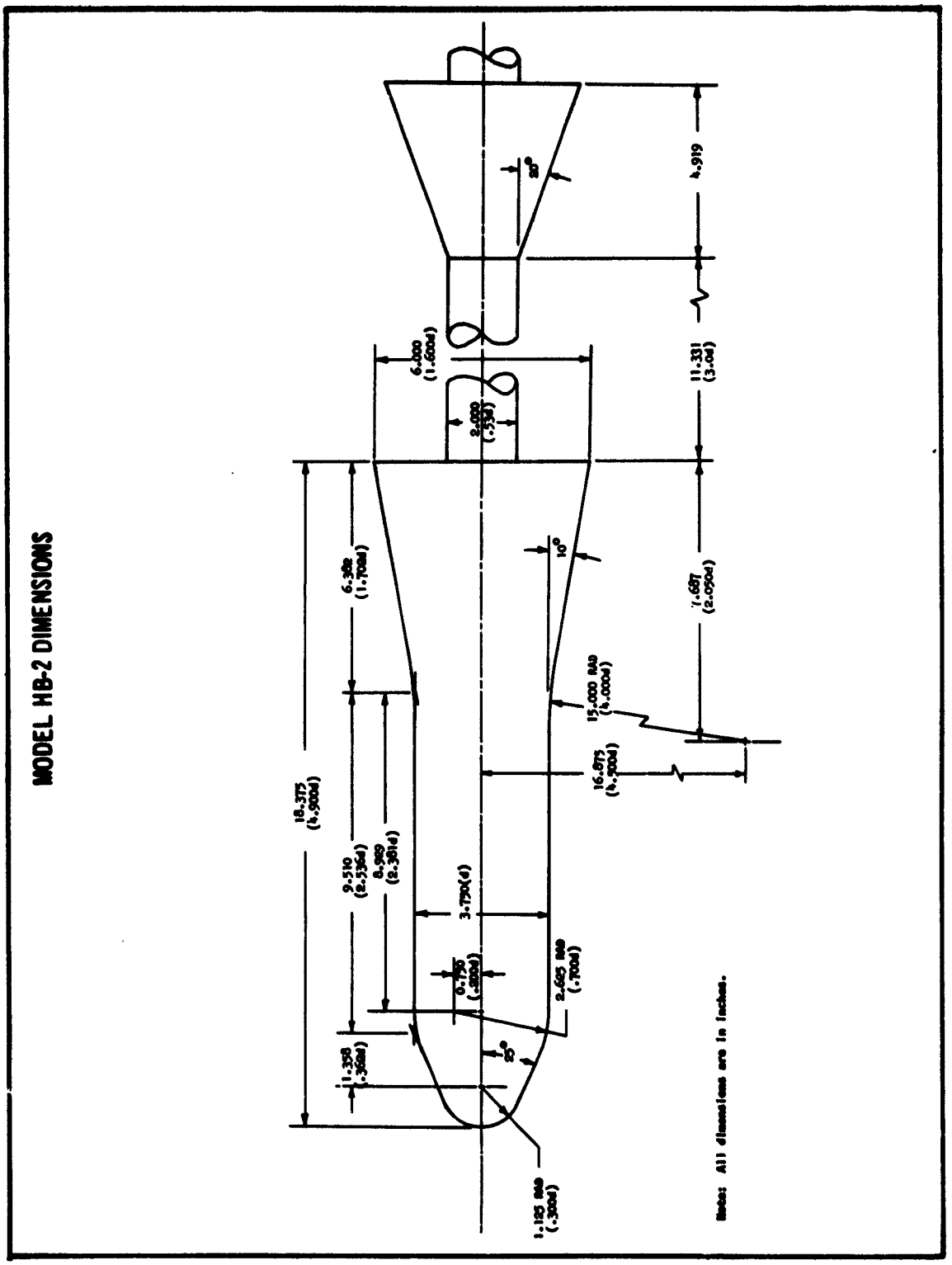
MODEL HB-2 DIMENSIONS
4.919
6.000 (1.600d)
2.000 (.533)
11.331 (3.0d)
20°
10°
6.388 (1.700d)
7.697 (2.050d)
15.000 R&D (4.000d)
16.875 (4.500d)
18.375 (4.900d)
9.510 (2.536d)
8.989 (2.397d)
3.750(d)
0.795 (.200d)
2.625 R&D (.700d)
1.350 (.360d)
20°
1.125 R&D (.300d)
Note: All dimensions are in inches.

FIGURE 2

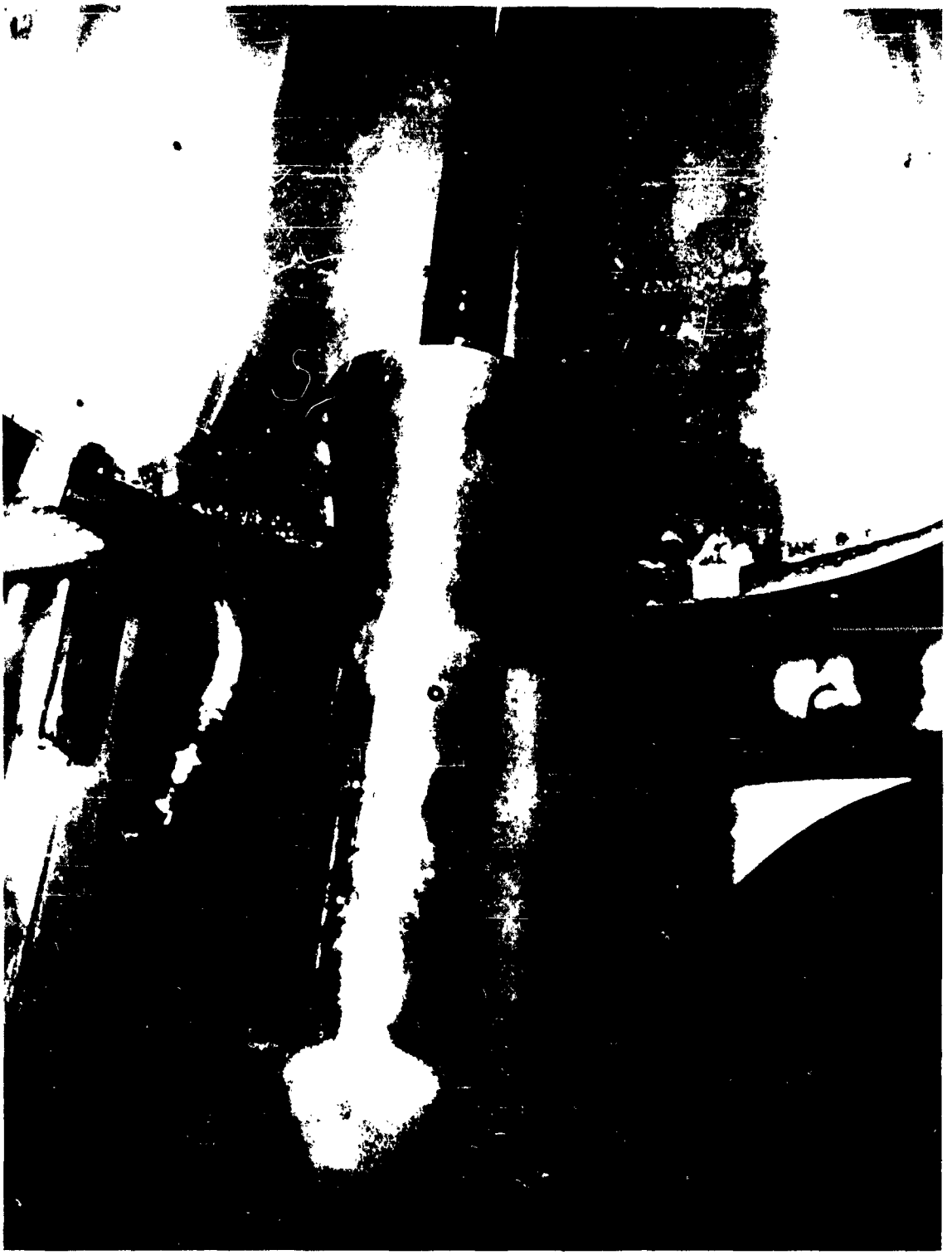

MODEL HB-2 INSTALLATION

FIGURE 3

PRESSURE DISTRIBUTIONS

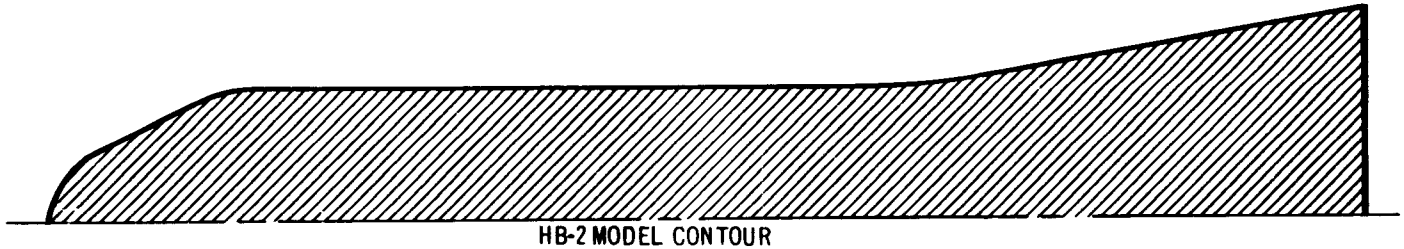

HB-2 MODEL CONTOUR

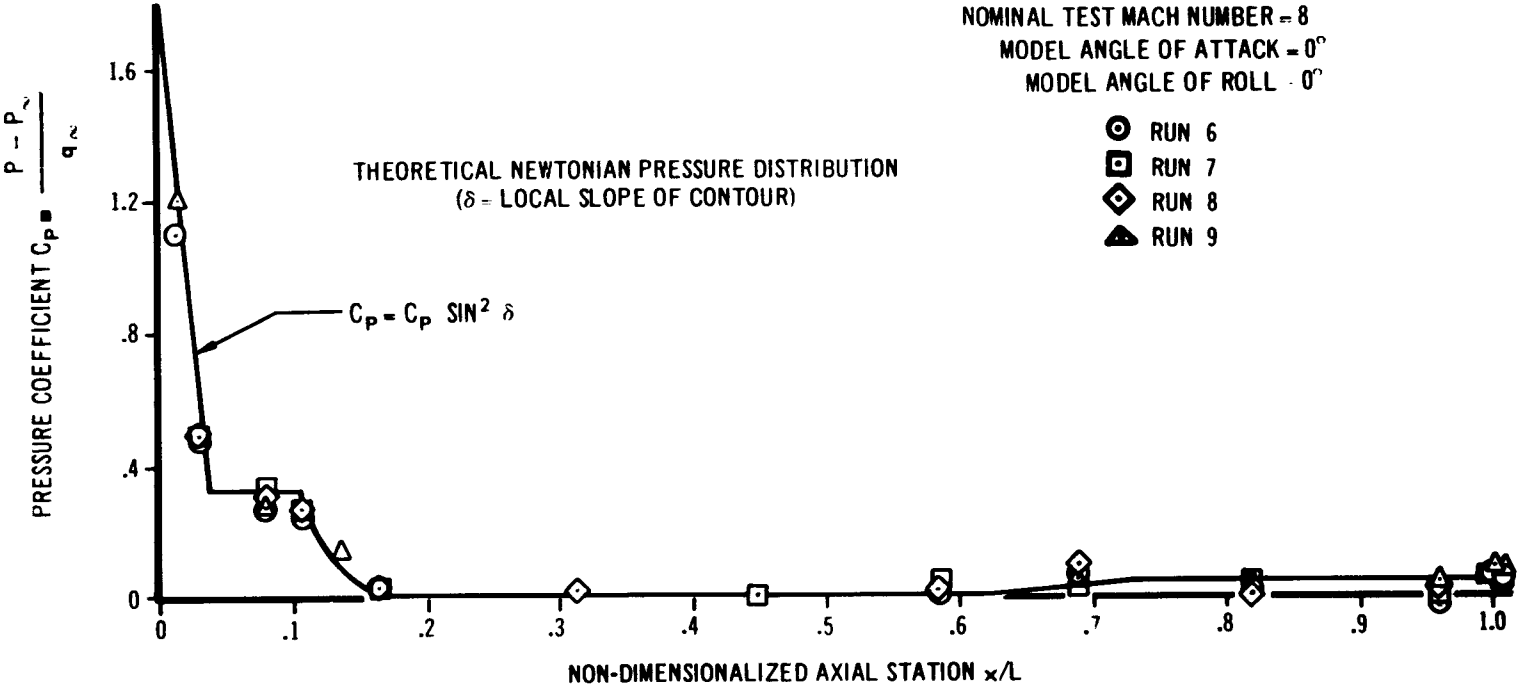

FIGURE 4

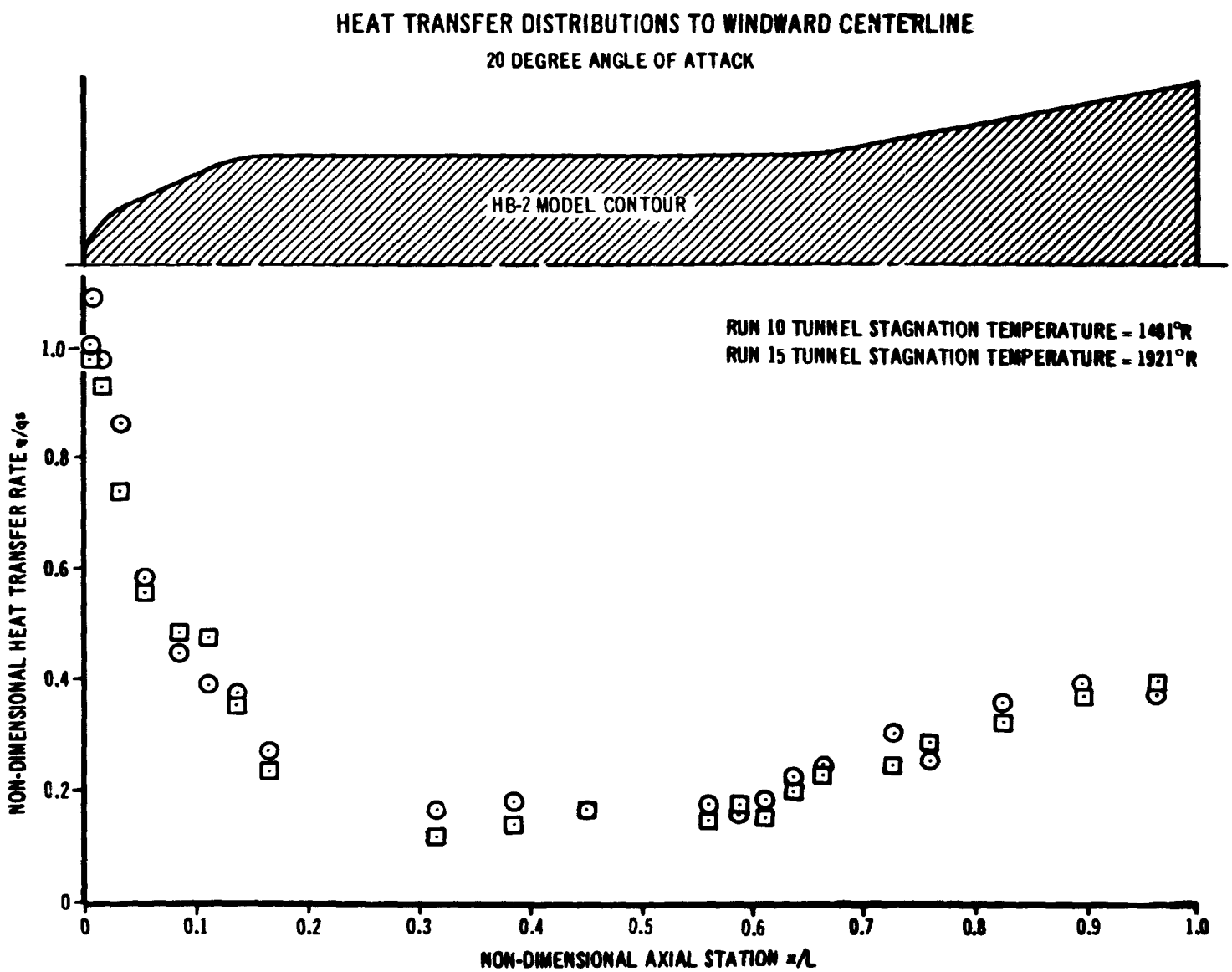
HEAT TRANSFER DISTRIBUTIONS TO WINDWARD CENTERLINE
20 DEGREE ANGLE OF ATTACK
HB-2 MODEL CONTOUR
RUN 10 TUNNEL STAGNATION TEMPERATURE = 1481°R
RUN 15 TUNNEL STAGNATION TEMPERATURE = 1921°R
NON-DIMENSIONAL HEAT TRANSFER RATE q/qs
NON-DIMENSIONAL AXIAL STATION x/L
0
0.2
0.4
0.6
0.8
1.0
0.1
0.3
0.5
0.7
0.9

FIGURE 5

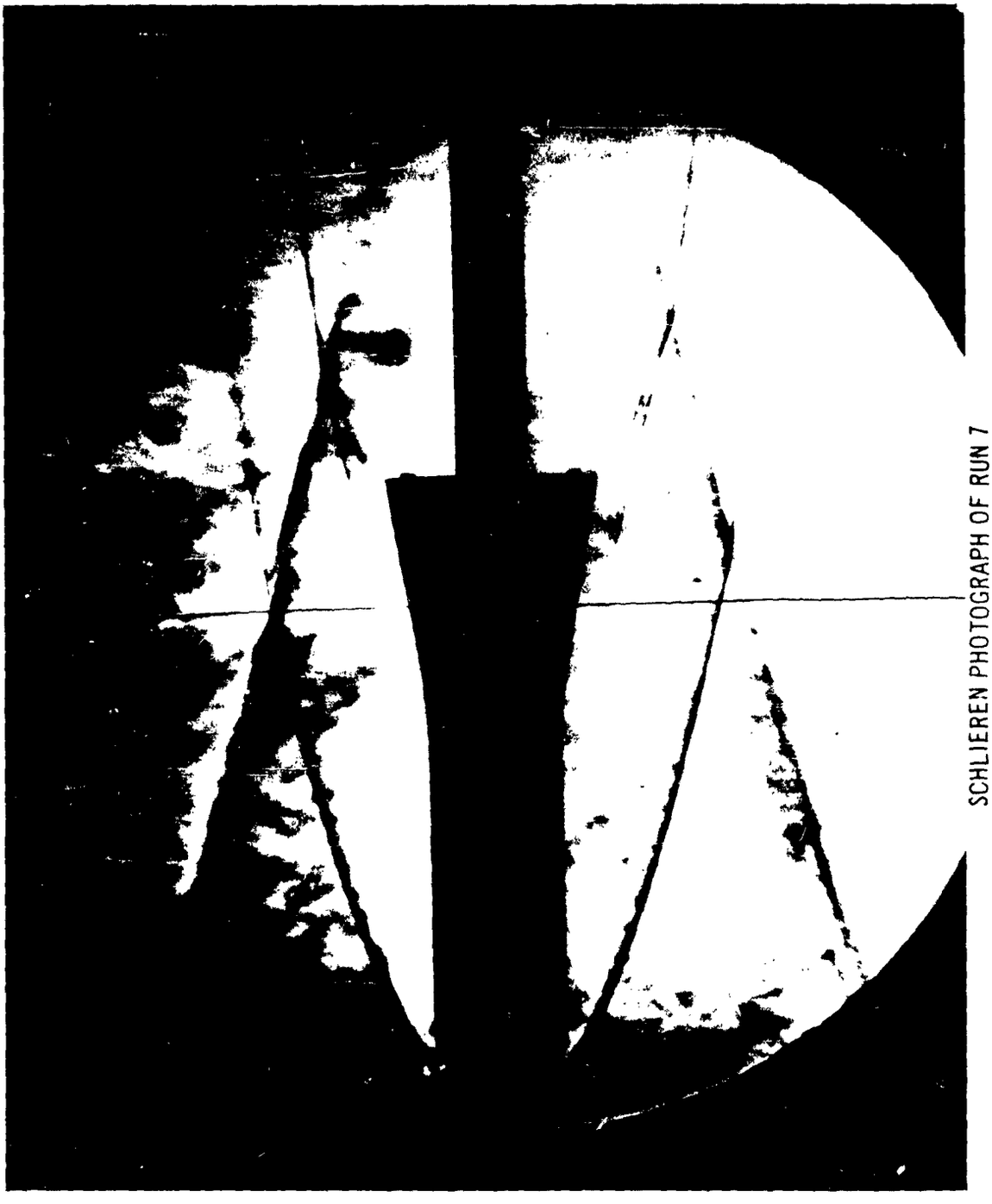

SCHLIEREN PHOTOGRAPH OF RUN 7

FIGURE 6

COMPARISON OF MEASURED AND THEORETICAL STAGNATION POINT HEAT TRANSFER RATES

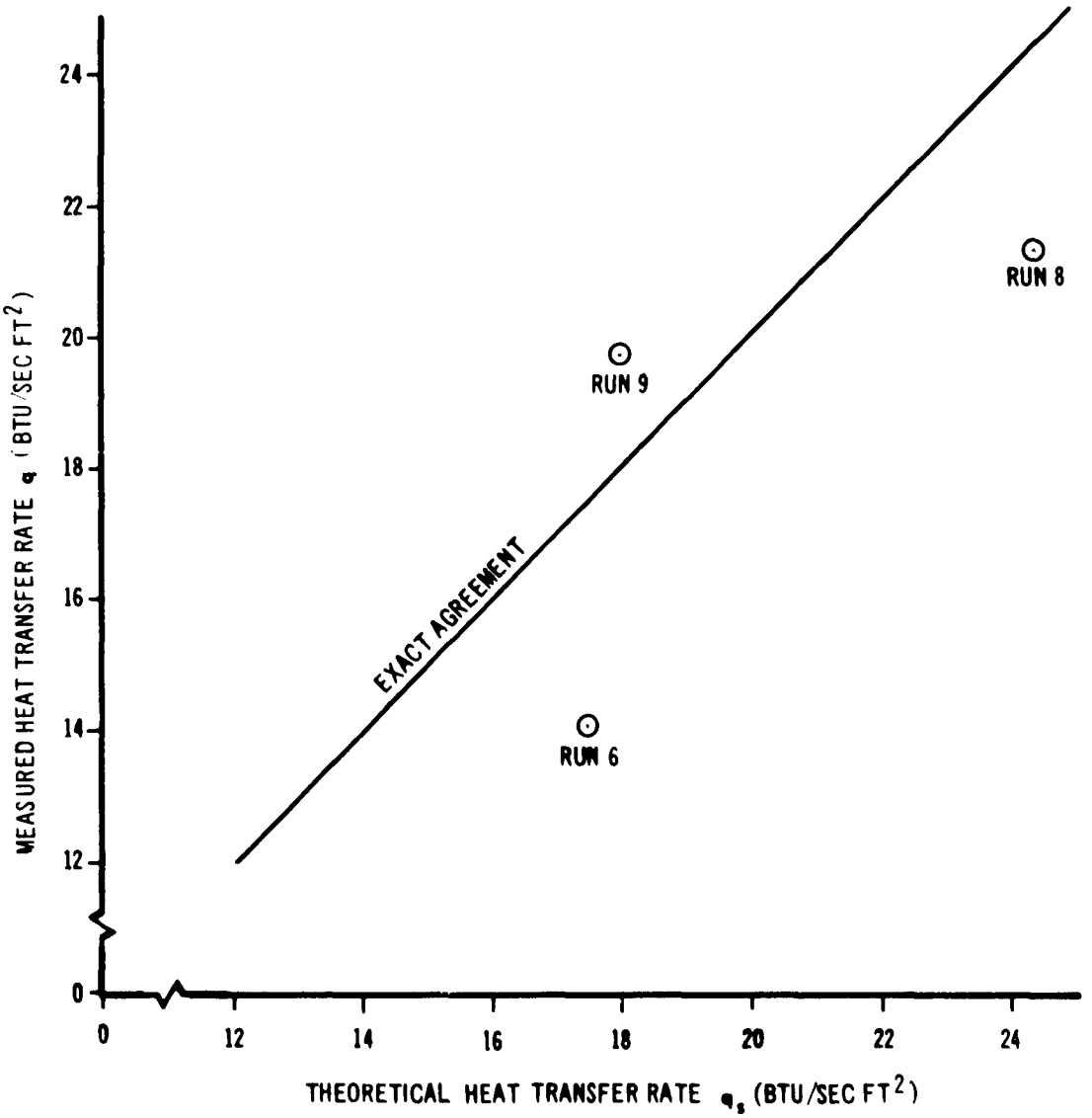

FIGURE 7

Section 3

Hypervelocity Studies Using Hypervelocity Impulse Tunnel

J.A. Copper

January 1, 1963

Report Number SM-41379-3

Sales Order: 81280-187
Engineering Work Order: 51902
Job Work Order: 0001

SUMMARY

Gasdynamic techniques required to enable the Hypervelocity Impulse Tunnel to reach its designed limits of performance, including velocities up to 20,000 ft/sec and run times of at least 10 milliseconds, have been tentatively verified in auxiliary experiments. Operation and control of a combustible mixture of hydrogen and oxygen, diluted by helium or nitrogen, have been demonstrated in the drive section of a three-inch shock tube, and have subsequently been applied with good results in the six-inch drive section of the HIT. Likewise, the tailored-interface and equilibrium-interface techniques and the steady driver expansion technique at the principal diaphragm have been practiced successfully in the three-inch shock tube, all with a combustion drive. However, the use of an orifice at the principal diaphragm to prolong the steady test duration appears to be of marginal value in the range of conditions studied. Analytical methods for determining airflow test conditions have been investigated. Instrumentation suitable for the shock tunnel environment is being developed. Progress therein, as well as preliminary tunnel calibration, is reported.

TABLE OF CONTENTS

LIST OF ILLUSTRATIONS

1. INTRODUCTION

Since complete laboratory simulation of the altitude and velocity range of current interest is out of the question, experimental hypersonic research must be conducted under conditions of partial simulation, as discussed in reference 1. In order to partially simulate conditions of interest to real gas studies, this investigation has been undertaken with the goal of generating uniform flow at velocities up to 20,000 ft/sec.

The DAL Hypervelocity Impulse Tunnel (HIT) is designed to generate air velocities up to 20,000 ft/sec with test durations on the order of 10 milliseconds. This 30-inch shock tunnel, currently in an early stage of calibration, is described in reference 2. During FY 1962, as part of a continuing IR&D investigation, several gasdynamic techniques crucial for ultimate attainment of the designed performance limits have been tentatively verified in auxiliary experiments. For example, the tailored-interface technique (references 3 and 4) at high shock Mach numbers and the "steady" diaphragm configuration (reference 3) have been utilized. To obtain even higher performance it is planned to use the equilibrium-interface technique (references 4 and 5). To demonstrate that these techniques can be utilized is, in fact, one goal of this program; the other goal is to investigate, as thoroughly as possible, the flow in the test section of the HIT.

2. COMBUSTION STUDIES

To obtain the stipulated enthalpies and testing times in the HIT, it is appropriate to use a combustion driver and either the tailored-interface technique or the equilibrium-interface technique. The technique of using the exothermic combustion of a hydrogen-oxygen mixture to heat either a helium or a hydrogen driver gas is attractive in principle since the pressure vessel used to contain the mixture does not have time to heat up appreciably. However, obtaining satisfactory combustion is not a trivial problem; for example, the use of combustion drivers is regarded as unsatisfactory at the Cornell Aeronautical Laboratory due to excessive shock wave attenuation (reference 6), poor repeatability, and a tendency for the mixture to detonate. These factors, of course, make it difficult to attain tailored-interface conditions. For these reasons it is necessary to determine whether a combustion technique can be developed which would permit successful tailoring.

In order to obtain good combustion results, it is necessary to have a homogeneous mixture of the constituent gases (reference 7). In addition, the flame path after ignition must be kept short; in other words, if the mixture is contained in a long tube, it must be ignited in a number of places. In order to get a satisfactory mixture, it is necessary to use positive means of mixing rather than to rely simply on thermal diffusion. This may be seen by noting that the characteristic time for one gas to diffuse a distance δ through another gas may be expressed as δ^2/D_{12}. Now for hydrogen diffusing into helium, the coefficient of diffusion D_{12} is about 2×10^{-3} ft^2/sec so that, if δ is 34 feet (the length of the driver tube), the characteristic diffusion time becomes 6×10^5 seconds or about one week.

To aid in mixing the combustible mixture, a feeder tube is installed inside the driver section along its entire length. When the driver tube is to be filled, the gases enter one end of the feeder tube and are sprayed from many small orifices distributed along its length. Since there is an appreciable pressure drop in the feeder tube, the distances between orifices decrease exponentially with the distance from the start of the feeder tube. This orifice arrangement permits nearly constant mass addition along the axis of the driver section. When filling the driver, sonic flow through the orifices is maintained. This high-speed flow produces a swirling motion which promotes turbulent mixing.

The gas mixture is ignited by heating an ignition wire which runs axially along the centerline of the driver tube. Various methods of heating the ignition wire have been investigated in the three-inch shock tube. These range from exploding small (0.003-inch-diameter) copper and aluminum wires to both "fast" and "slow" heating of a 0.010-inch-diameter tungsten wire. "Fast" heating utilizes the discharge of a capacitor bank while "slow" heating is accomplished with domestic 440-volt power. The "fast" heating of the 0.010-inch-diameter tungsten wire is judged to be the most satisfactory ignition method, with about 60 joules/foot of energy being required for ignition.

The combustion technique described above produces the best results in the three-inch shock tube. Although most experimental pressure traces exhibit some pressure oscillations (fig. 1), it is possible to obtain tailored-interface conditions as shown in fig. 2(a). On several runs where the diaphragm pressure ratio was not correct for tailoring, the reservoir pressure adjusted itself to a steady value within 1 or 2 milliseconds. This gives support to the hope that it will be possible to use the equilibrium-interface technique to increase the HIT performance beyond that obtainable with the tailored-interface technique. However, even though the equilibrium-interface technique can apparently produce steady reservoir pressure, the enthalpy distribution in the test section must be measured before the usefulness of this method can properly be assessed. This is necessary because there may be appreciable mixing of the driver and driven gases which can produce nonuniformities in the enthalpy level while maintaining a constant pressure.

The oscillations on the driver pressure trace (fig. 1) correspond to a weak shock wave which propagates back and forth in the closed driver tube. As richer mixtures are used and detonation mixtures are approached, this wave becomes stronger. Now, when the diaphragm opens, this wave propagates down the driven tube and affects the reservoir conditions deleteriously. An example of this disturbance terminating steady conditions in the reservoir is shown in fig. 2(b).

Several constant-volume combustion tests have been made in the HIT to check out the supporting equipment and instrumentation and to determine whether the technique developed in the three-inch shock tube would give satisfactory results in the larger tube. It is found that a stoichiometric oxygen-hydrogen mixture, diluted with about 84.5% helium, gives the best results. This mixture is quite lean, barely rich enough to sustain burning, and the resulting combustion is quite gentle as illustrated in fig. 3. For this mixture the final sound

speed a_f is 7100 ft/sec, as compared with the maximum sound speed of about 7500 ft/sec which is theoretically obtained with a mixture diluted with only 73% helium (fig. 4). However, when mixtures richer than about 84% helium were tried in the HIT, violent pressure fluctuations were obtained. Studies are currently under way to extend the range over which good combustion can be obtained.

3. STEADY DRIVER EXPANSION CONFIGURATION

For a shock tube with the dimensions of the HIT and operating under tailored-interface conditions, the first disturbance that arrives at the reservoir region is the result of the interaction of the reflected shock wave and the tail of the expansion wave (fig. 5). It is normal, then, to assume that this disturbance terminates the useful test time. In theory, it is possible to eliminate this disturbance by eliminating the portion of the nonsteady expansion wave that expands the flow supersonically. This is done by placing a throat at the diaphragm section and a diverging nozzle downstream of it. This modification has been called the steady configuration (reference 3) because the supersonic expansion proceeds here in a steady rather than a nonsteady fashion. In theory, the use of the steady driver expansion technique usually increases the test time by a factor of two or three at the expense of a lower shock Mach number M_s for a given diaphragm pressure ratio. The reason for this decrease in M_s is that a steady expansion is less efficient* than a nonsteady expansion in supersonic flow.

Diaphragm throat-nozzle inserts, designed for $M_s = 6$ and $M_s = 10$, have been fabricated for the three-inch shock tube. However, it is difficult to detect any difference in performance between runs when these inserts are used and when they are not. In general, the useful run times seem to be as long as one would expect with the steady modification, even when the throat-nozzle insert is not installed. This tentative conclusion has been substantiated by the limited results obtained in the HIT. One reason for this apparent independence of diaphragm configuration is that the disturbance resulting from the interaction of the reflected shock wave and the tail of the expansion wave is in many cases quite weak (reference 5). Perhaps for the range of HIT operating conditions, this disturbance does not significantly affect the steadiness of the reservoir pressure.

---

* The expansion process that produces the largest velocity increase for a given pressure decrease is defined as the most efficient.

4. CALCULATED PERFORMANCE

The HIT test section conditions were predicted prior to actual tunnel operation by using an empirical boundary layer theory (reference 8) to calculate the effective area ratio (A/A*), and by assuming a one-dimensional, isentropic expansion of air in equilibrium (as described in reference 9). The results of these calculations are shown in figs. 6 to 8. The variation in test section Mach number with reservoir conditions is shown in fig. 6. Here it is seen that the test-section Mach number may be varied between 9.5 and 28. Fig. 7 shows the extent of the core of inviscid flow in the test section. The usable core varies from nearly 13 inches (for nozzle throat diameter d* = 0.840 in. and air reservior pressure p_5 = 30,000 psi) to about 3.5 inches (for d* = 0.030 in. and p_5 = 1,000 psi). Fig. 8 shows the operating envelope in terms of Reynolds number and test Mach number. The Reynolds number ranges between 300 and 3×10^7 per foot.

The theoretical performance curves provide a reference for the correlation of actual calibration data, they give operating envelopes to be used in the design of instrumentation, and they provide an idea of the simulation capabilities of the HIT.

5. CALIBRATION TECHNIQUES

Several methods for determining the test-section conditions in the HIT have been analyzed. The simplest of these techniques requires only a pitot pressure measurement in the test section in addition to knowledge of the reservoir pressure which may be either measured directly or calculated from the measured M_s. All other test section properties can then be found from real-gas tables (for example, references 10 and 11), if the nozzle flow is considered to be an isentropic expansion of equilibrium air. However, several other methods have been considered where it is not necessary to assume isentropic flow in the nozzle and no dependence is made on the reservoir conditions. One such method makes use of a stagnation-point heat-transfer measurement while another technique utilizes a direct test-section velocity measurement by opitcal means.

The Fay and Riddell equation for heat transfer from a gas in equilibrium to a stagnation point (reference 12) has been well verified experimentally in shock tubes and shock tunnels (for example, references 13 and 14). The total enthalpy of the airflow in the HIT test section can be found from this equation after measuring the pitot pressure and the heat transfer rate to the stagnation point of a simple body, such as a sphere. Once the stagnation conditions are known, the free-stream conditions can be determined from the normal shock wave equations limited by the assumption that the flow in the shock layer is incompressible.

Another technique to evaluate the enthalpy level in the test section is to measure the free-stream velocity optically (for example, references 15 and 16). The velocity is determined by generating a disturbance at the upstream end of the test section and photographing (with the help of a spark-schlieren system) the position of this

disturbance a known time interval later. In addition, experimental studies are presently under way to try to relate (using blast-wave theory) the rate of expansion of this disturbance wave to the free-stream density. If a static property such as the density can be determined, the degree of nonequilibrium present in the test section can be evaluated.

If the flow in the nozzle can be considered isentropic, the degree of nonequilibrium in the test section can be evaluated by obtaining one test-section measurement in addition to the pitot pressure (reference 17). For given free-stream stagnation conditions, appropriate curves can be constructed using reference 10. It is assumed in this method that air is in equilibrium up to a point, then chemical composition suddenly becomes frozen until the air passes through a normal bow shock wave, after which it is assumed to be in equilibrium again. Fig. 9 is an example of such a plot with pitot pressure plotted against static pressure. From this plot, the point where the composition freezes, and hence the chemical composition ahead of the bow shock wave, can be determined.

6. INSTRUMENTATION

Shock-wave velocity, shock-tube pressures, test-section pressures and test-section heat transfer have been measured during the course of this investigation. The systems used to measure these quantities are briefly described below.

An average shock-wave velocity is determined by measuring the shock transit time between two stations. The shock wave is detected either by a thin-film resistance thermometer, which senses the temperature rise behind the shock wave, or by a transducer which detects the ionization behind the shock wave. The ionization detectors are much less troublesome as they use a passive electronic circuit and their signal does not require amplification. Unfortunately, they cannot be used for shock waves weaker than about shock Mach number 6, as below this value the ionization level behind the shock wave is too low.

Shock-tube pressures between 100 and 6000 psi have been measured with Kistler Model 605 quartz piezoelectric pressure transducers. The charge amplifiers (Kistler Model 565) that complete the measuring system have a sufficiently long time constant to allow static calibration of this system.

Several pressure transducers are being evaluated for the low (0.03 to 50 psi) test-section pitot pressure measurements required. These transducers include Kistler Models 701 and 401 and Atlantic Research Corp. Model LC-60. When used with Kistler Model 568 charge amplifiers, the Model 401 and 701 transducers can also be calibrated statically. The calibrated sensitivities of these Kistler transducers is within 30% of their advertised values. It appears that the Model 401 and 701 transducers are limited by noise to pressures above about 0.1 psi. Based on their theoretical sensitivity, the ARC transducers should be capable of pressure measurements to 0.01 psi, and possibly even lower. In order to calibrate these ARC transducers it was necessary to develop

special low-range calibration techniques. The sensitivity of these transducers dictates that they must be isolated from any mechanical valving device, and their transient response characteristic necessitates that the pressure step have a rise time of one millisecond or less. It has not been possible as yet to obtain a calibration which agrees with the calibration supplied with the ARC transducers. In addition, these transducers do not give a step output when exposed to what all other evidence* indicated was a step input in the HIT test section. The three-inch shock tube is currently being prepared as a calibration device to supply a known shock-wave pressure change to these transducers so that their characteristics can be examined more carefully.

Two different techniques are to be used to obtain heat-transfer rate measurements in the HIT. One technique uses a thin-film resistance thermometer while the other uses a calorimeter. The thin-film transducer consists of a thin metallic film applied over an insulator backing which can be considered to be of infinite thickness for run durations typical of the HIT. The thin-film element then senses the surface temperature of the backing material, indicating its temperature change with a change in resistance. From the surface temperature history of the backing material the heat-transfer rate can be calculated from the known solution for one-dimensional heat conduction to a semi-infinite body.

The calorimeter incorporates a thermal mass which retains the heat transferred to it. Hence the heat-transfer rate is proportional to the time rate of change of the average temperature of the thermal mass. Stagnation point heat-transfer measurements have been made in the HIT test section using a calorimeter (Hidyne Model HT-100), which is calibrated by the manufacturer and is extremely simple to use.

As noted in the previous section, static pressure measurements are extremely valuable in evaluating nonequilibrium effects. However, no commercially available transducers seem to be capable of measuring these extremely low pressures (0.36 to 0.00004 psi). For these reasons, a transducer similar to that developed at Cornell Aeronautical Laboratory (reference 18) is being designed and built for evaluation at D.A.L. This transducer utilizes a bimorph lead zirconate titanate beam which is loaded in bending (fig. 10). The piezoelectric crystal is protected from temperature effects and acceleration compensation is built into the transducer through the use of a second diaphragm and crystal. This transducer should have a natural frequency of about 10,000 cps and a range from about 0.001 to 1 psi.

---

* The reservoir pressure and two other pitot-pressure measurements, all made with Kistler transducers, indicated a step input of pressure.

7. PRELIMINARY RESULTS OF TUNNEL CALIBRATION

Some initial calibration results have been obtained in the HIT at the nominal Mach 10 cold operating point (reference 2). For this enthalpy level, the shock Mach number required for tailoring is about 2.7; this can be obtained with a driver gas mixture of 92% helium and 8% nitrogen, both at room temperature. Several runs have been made using a driver mixture nominally consisting of 90% helium and 10% nitrogen at 1000 psi. Fig. 11 shows that the experimental diaphragm pressure ratio (p_4/p_1) required for shock strengths in this range correlates better with the theoretical curve for a straight shock tube than with the curve for a tube with the HIT geometry of 36/25 area convergence at the diaphragm section. The amount of shock-wave attenuation measured during these runs is negligible. An example of the reservoir pressure under these conditions is shown in fig. 12(a). Here it is seen that the run time (time of constant reservoir conditions) is about 23 milliseconds with the pressure constant to within ±5%.

Fig. 12(b) shows a typical pitot-pressure record obtained on the test section centerline, 2 inches aft of the nozzle exit. Here it is seen that the pressure is constant for at least 15 milliseconds. Measurements taken 6 and 11 inches from the centerline exhibit this same constant pressure behavior. On this run the test section Mach number determined from the pitot pressure measurements (M_∞ = 10.6) agrees with the predicted value of M_∞ = 11.1 (fig. 6) within the limit of experimental accuracy.

During this series of runs one stagnation point heat transfer measurement was made with a calorimeter*. The oscilloscope record is shown in fig. 13. A constant slope indicates a constant heat transfer rate or that the enthalpy level in the test section is constant. It is seen that the heat transfer rate is indeed constant for at least 15 milliseconds. On this run the heat transfer rate is within 1% of that predicted by the Fay-Riddell theory for the measured reservoir conditions.

*The transducer was damaged during the run; this damage is believed to be the result of faulty transducer construction, not foreign particles in the airstream.

8. REFERENCES

1. Moulin, L. (editor), An Assessment of Our Present Status and Future Requirements for High Temperature Hypersonic Facilities, Round Table Discussion held in Brussels, Training Center for Experimental Aerodynamics, TM-14, April 6, 1962.

2. Copper, J. A., The Hypervelocity Impulse Tunnel: Facility Description and Expected Performance, Douglas Aircraft Company Inc., Santa Monica Report No. SM 41377, November 2, 1962.

3. Wittliff, C. E., M. R. Wilson, and A. Hertzberg, The Tailored-Interface Hypersonic Shock Tunnel, J. of the Aerospace Sciences, Vol. 26, No. 4, pp 219-228, April 1959.

4. Hertzberg, A., W. E. Smith, H. S. Glick, and W. Squire, Modifications of the Shock Tube for the Generation of Hypersonic Flow, Cornell Aeronautical Laboratory Report No. AD-789-A-2, March 1955.

5. Copper, J. A., Experimental Investigation of the Equilibrium Interface Technique, The Physics of Fluids, Vol. 5, No. 7, pp 844-849, July 1962.

6. Wittliff, C. E., and M. R. Wilson, Shock Tube Driver Techniques and Attenuation Measurements, Cornell Aeronautical Laboratory Report No. AD-1052-A-4, August 1957.

7. Nagamatsu, H. T., and E. D. Martin, Combustion Investigation in the Hypersonic Shock Tunnel Driver Section, J. of Applied Physics Vol. 30, No. 7, pp 1018-1021, July 1959.

8. Burke, A. F., and K. D. Bird, The Use of Conical and Contoured Expansion Nozzles in Hypervelocity Facilities, Advances in Hypervelocity Technique, Plenum Press, pp 373-424, March 1962.

9. Kaegi, E. M., and W. R. Warren, Free Stream Properties of Argon-Free Air in Chemical Equilibrium for a One-Dimensional, Isentropic, Expansion Process, General Electric Report R61SD111, December 1961.

10. Yoshikawa, K. K., and E. D. Katzen, Charts for Air-Flow Properties in Equilibrium and Frozen Flows in Hypervelocity Nozzles, NASA TN D-693, April 1961.

11. Jorgensen, L. H., and G. M. Baum, Charts for Equilibrium Flow Properties of Air in Hypervelocity Nozzles, NASA TN D-1333, September 1962.

12. Fay, J. A., and F. R. Riddell, Theory of Stagnation Point Heat Transfer in Dissociated Air, J. of the Aeronautical Sciences, Vol. 25, No. 2, pp 73-85, February 1958.

13. Rose, P. H., and W. I. Stark, Stagnation Point Heat-Transfer Measurements in Dissociated Air, J. of the Aeronautical Sciences, Vol. 25, No. 2, pp 86-97, February 1958.

14. Nelce, S. E., R. W. Rutowski, and K. K. Chan, Stagnation-Point Heat-Transfer Measurements in Hypersonic, Low-Density Flow, J. of the Aerospace Sciences Vol. 27, No. 5, pp 387-388, May 1960.

15. Cunningham, B. E., and S. Kraus, Experimental Investigation of the Effect of Yaw on Rates of Heat Transfer to Transverse Circular Cylinders in a 6500-Foot-per-Second Hypersonic Air Stream, NACA RM A58E19, August 26, 1958.

16. Karamcheti, K., W. Vali, J. B. Kyser, and M. L. Rasmussen, Measurements of Pressure and Speed of Flow in a Spark-Heated Hypersonic Wind Tunnel, AEDC TDR 62-218, November 1962.

17. Haymon, Jr., L. O., and R. B. Stewart, A Technique for Determining the Nozzle-Flow Properties of Air in an Equilibrium, Nonequilibrium, or Frozen State, J. of the Aerospace Sciences, Vol. 29, No. 2, p. 245, February 1962.

18. Martin, J. F., G. R. Duryea, and L. M. Stevenson, Instrumentation for Force and Pressure Measurements in a Hypersonic Shock Tunnel, Advances in Hypervelocity Techniques, Plenum Press, pp 145-186, March 1962.

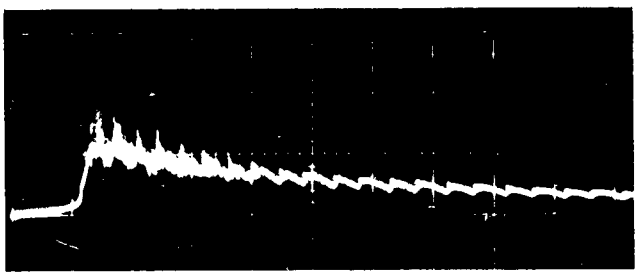

Sweep: 20 milliseconds/division

Sensitivity: 680 psi/division

Initial Pressure: 200 psia

Initial Mixture: 7.2% O_2, 11.8% H_2, 81% He

FIGURE 1. PRESSURE HISTORY OF CONSTANT VOLUME COMBUSTION IN THE THREE-INCH SHOCK TUBE DRIVER

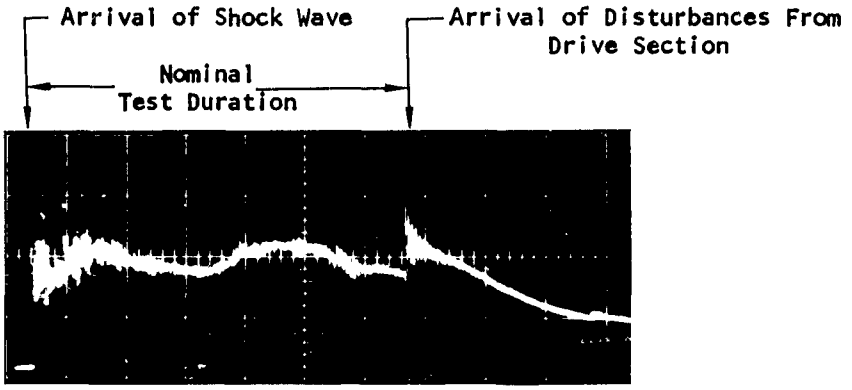

(a) Near Tailoring with Combustion Driver

Shock wave Mach number M_s = 10.4; Initial air pressure = 1.01 psia
Sweep: 1 millisecond/division
Sensitivity: 720 psi/division

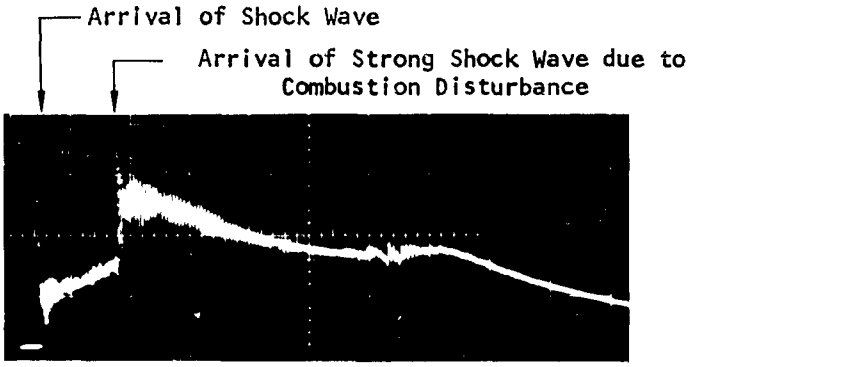

(b) Effect of Combustion Disturbance

Shock wave Mach number M_s = 8.9; Initial air pressure = 0.98 psi
Sweep: 1 millisecond/division
Sensitivity: 720 psi/division

FIGURE 2. PRESSURE RECORDS AT DOWNSTREAM END OF DRIVEN TUBE

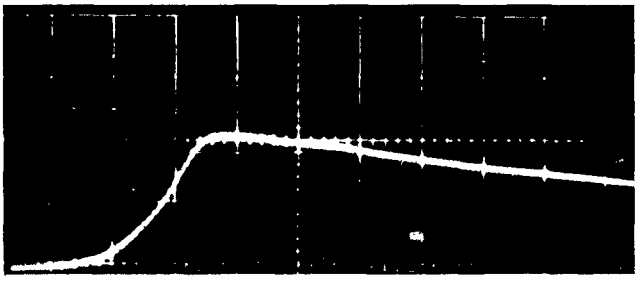

Initial Pressure: 630 psi
Initial Mixture: 5.1% O_2, 10.3% H_2, 84.6% He
Sweep: 200 milliseconds/division
Sensitivity: 1030 psi/division

FIGURE 3. PRESSURE HISTORY OF CONSTANT VOLUME COMBUSTION IN SIX-INCH-DIAMETER DRIVER

THEORETICAL PERFORMANCE OF CONSTANT VOLUME COMBUSTION
OF A MIXTURE OF HELIUM AND STOICHIOMETRIC OXYGEN AND HYDROGEN
(ASSUMING NO HEAT LOSS)

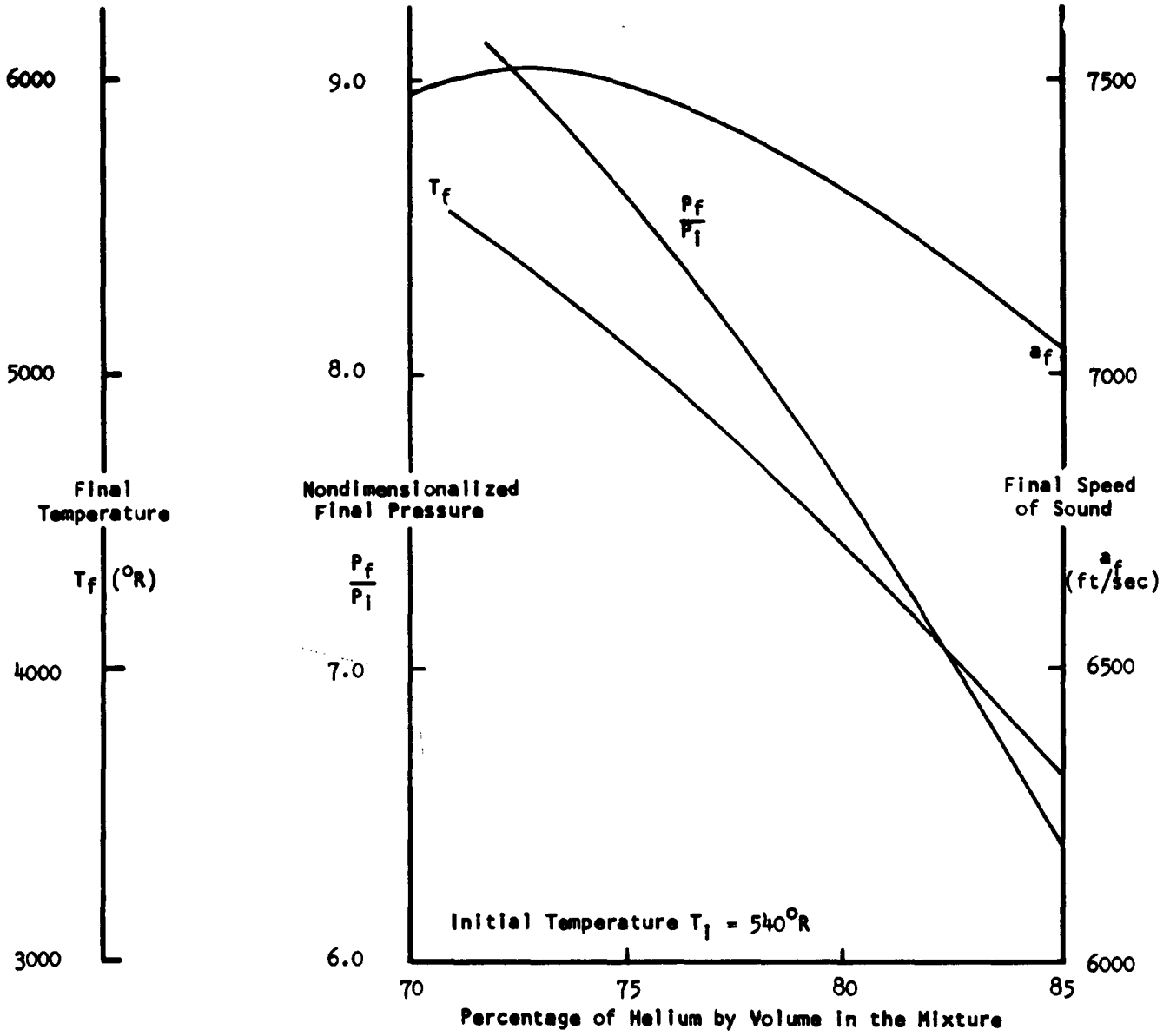

FIGURE 4

WAVE DIAGRAM OF SHOCK TUNNEL USING TAILORED INTERFACE TECHNIQUE

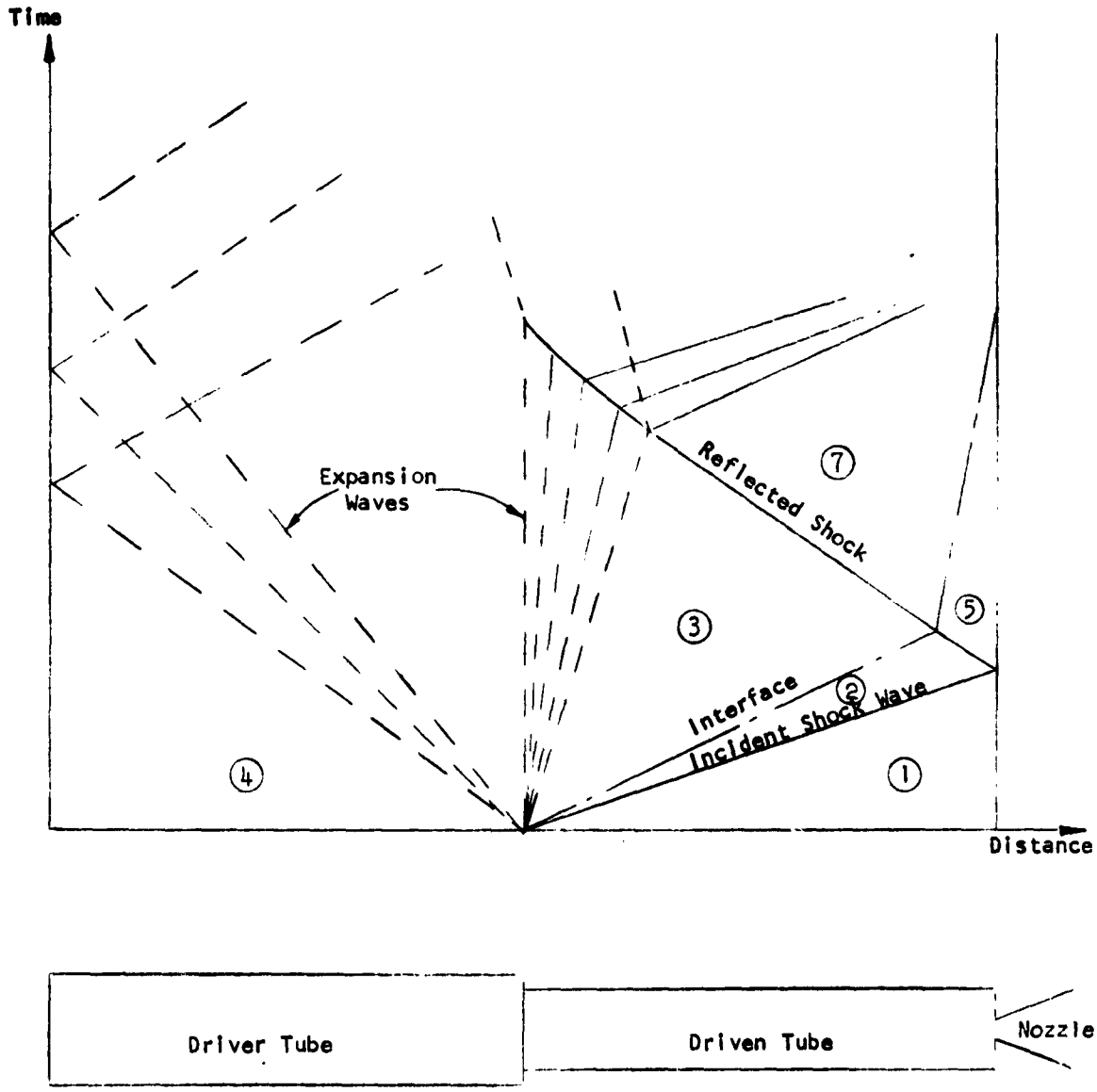

FIGURE 5

DEPENDENCE OF TEST SECTION MACH NUMBER
ON AIR RESERVOIR CONDITIONS

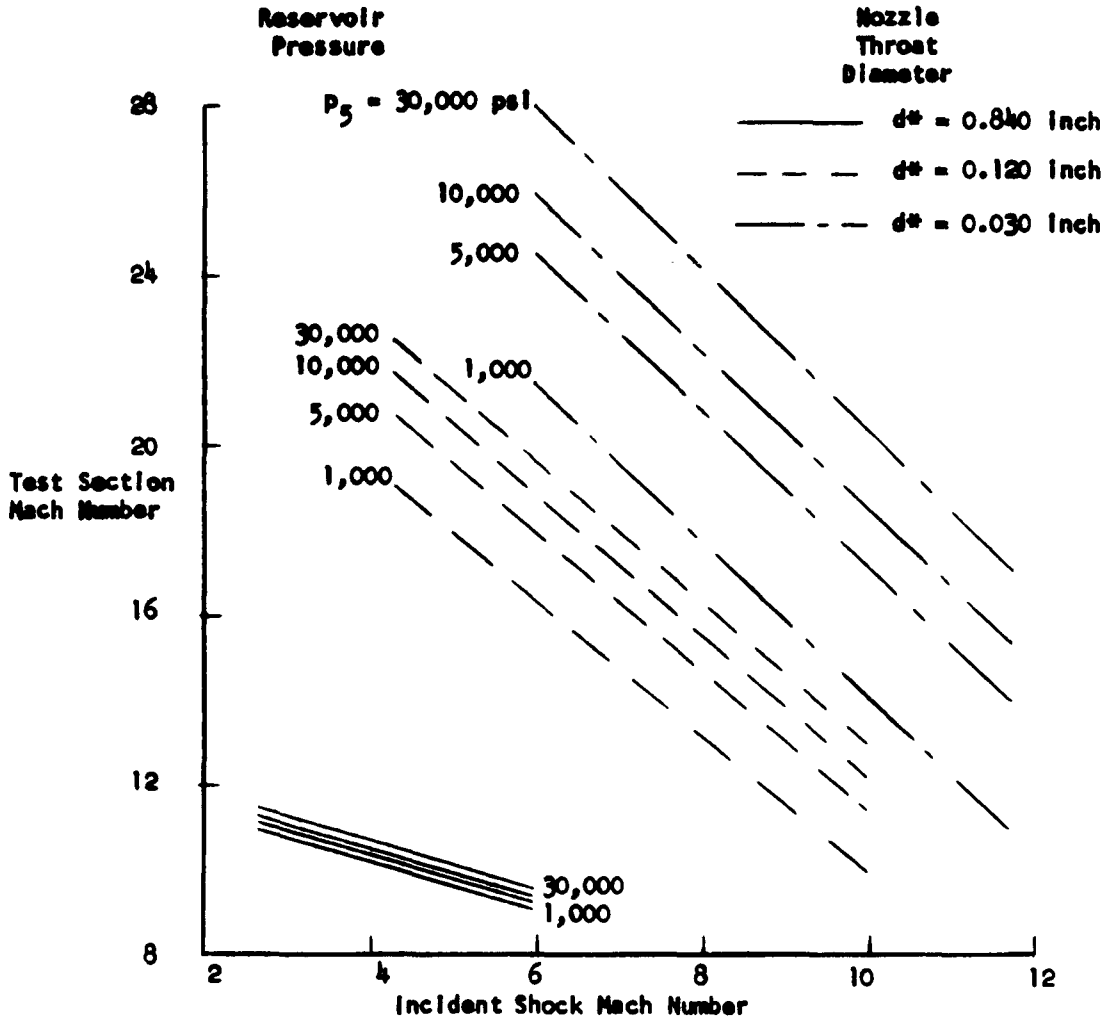

FIGURE 6

RADIUS OF INVISCID TEST AIR CORE IN
HYPERVELOCITY IMPULSE TUNNEL

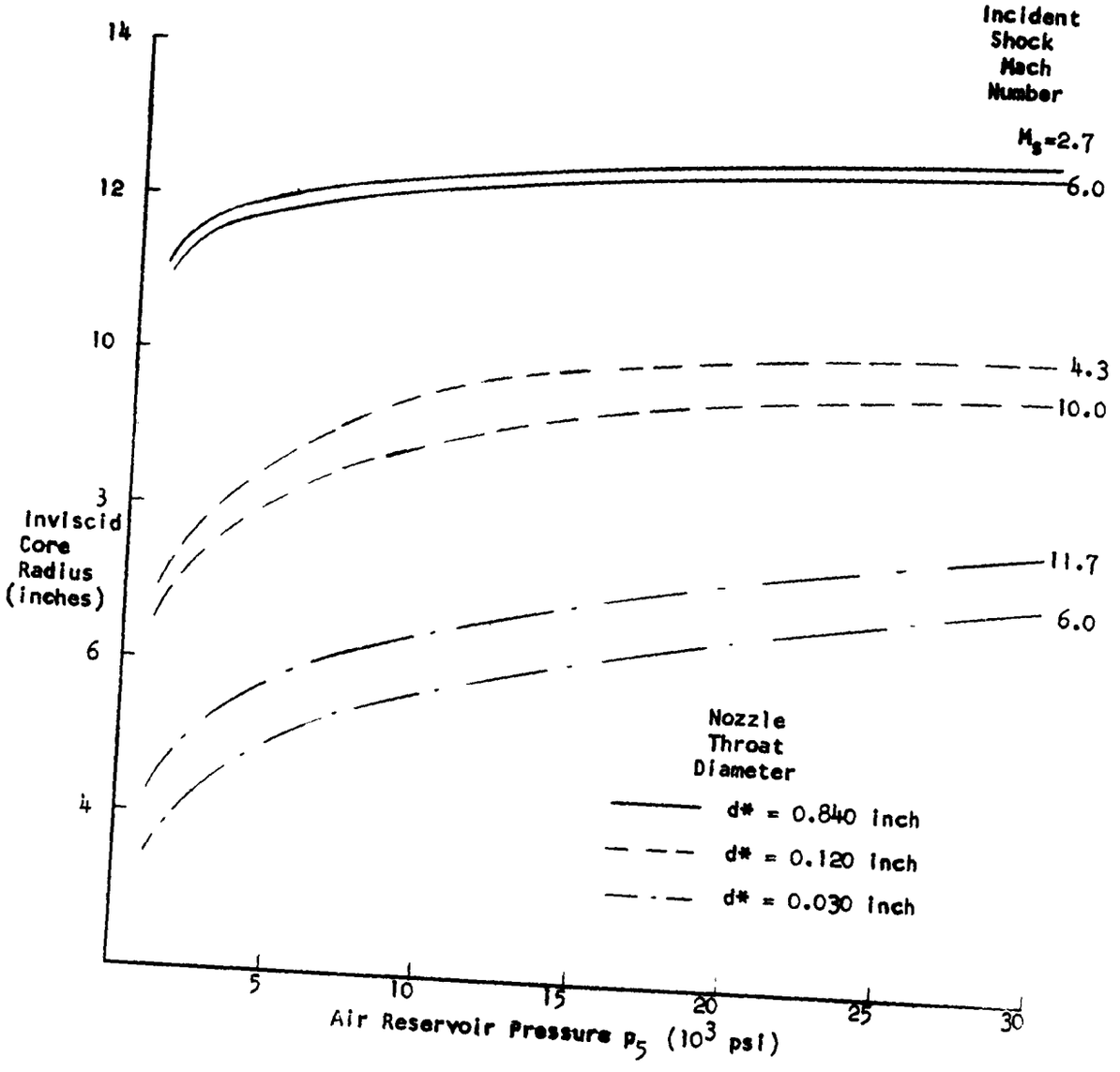

FIGURE 7

REYNOLDS NUMBER PER FOOT VS. TEST SECTION MACH NUMBER
IN THE HYPERVELOCITY IMPULSE TUNNEL

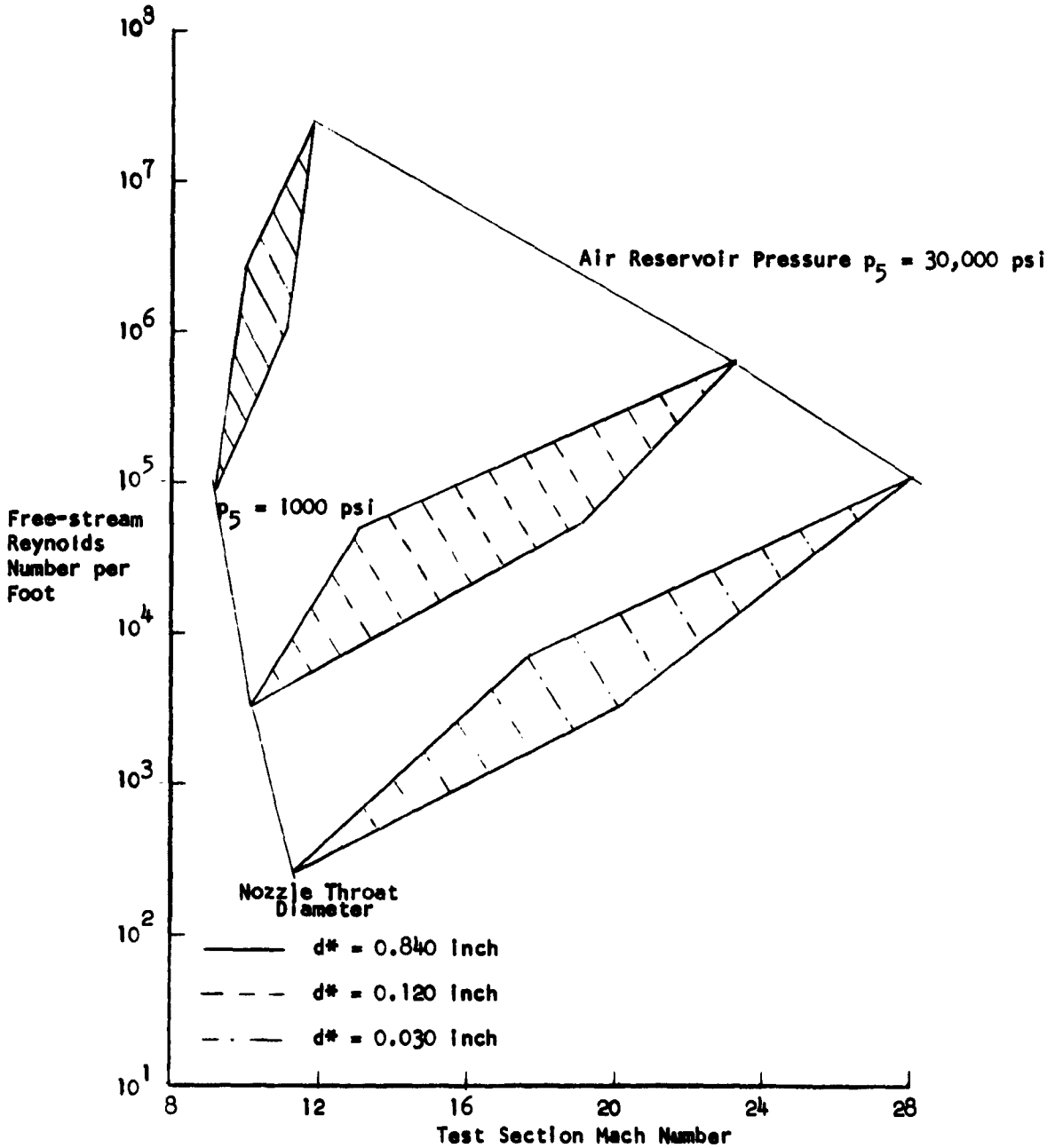

FIGURE 8

VARIATION OF PRESSURE BEHIND NORMAL SHOCK
WITH FREE STREAM STATIC PRESSURE

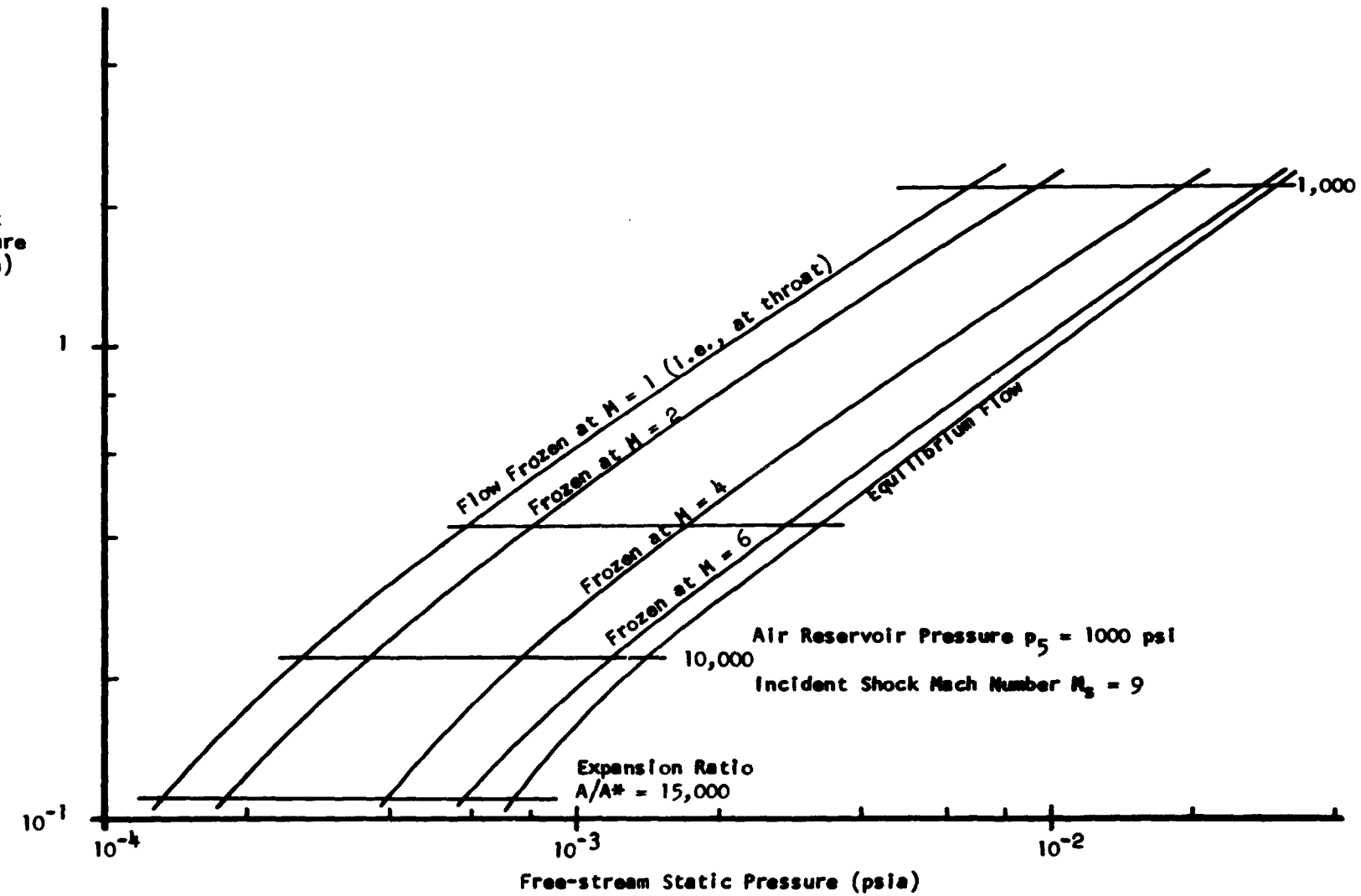

FIGURE 9

LEAD ZIRCONATE TITANATE (PZT) TRANSDUCER
(FROM REF 18)

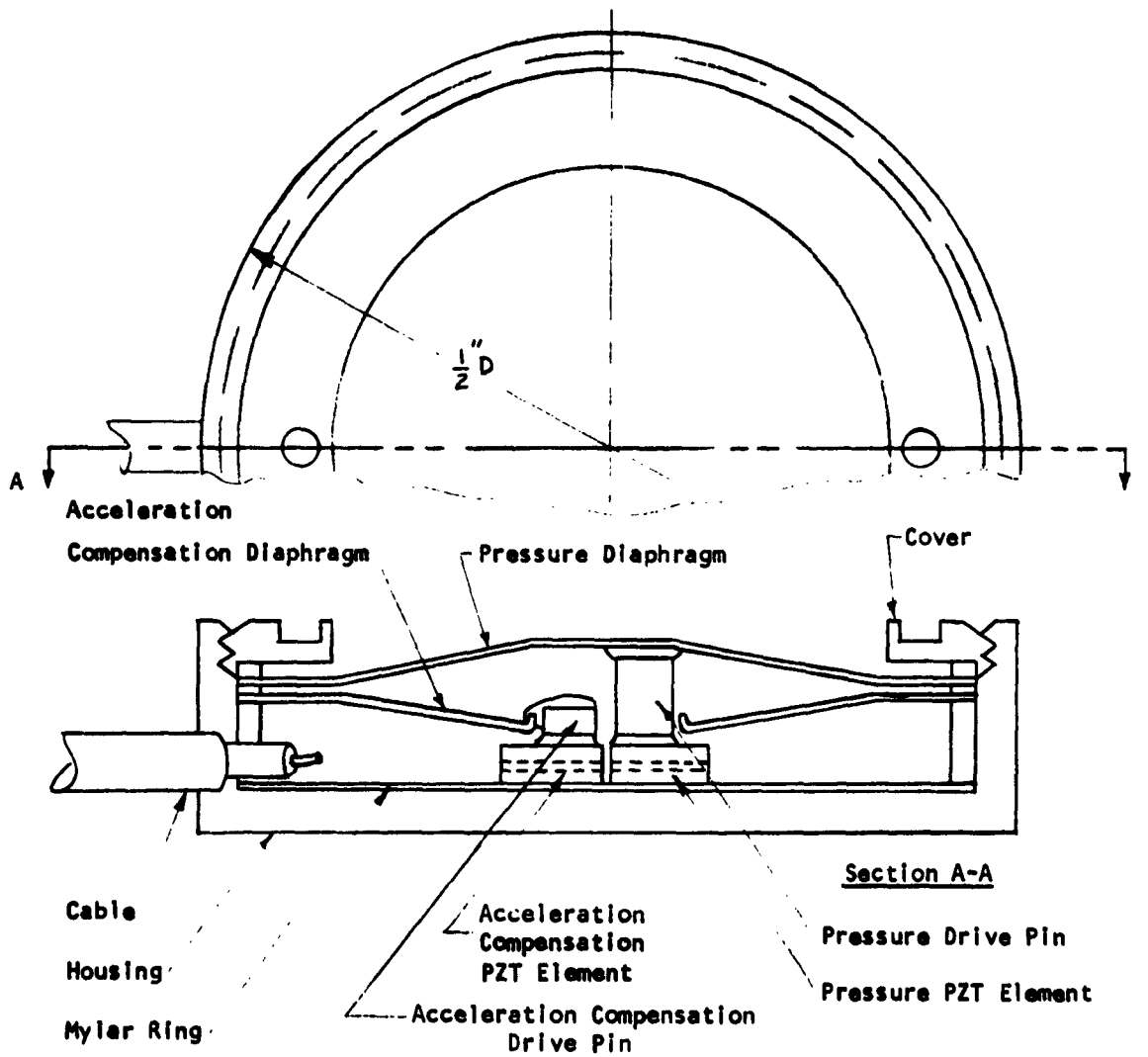

FIGURE 10

SHOCK TUBE EXPERIMENTAL RESULTS

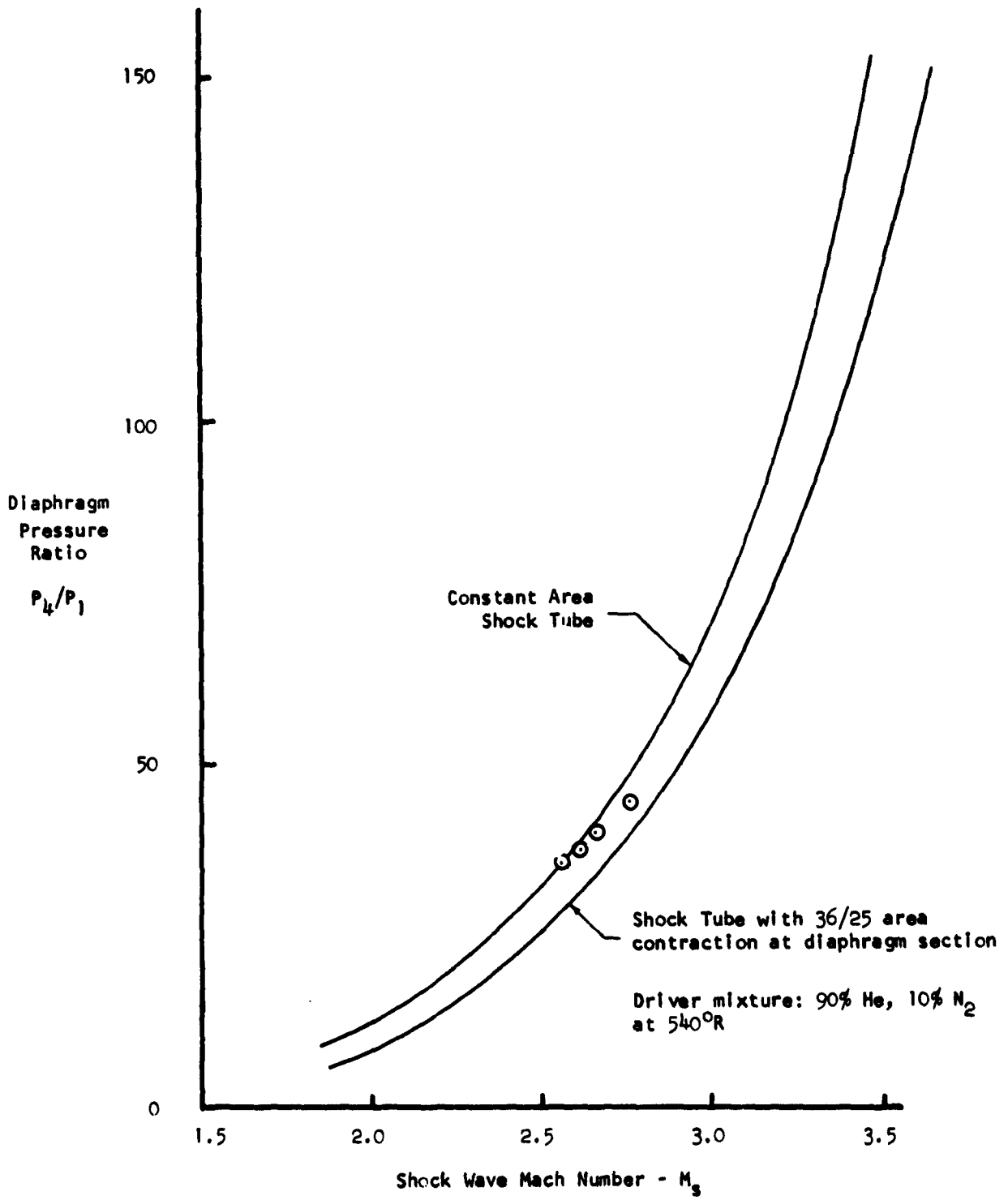

FIGURE 11

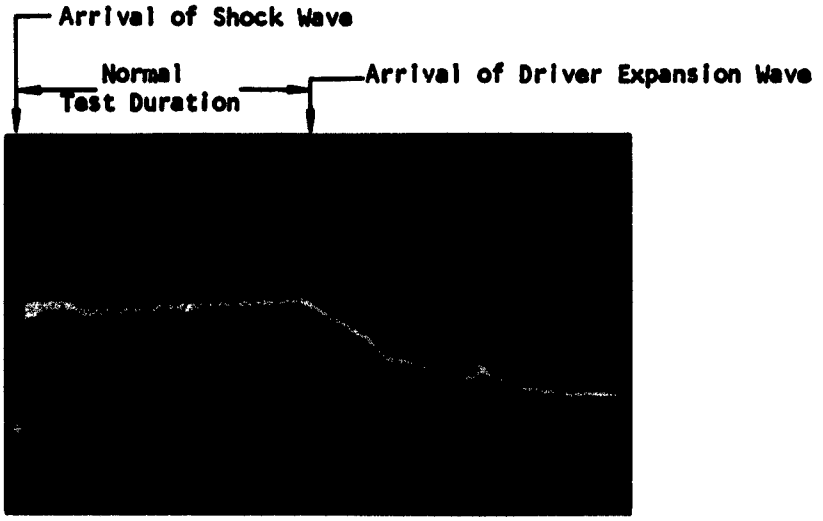

(a) Reservoir Pressure

Sweep: 5 milliseconds/division
Sensitivity: 420 psi/division
Shock Mach Number = 2.56

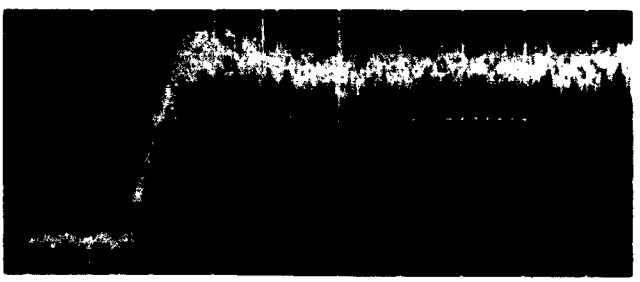

(b) Test Section Pitot Pressure

Sweep: 2 milliseconds/division
Sensitivity: 0.45 psi/division
Test Section Mach Number = 10.6

FIGURE 12. TYPICAL RESULTS OF HYPERVELOCITY IMPULSE TUNNEL CALIBRATION

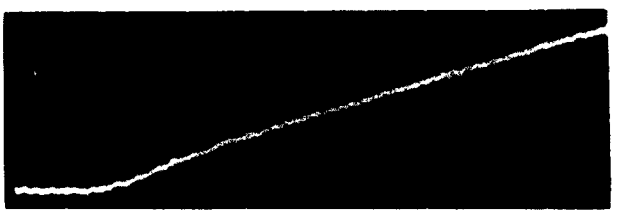

Shock wave Mach number $M_s = 2.76$
Pitot pressure $p_s = 2.22$ psi
Sensitivity: 200 μv/division

FIGURE 13. CALORIMETER RECORD OF THE TEST SECTION STAGNATION-POINT HEAT-TRANSFER RATE

Section 4
Hypervelocity Studies Using Light Gas Gun And Ballistic Range

W.B. Covey

January 1, 1963

Report Number SM-41379-4

Sales Order: 81280-187
Engineering Work Order: 51902
Job Work Order: 0002

SUMMARY

A two-stage light-gas gun and 100-foot ballistic range are in an early stage of development and operation at DAL. Principles of design and operation are reported in support of the proposed limits of performance, viz., 15,000 ft/sec from a single-stage gun of 1.5-inch bore and 30,000 ft/sec from a two-stage gun of 0.25-inch bore. Several types of initial experiments have been performed. For example, 50-gram models have been launched from the single-stage gun at velocities ranging up to 15,000 ft/sec. Instrumentation systems, with emphasis on telemetry, are in an early developmental stage. Encapsulated, microminiature, telemetry carrier oscillator circuits, 0.5-inch diameter by 1.1-inch long, have been built and transmit at frequencies to 80 megacycles. It is estimated that 3 to 7 channels of pressure or temperature information can be telemetered from a model by frequency modulation of a 110-megacycle carrier.

TABLE OF CONTENTS

LIST OF ILLUSTRATIONS

NOTATION

a_c	Speed of sound in the products of gun powder combustion in the pump tube
a_1	Initial speed of sound in the gas in the pump tube
a_5	Speed of sound of the gas acting initially on the model or piston in the first launch tube after establishment of the reflected shock wave in the pump tube
A	Cross-section area of the launch tube and frontal area of the projectile
C	Capacitance
C_D	Drag coefficient
J	Energy
L	Length of the launch tube
m	Mass of the projectile, model or piston
p_c	Pressure of the products of gun powder combustion in the pump tube
p_1	Initial pressure in the pump tube
p_2	Static pressure behind the incident shock wave in the pump tube
p_5	Pressure acting initially on the model or piston in the first launch tube after establishment of the reflected shock wave in the pump tube
p_B	Pressure on the model base
R	Resistance
t	Time, or time constant of spark
T_1	Temperature of the gas initially in the pump tube
T_5	Temperature of the gas acting initially on the model or piston in the first launch tube after establishment of the reflected shock wave in the pump tube
u_2	Gas velocity behind the incident shock wave in the pump tube
U	Projectile velocity
U_L	Muzzle velocity of the projectile
V	Voltage
x	Coordinate along the flight path
γ	Ratio of specific heats in the gas in the pump tube and behind the model or piston in the first launch tube
γ_c	Ratio of specific heats in the products of gun powder combustion in the pump tube
ρ	Ambient density

1. INTRODUCTION

The following quotation from reference 1 records the need for facilities to augment supersonic wind tunnels at higher Mach numbers: "The number of new aerodynamic and thermodynamic effects encountered in air flows at hypersonic speed which are not well understood theoretically has made it necessary to rely heavily on experiment in this speed range. Methods for making suitable experiments have themselves posed formidable problems. It has proved to be inherently difficult to establish, in wind tunnels, condensation-free air flows with speeds of the order of (or greater than) 10 times the speed of sound in the free stream. It is still more difficult to maintain in these flows, on even a short-duration basis, stagnation temperatures equal to those for flight at the test Mach number, as is necessary for simulating the characteristics of the air when molecular vibration, dissociation, ionization, and other physical and chemical reactions occur in the disturbed flow field. Furthermore, to maintain the Reynolds number in the range of interest for flight, it is necessary to make very large wind tunnels and to operate them at stagnation pressures measured in tens or hundreds of atmospheres. These difficulties, while counter-balanced by the convenience and utility of wind tunnel testing, are so formidable that they have led to a search for alternate methods of making hypersonic experiments."

One alternate method, the subject of this research and development program, is free-flight testing of laboratory-scale models which are flown at the full velocity of the missile. In this type of test, temperatures are approximated and aerodynamic heating of the model is representative of that experienced by the missile in hypervelocity flight. This type of facility, originally developed for measurement of drag and stability of artillery projectiles, is still referred to as the ballistic range.

The DAL Light-Gas Gun Ballistic Range is designed to fire a projectile at hypervelocity into a controlled atmosphere. The projectile is launched by the action of a light, compressed gas produced in a gun by combustion of rifle powder. Design limits are 15,000 ft/sec from a single-stage gun of 1.5-inch bore and 30,000 ft/sec from a two-stage gun of 0.25-inch final bore. The light gas gun and 100-foot range are currently in an early stage of development and operation.

During FY 1962, as part of a continuing IR&D study, several types of initial experiments have been performed and theoretical performance analyses and instrumentation system analyses have proceeded. The gas-dynamics and ballistics of the one- and two-stage guns have been analyzed for prediction of ultimate performance. Techniques for measuring drag coefficients and, ultimately, complete stability data from optical observations, have been worked out. Optical and timing systems have been checked by firing a 30-caliber rifle in the range tank. The ultimate utility of this facility will be realized when the required information can be telemetered from the model during flight. To this end, telemetry systems are being developed which are compatible with the model scale and with the dimensions of the range tank, and which can operate after accelerations approaching 10^6 g.

2. FACILITY

Figure 1 is a schematic representation of the DAL Light-Gas Gun Ballistic Range. The major components are the launcher, blast receiver, and test chamber.

The launcher is a light-gas gun that accelerates the model to the test velocity. It consists of a 3.5-inch-bore pump tube, 15 feet in length, capable of operating at peak pressures as high as 38,000 psi, and a launch tube, 1.5-inch smooth bore by 26.3 feet long, in which the model is accelerated. Typically, prepressurized helium is further compressed in the pump tube by burning a gun powder charge at the breech. The helium propels the model through the pre-evacuated launch tube to a velocity as high as 15,000 ft/sec. A second gun configuration is available by adding as a second stage a 0.25-inch smooth-bore barrel at the muzzle end of the 1.5-inch launch tube. In this arrangement, the piston driven through the 1.5-inch tube compresses helium or hydrogen which then propels the 0.25-inch model through the second stage. The 1.5-inch piston deforms and flows plastically into a convergent section at the downstream end of its tube while the model is traversing its tube; this alleviates inertial loading of the model with no sacrifice in muzzle velocity. The two-stage gun is capable of launching small particles at velocities in excess of 20,000 ft/sec, perhaps at 30,000 ft/sec.

After leaving the gun muzzle, the model or particle enters the pre-evacuated blast receiver, an 800-cubic-foot tank containing seven baffle plates. The model flies through holes provided in the baffle plates, while the sabot or its fragments, being aerodynamically unstable, leave the flight path and impact on the baffles. The blast from the gun is attenuated also by these plates by expansion of the helium propellant and of the gaseous products of gun powder combustion into the voids between baffles, and thus out of the flight path.

After leaving the blast receiver, the model passes through a quick-operating valve. This valve is closed prior to model launch initiation and opens in sychronism with the model motion. The purpose of this device is to separate the atmospheres in the two tanks, blast and range, which frequently have a pressure differential. The valve closes quickly behind the model about 0.1 second after opening.

The range tank, currently 100 feet long by 10 feet in diameter, is the test chamber. It contains the instrumentation necessary for observation of model parameters during free flight. At the end of the range, the test model is stopped by the model catcher, a thick-walled container filled with fire-resistant cotton waste.

3. THEORETICAL PERFORMANCE OF THE LIGHT-GAS GUN

A test in the ballistic range begins with launching the model. Therefore prime consideration must be given to the accelerating device. If the flights are to be made at hypervelocities, one cannot employ a conventional military cannon or conventional ordnance technology. The muzzle velocity of a gun powered by combustion of nitrocellulose gun powder is limited theoretically to 10,000 ft/sec if fired into the atmosphere, or to 28,000 ft/sec if fired into a vacuum.

These are ideal performances based upon assumptions of infinite pressure, infinite length and a frictionless, adiabatic barrel wall, and are not actually obtainable in practice. Maximum performance of the best nitrocellulose gun with an evacuated barrel is limited in practice to about 10,000 ft/sec.

The requirements for the DAL Ballistic Range are velocities in excess of 10,000 ft/sec for aerodynamic studies and greater than 20,000 ft/sec for impact testing. Consequently, the design goals are, respectively, 15,000 and 30,000 ft/sec.

The principal limitation on performance of conventional guns is due to the high molecular weight of the propellant gases. The products of combustion of gun powder, which drive the projectile out of the barrel, have a molecular weight of 24 to 28. Therefore, a relatively large proportion of the available energy must go into the acceleration of the propellant gases. To overcome this limitation, one employs the light-gas gun, wherein a low-molecular-weight gas such as helium or hydrogen is substituted as the propellant gas. Less energy is absorbed by accelerating the gas and correspondingly more energy is imparted to the model or projectile.

In the study that was undertaken to design the DAL light-gas gun and to evaluate its optimum performance, numerous reports of similar facilities have been reviewed. References 1 to 4 are important reports of different types of light gas guns.

3.1 Pump Tube

The pump tube is 3.5 inches inside diameter, 15 feet long, with a bag of gun powder filling 12 inches at the breech end, and is designed for operating pressures up to 38,000 psi. The tube is prepressurized to p_1 with helium at room temperature. Combustion of the gun powder compresses the helium in a manner not unlike the action in a common shock tube. In fact, assumptions by which to analyze this compression process are evolved to capitalize on the similarities.

It is assumed that, instantaneously after ignition of the gun powder, a large volume of the hot, pressurized, heavy products of combustion begin to work on the helium, and that the combustion proceeds steadily in such

a way that these driving conditions remain constant during helium compression. This is equivalent to assuming that the helium is suddenly exposed to an effectively infinitely large chamber filled with the products of combustion at the stipulated conditions, an assumption validated by experience with other light-gas guns of similar configurations. The instantaneous ignition and sudden establishment of driver conditions generates a shock wave, called the incident shock wave, which compresses the helium and accelerates it toward the model (or piston). This shock-processed helium is brought to rest momentarily at the downstream end of the pump tube as the shock wave is reflected upstream by the initially stationary model. The stagnant, twice-shocked helium acts instantaneously on the model and launches it. The state of the compressed helium gradually relaxes from this initial condition as the model shears from its flange and accelerates through the launch tube.

It is a simple matter to calculate this initial condition of the stagnant, compressed helium, which characterizes the performance of the pump tube, by applying perfect gas relations to the combustion products and to the helium. These relations are given, for example, in reference 5, and are well verified in practice (see reference 6, for example). Subscripts 1, 2, and 5 identify the helium in its initial state after passage of the reflected shock wave; subscript c identifies the products of combustion of the powder charge.

Since helium is a perfect gas (for example, its ratio of specific heats γ is a constant, 5/3) in the range of interest, its constant velocity u_2 behind the incident shock wave is

$$u_2 = a_1 \left(\frac{p_2}{p_1} - 1\right)\left(\frac{1}{2\gamma}\left[(\gamma+1)\frac{p_2}{p_1} + \gamma - 1\right]\right)^{-1/2}$$

where a_1 is the initial speed of sound in the helium. It is convenient, then, to specify a pressure ratio p_2/p_1 across the incident shock wave in order to calculate the desired conditions. The cross-sectional area of the driver section of the equivalent shock tube has been assumed to be so large relative to the area of the pump tube that the velocity of the combustion products traversing the hypothetical driver section is negligible compared to the local speed of sound a_c. Furthermore, in the range of interest, the driver pressure p_c is sufficiently great relative to the initial helium pressure p_1 that the flow of combustion products into the helium zone is choked, i.e., proceeds from sonic speed through a nonsteady expansion to supersonic speed. Under these conditions, the pressure at which the combustion products are supplied is

$$p_c = p_2\left[\frac{\gamma_c + 1}{2} - \frac{(\gamma_c - 1)}{2}\frac{u_2}{a_c}\right]^{-2\gamma_c/(\gamma_c - 1)}$$

The pressure and temperature of the helium acting initially on the model, behind the reflected shock wave, are

$$p_5 = p_2 \left[\frac{(3\gamma - 1)\, p_2 - (\gamma - 1) p_1}{(\gamma - 1)\, p_2 + (\gamma + 1)\, p_1} \right]$$

and

$$T_5 = T_1 \left[\frac{(3\gamma - 1)\, p_2 - (\gamma - 1) p_1}{(\gamma + 1)\, p_2 + (\gamma - 1)\, p_1} \right] \left[\frac{(\gamma - 1)\, p_2 + p_1}{\gamma\, p_1} \right]$$

The properties of the products of combustion are assumed to be those of a gas produced by a typical nitrocellulose powder, namely a ratio of specific heats γ_c of 5/4 and a speed of sound a_c of 3800 ft/sec (reference 6). If the helium is initially at 80°F, its speed of sound a_1 is 3340 ft/sec. The foregoing relations become

$$u_2 = 4480 \left(\frac{p_2}{p_1} - 1\right) \left(4 \frac{p_2}{p_1} + 1\right)^{-1/2} \quad \text{(ft/sec)}$$

$$p_c = p_2 \left(1.061 - \frac{u_2}{30,400}\right)^{-10}$$

$$p_5 = p_2 \left(\frac{6\, p_2 - p_1}{p_2 + 4\, p_1}\right)$$

$$T_5 = 540 \left(\frac{6\, p_2 - p_1}{4\, p_2 + p_1}\right) \left(\frac{2\, p_2 + 3\, p_1}{5\, p_1}\right) \quad (^\circ R)$$

The unbroken curves in figure 2 show the pressure p_5 and temperature T_5, in terms of initial values, which can be expected to act on the model at the start of its run as functions of the ratio of combustion pressure p_c to initial pressure p_1, within the framework of assumptions. The condition that the flow of combustion products into the helium zone be choked is fulfilled when the helium velocity behind the incident shock wave u_2 is greater than, or equal to, $a_c \sqrt{2/(\gamma_c + 1)}$ or 3590 ft/sec in this case, i.e., when p_c/p_1 is greater than 7.

To evaluate the interpretation of the burning powder as providing a reservoir of effectively infinite cross section, a similar analysis can be made of the case when the combustion pressure acts on the helium like a shock-tube driver with no area change at the diaphragm. The foregoing equation for p_c is then replaced by

$$p_c = p_2 \left[1 - \frac{(\gamma_c - 1)}{2} \frac{u_2}{a_c} \right]^{-2\gamma_c/(\gamma_c - 1)}$$

The broken curves in figure 2 show the corresponding solutions of this more pessimistic case.

Figure 3 is a restatement of figure 2 for the special case of p_c = 38,000 psi, the safe operating limit of the present pump tube. It is planned to assess the performance of the pump tube by correlating measurements of p_c, p_5, and T_5 with the foregoing analysis.

3.2 Single-Stage Launch Tube

The first-stage launch tube is 1.5 inches inside diameter and 26.3 feet long. The velocity of a projectile (model or piston) in the pre-evacuated tube depends on its mass, the tube dimensions, and the condition (state number 5) of the stagnant, shock-processed helium prior to release of the projectile. Acceptable common practice is to calculate the muzzle velocity U_L, within the framework of assumptions discussed in reference 2, by the following relation:

$$\frac{p_5 A L}{m a_5^2} = \frac{2}{\gamma-1}\left[\frac{\frac{2}{\gamma+1} - \left(1 - \frac{\gamma-1}{2}\frac{U_L}{a_5}\right)}{\left(1 - \frac{\gamma-1}{2}\frac{U_L}{a_5}\right)^{(\gamma+1)/(\gamma-1)}} + \frac{\gamma-1}{\gamma+1}\right]$$

where A is the cross-section area of the launch tube, L is its length, and m is the mass of the projectile. The pressure, temperature, and sound speed in region 5 are related to p_c/p_1 as described in section 3.1.

In the present case, A = 0.01227 ft^2, L = 26.3 ft, and γ = 5/3. The above relation can be written as

$$2.26 \times 10^5 \frac{p_5}{m a_5^2} = \frac{\frac{U_L}{3 a_5} - \frac{1}{4}}{\left(1 - \frac{U_L}{3 a_5}\right)^4} + \frac{1}{4}$$

where p_5 is in psia, m is in grams, and a_5 and U_L are in ft/sec. The relation has been solved for the muzzle velocity U_L for the case of effectively infinite chamberage, p_c = 38,000 psia, $10{,}000 \leq p_5 \leq 40{,}000$ psia, and $20 < m < 100$ grams, and for the conditions stated in figures 2 and 3. The performance of the launch tube is shown in figure 4. In this case, it is unnecessary to consider higher initial pressures p_1 than that producing the optimum pressure p_5 which generates the maximum launch velocity.

3.3 Two-Stage Launch Tube

The launch tube for two-stage operation is 0.25 inch inside diameter and 50 inches long. As discussed in section 2, a deformable piston compresses a light gas in the first stage launch tube which terminates in a convergent section. This arrangement, analyzed in reference 7, tends to provide a constant pressure at the base of the model during

its run in the launch tube. That analysis gives the muzzle velocity of the model as

$$U_L = \sqrt{\frac{2 A L p_B}{m}}$$

where p_B is the model base pressure. The remaining symbols have been defined in section 3.2. The resulting performance is shown in figure 5 for $10^4 < p_B < 6 \times 10^4$ psia and $0.10 < m < 0.60$ grams.

3.4 Drag Measurement

Drag data can be derived from measurements at three stations, following a procedure given in reference 8. The average velocity in the two successive intervals decreases and the rate of decrease is a measure of drag. Although the flight path may be slightly misaligned with the range axis and the model may oscillate somewhat in pitch, the angles of misalignment and of pitch and yaw can be considered small, in general. The components of lift and side force along the range axis, then, remain negligible and the drag of the model is essentially the drag component along the range axis, the product of its mass and the component of acceleration along that axis, viz.,

$$\frac{C_D \rho U^2 A}{2} = - m \frac{dU}{dt} = - m \frac{d^2 x}{dt^2}$$

To assume that the drag coefficient C_D is constant over the interval observed is consistent with the previous assumptions. The above expression can then be integrated once over the interval between any two stations to obtain

$$\frac{C_D \rho A (t_{i+1} - t_i)}{2 m} = \frac{1}{U_{i+1}} - \frac{1}{U_i}$$

or twice over the same interval to obtain

$$\frac{C_D \rho A (x_{i+1} - x_i)}{2 m} = \ln \left[1 + \frac{C_D \rho A U_i (t_{i+1} - t_i)}{2 m} \right]$$

If three successive stations are equidistant, the drag coefficient is found from the foregoing relations to be expressible entirely in terms of observables as

$$C_D = \frac{2 m}{\rho A (x_{i+1} - x_i)} \ln \left(\frac{t_{i+2} - t_{i+1}}{t_{i+1} - t_i} \right)$$

Likewise, the velocities at these stations are found in terms of observables and the previous velocity as

$$U_1 = \frac{2m}{C_D \rho A (t_{i+1} - t_i)} \left(\frac{t_{i+2} - t_{i+1}}{t_{i+1} - t_i} - 1\right)$$

$$U_{i+1} = U_1 \left(\frac{t_{i+1} - t_i}{t_{i+2} - t_{i+1}}\right)$$

$$U_{i+2} = \frac{1}{\frac{C_D \rho A (t_{i+2} - t_{i+1})}{2m} + \frac{1}{U_{i+1}}}$$

Thus the drag force can be obtained at each station.

4. OPERATION OF THE LIGHT-GAS GUN

The first combustion tests in the light-gas gun have been performed in the sealed pump tube. Several launches from the single-stage configuration have been accomplished during the final month of the report period.

4.1 Closed-Bomb Tests

Closed-bomb tests have been conducted to establish empirical relationships between powder charge, initial helium pressure, and subsequent peak helium pressure. A heavy plug, similar to the breech plug, has been fabricated to seal the downstream end of the pump tube. A measured charge of gun powder is placed in the tube which is then evacuated and pressurized with a designated amount of helium. After electrical ignition of the gun powder, a pressure history at each end is measured by means of a piezoelectric gage and recorded on an oscilloscope. A plot of peak pressure versus rifle powder weight in closed-bomb tests is shown in figure 6 by the open symbols. The pressure is measured at the center of the plug at the muzzle end.

Initially it was thought that the powder must be ignited at many points simultaneously in order to obtain even combustion. The IMR-4895 or 4198 powder was packaged in a cylindrical-shaped cloth bag with a high velocity fuse, Pyrocore, at the axis of the charge. Since the fuse burns at a very rapid rate, it was presumed that the powder would be ignited at all points along the axis simultaneously. However, in practice, the powder did not ignite at all. The shock associated with the violent burning of the fuse broke open the bag and scattered the powder. Since the powder is relatively slow-burning and slow-starting, it would not respond to the rapid flame front associated with the Pyrocore fuse.

The device at present being used to initiate combustion is a DuPont S-67 electric match. This is a relatively slow-starting and long-burning fuse similar in burning to a household match head. The electric match proved to be very reliable in igniting slow-burning powders; however, the power supply fuse failed during some of the firings.

An investigation revealed that, when fired alone, the match caused a current drain of less than 0.5 amp, but when associated with a powder charge the 10-amp fuse occasionally burned out. It was reasoned that the violence of the powder combustion would cause the connecting wires to become shorted, thus increasing the current drain.

In order to alleviate this problem, it was decided to energize the match by means of a capacitor discharge instead of directly from the power supply. Tests indicated that a 48-microfarad capacitor charged to 28 volts supplies sufficient energy to ignite the match and subsequently the powder reliably.

At first, it was awkward to place the powder into the gun breech properly. The nonrigid powder bag tended to be pinched between the breech block and the pump tube in the vicinity of the O-ring (see figure 7). The alternative of containing the charge within a rigid shell casing is unacceptable because of the difficulty in connecting the firing wires between the casing and the breech. Several powder bag supports were tried with the following general results:

1. supports not connected to the breech were accelerated to the opposite end of the pump tube and were damaged;
2. supports that had large areas of flat material were destroyed, even though connected to the breech.

One satisfactory device, shown in figure 7, consists of a steel drill rod threaded into the breech. The powder bag is given rigid support by being tied to this rod and is inserted easily into the gun.

4.2 Single-Stage Launches

These tests have been conducted for the purpose of light-gas gun calibration and development of launch techniques. Simple cylindrical models, fabricated from lexan plastic, have been launched. All the model weights range from 45 to 56 grams.

Two types of model release have been used (see figure 8). One method is to machine a tapered flange on the base of the model. This flange, whose outer diameter is approximately 3/8 inch larger than the launch tube bore, is installed in the tapered muzzle of the pump tube. The

initial helium charge in the pump tube is sealed from the launch tube by the fit of this flange into the taper. The peak helium pressure is sufficient to compress and deform the lexan so that the flare is extruded into the launch tube bore, thus launching the model. The second type of model release is based on an oversized model outer diameter. Friction because of the tight fit in the launch tube is sufficient to resist movement when subjected to the initial helium charge pressure. The peak helium pressure overcomes this friction to launch the model.

The first method, flared-base models, has the advantage of prohibiting premature launches; however, there are two problems associated with this configuration. First, this type usually launches prematurely. Further development will include strengthening the flare to resist movement until higher pressure develops. The second problem occurs when part of the base shears and part deflects, creating a situation where deformation of the body probably would cause unsatisfactory sabot separation.

The main problem noted with the drive-fit method of model release is premature release. In one case a model whose diameter exceeded the launch tube bore by 0.020 inch was driven out by a prepressure differential of only 95 psi. In order to effect a satisfactory launch, the model or sabot must resist 320 pounds for a prepressure of 180 psi. Planned prepressures, approaching 1000 psi, require an extremely tight sabot in order to resist 1770 pounds. Under these circumstances, it may be impossible to install the sabot without damage.

Other methods under development but not yet practiced are release of the model by shear from a clamped flange, by means of a break valve, and by means of a frangible diaphragm. Results of these first shakedown firings are varied and the data are scattered. Peak pressures, measured at the pump tube wall 18 inches upstream of the initial model position, are shown in figure 6. All of the launches were performed with 180 psi initial (precompression) helium pressure. Premature model release is indicated by the extent to which peak closed-bomb pressures exceed peak launch pressures. Figure 9 is a plot of model velocity in the range tank about 20 feet from the muzzle. Model weight is neglected since all models were within 10% of 50 grams. No trend can be noted from the plot; however, one area of repeatability exists at a powder weight of 1.2 kilograms, where three launches resulted in approximately 10,000 feet per second.

The probable causes of scatter in these data are:

1. Inconsistent model-release techniques causing variation in peak pressure.
2. Contamination of helium due to incomplete purge of air prior to filling.

3. Variation of powder type (two types used were IMR 4895 and IMR 4198).
4. Variation in blast receiver pressure.
5. Instability resulting in tumbling and increased drag in some models.

Further studies are aimed at improving repeatability, increasing velocity, and improving sabot separation. The variables listed above will be better controlled by the use of identical models and improved techniques. By improving the model-release methods, higher peak pressures and increased model accelerations will be obtained. A study will be initiated using larger powder charges and faster burning types in an attempt to reach the maximum pump-tube operating pressure of 38,000 psi. Higher initial helium charge pressures will be evaluated with the goal of improving energy transfer to the model. In the one sabot shot made in the initial group of launches, the sabot separated by only a few inches and impacted along with the model on the target. Lack of success was due probably to the blast receiver pressure being too low for proper separation. Studies are being initiated to optimize blast receiver pressure and develop equipment to slow and stop the sabot parts.

5. INSTRUMENTATION

Because of the nature of the ballistic range operation, the problem of obtaining useful data is very different from that encountered in a wind tunnel or a shock tunnel. Not only are the phenomena transient, but the data must be gathered from a small body in hypervelocity free flight. Further problems are introduced by conducting the test at nonambient pressure or even in a toxic atmosphere. Frequently, the model is accompanied by flame, smoke, and foreign matter resulting from the launch cycle.

5.1 Optics for Model Detection and Observation

A primary function of instrumentation in dynamic tests is to observe and record the motions of the model during flight. Ideally, such instrumentation should show the position and attitude of the model continuously during the flight through the range tank. From measurements in the six degrees of freedom and from knowledge of the model center of gravity and moments of inertia, the aerodynamic stability can be determined.

For lack of a method of accomplishing the ideal system, a compromise system has been developed. This is a shadowgraph system which observes the location of the model in three space coordinates (and possibly observes the attitude of unsymmetrical models under certain conditions) at measured times in the vicinity of fixed stations along the flight path. As the model passes a given point its position and the time are

recorded. If enough of these position-time recordings are made during the flight a plot of flight path can be made. In ballistic range practice, at least five stations are required to generate data on natural frequencies of oscillation.

The initial system capability consists of three optically instrumented stations. Three-station operation does not permit determination of stability and control characteristics, but does allow two velocity measurements from which the drag coefficient can be calculated (see section 3.4). Each of the instrumentation stations must have the ability to produce a shadowgraph image of the model somewhere in the field of view. The image must be of sufficient quality to be located relative to the image of the fiduciary system. The concept of this shadowgraph system is based on the capability to photograph an object travelling many thousands of feet per second. There are two basic methods which can be used to stop high-speed action photographically. One is to use a steady light source and to activate a fast shutter. The other is to activate a short-duration light source. In either case, the light intensity must increase as the exposure time decreases in order to obtain satisfactory film contrast. If a blur of 0.010 inch on the film is acceptable, the corresponding model motion is 0.033 inch during the exposure, because the image is reduced to three-tenths in the present system. If the model speed is 25,000 ft/sec, its illumination must be limited to 10^{-7} second. Since it is difficult to operate a mechanical camera shutter faster than 10^{-3} second, it appears that ballistic range requirements can be fulfilled only by a spark-discharge light source. In general, a spark source with no shutter is adequate for an exposure time on the order of 10^{-7} second. For still shorter exposures, an electronic shutter must be added to the optical train. In the latter case, a spark-light source would still be dictated by the light-intensity requirements. A spark source without a shutter has been selected for the present system; see section 5.2.

The shadowgraph system is a folded, single-pass system centered in the vertical transverse plane; see figure 10. The spark light source, discussed above and in section 5.2, is the only element not inside the range tank. The 12-inch-diameter primary mirrors, spherical mirrors which provide parallel light through the test corridor, have a 96-inch focal length. The choice of polaroid 4- by 5-inch cut film limits the usable diameter of the image at the film plane to 3.62 inches. The magnification of the system is therefore designed to be 0.30. A standard spectacle lens of 666 mm focal length is used as the focussing lens. At present, six shadowgraph systems are operative, providing vertical and horizontal observation at three stations.

The spark light source at each station is triggered by a signal from a separate optical system, illustrated in figure 11. Each model-detection module consists of a continuous lamp, a cylindrical mirror, a photocell, and auxiliary lenses. A thin light screen is produced from the long, thin filament of the lamp by an appropriate lens and aperture. The image of this source is at, or near, the center of curvature of the

mirror, a section of a circular cylinder. The light thus traverses the expected flight path twice and is focussed (in one dimension) at the photosensitive detector. A lens associated with the photocell focuses an image of the model on the anode. The coplanar configuration shown in figure 11 is chosen over the coaxial configuration because it produces a greater light change at the photocell for a given model size. By this system, a nonluminous model is detected by the decrease in background illumination. When the model is moving at conditions which cause self-luminosity, the same system, with lamp off, can detect its passage.

5.2 Electronics for Model Detection and Observation

The electronic system for model observation is required to flash two high-intensity short-duration light pulses at each station upon detection of a small change in nearby light level. A block diagram of one channel of this system appears in figure 12. Arrival of the model in the shadowgraph field of view is detected by the photocell as a small change in light level; see section 5.1. The photocell responds by producing a current of a few microamperes. Immediately adjacent to the photocell is a small solid-state amplifier which boosts the pulse power to a level that can be transmitted successfully through a cable. The preamplifier and photocell circuits are shown in figure 13.

The pulse amplifier, located in the control room, receives this pulse, amplifies it to the 20-volt level, and applies it to the control grid of a thyratron. A block diameter of the pulse amplifier is shown in figure 14. Conduction of this high-power tube produces the 200-volt spike that is necessary to trigger the spark light sources. In order to have the capability of firing the spark from either a positive or negative change in light level, a phase reversal circuit is included in the pulse amplifier.

Since this equipment must be very sensitive to the photocell signal, it is also sensitive to stray electromagnetic disturbances (noise). To prevent inadvertent triggering of the system, a blanking circuit is incorporated in the pulse amplifier. This circuit prohibits thyratron conduction except during a 200-millisecond period. This unblank period is initiated, as the model enters the range tank, by a signal from a timer which is started by the firing switch.

The primary requirements of a light source for model imagery are high intensity and short duration. This goal is achieved by utilizing the light produced by discharging the electrical energy, stored in a capacitor, across an atmospheric air gap between two electrodes. Until required, the discharge is prevented by the interelectrode separation. When discharge is desired, ions are injected into the gap,

reducing the gap resistance and effecting energy discharge. The duration of the spark light source is typified by its time constant $t = RC$, and the light intensity depends on its energy $J = CV^2/2$. In order to produce a short-duration, high-energy light, the capacitance C and resistance R must be low and the voltage V high. In the present spark light source, the capacitance is variable from 0.01 to 0.12 microfarad and the voltage is fixed at 10^4 volts. The resistance is made very low by the judicious arrangement of the components, see figures 15 and 16.

Tests have been made of the duration of the spark light source by observing the light output with a photocell and oscilloscope. With the 0.12 microfarad capacitor installed, i.e., with 6 joules of available energy, the duration of the light was measured to be 2×10^{-7} seconds. If this duration is equated to the time constant, 30 megawatts of power are produced and the average current is 3000 amperes. These estimates serve to illustrate the reason for the high intensity light output.

Discharge of the spark source is accomplished when the 200-volt pulse from the pulse amplifier is applied to the trigger input. This pulse is increased to 40,000 volts by the 1:200 set-up transformer. The 40,000-volt charge on the trigger capacitor discharges by arcing in the spark gap. This is a very low energy spark, but sufficient ionization occurs to cause the main capacitors to discharge across the large electrode creating the light used to photograph the model.

A secondary capacitor, 0.005 microfarad, also discharges through a voltage divider with a peak current of approximately one amp. This current creates a voltage pulse of 51 volts across the 51 ohm resistor used to trigger the counter. Several such counters provide the time base used in conjunction with physical measurements to calculate model velocity.

5.3 Rifle for Testing Systems

In order to evaluate and adjust the performance of such systems as the model detector, it is necessary to provide an actual moving projectile. A 0.30 caliber rifle has been purchased and installed in the range tank for this purpose; see figure 17. Its retractable mount allows the rifle to be fired on axis and to be moved out of the firing line of the light gas gun. An air cylinder raises the mount and a linkage actuates the trigger. A safety interlock on the range tank door prevents accidental discharge.

Figure 18 is a shadowgraph of a 0.30 caliber rifle bullet in flight. Figure 10 indicates that the optical system is designed so that two model images normally occur. The lower image is caused by the model intercepting the divergent light beam between the light source and first parabolic mirror. The smaller image in the center of view is the principal image and is used for data analysis.

5.4 Materials for Telemetry Packages

The ultimate value of this facility will be realized when the required information can be telemetered from a model during flight. At the present time, it is known that pressure and temperature can be converted to electrical signals by on-board instrumentation, and the signals can be transmitted to a ground station via a high-frequency radio link.

The Douglas light gas gun can launch objects up to 1.5 inches in diameter and 3 inches in length. Since most models must be launched in a sabot, the maximum diameter of the telemetry package can be about one inch and its maximum length about three inches. It is estimated that from three to seven channels of information can be telemetered during a single launching of such a package.

A simplified explanation of this multichannel operation follows: a single carrier oscillator is frequency modulated by subcarrier oscillators which are sensitive to the desired data characteristics. Frequency modulation, rather than amplitude modulation, is used because of the greater ease with which the data can be digitized and also because of better accuracy. The signal telemetered from the model is received via range antennas. The receiver drives a DC amplifier whose output is recorded on magnetic tape, typically at 60 inches per second. An oscillograph then records the data during playback of the tape, with the subcarrier frequency selected with a tunable discriminator. A transistorized current limiter is applied to the galvanometer to protect it from damage due to large, spurious noise signals. Speed of playback is reduced, typically by 32:1, to allow better time resolution of subcarrier frequency data. Time references, velocity information, and chamber pressure can also be recorded on the tape. This system is similar to one being used at the Arnold Engineering Development Center.

The first step in the modus operandi outlined above is to develop a miniature carrier frequency oscillator which can withstand high acceleration. A 40-gram model can be accelerated to 12,000 ft/sec in a launch tube of reasonable length, thereby experiencing about 10^6 g. Current telemetry practices for ballistic ranges at the Arnold Engineering Development Center and at the Canadian Armament Research and Development Establishment yield reliable data at only 2×10^5 g. Design trends are reviewed below and in references 9 through 15.

The carrier frequency, which is intended to measure a thermodynamic parameter, is influenced by mechanical changes due to stress and strain in miniature oscillator components. Thus all components are encapsulated and potted in place within the model. Certain static compression tests have been devised at AEDC to simulate dynamic operation. Stagnation pressure is selected as the variable most suitable to static calibration and to theoretical verification in flight tests. Subsequent flight tests validated static tests and calibrations and displayed transducer accuracies ranging from 4% to 14%.

Two major sources of error are subject to study. First, the body and encapsulation materials tend to acquire permanent sets during launching. The resulting stresses in the individual circuit components cause significant changes in their electrical characteristics. Furthermore, the electrical characteristics depend on the orientation of these stresses with respect to the components. Transistors are especially sensitive in these respects. Second, temperature changes in the transmitter after calibration and loading in the gun, but before launching, affect electrical parameters and produce frequency changes. The latter problem is simpler to solve.

Optimum orientations of components have been found through static and dynamic tests at AEDC. Transistor junctions are encapsulated separately in extremely rigid potting material, and the transistor is mounted near the model nose, in a specific attitude (base wafer parallel to stress vector), to reduce the inertial mass contributing to stresses within the transistor. Although 2N502 transistors have performed well, mesa transistors may prove to be superior.

Other components are oriented and potted with similar care. The induction coil is a major source of errors due to phase and frequency shifts. Four turns of number 24 enamelled wire with 0.1-inch pitch and 0.25-inch outside diameter is used in a 150 Mc oscillator at AEDC. The best orientation was found to be to place the coil at the front of the telemetry package with its axis longitudinal. At best, the coil has been responsible for a frequency shift of 10%.

The most successful battery is Mallory RM400R-T2, prepotted to avoid short circuits. However, a slightly larger battery, RM675R-T2, may prove better able to withstand current leakage because of its thicker cover. The best direction to load these disc-shaped batteries is along a diameter. This element appears to contribute 2% to frequency shift.

Two successful 0.1-watt resistors are Allen-Bradley TR-10 and Ohmite Little Devil. Negligible frequency shift occurs when the cylindrical resistor is loaded transversely. The best miniature glass capacitor is Corning CYFM10C. However, the best orientation was found to depend on the capacitor value.

Voids within the potting material deprive the components of structural strength; they provide points of stress concentration which lead to failure during loading. A technique at AEDC to preclude voids is to mix an epoxy under vacuum, to pour it into the outer shell and insert the telemetry package while vibrating the entire assembly, to replace the assembly in an evacuated chamber during early cure, and to pressurize the unit during the terminal curing stage.

The most desirable property of the resinous potting material is its low density which minimizes inertial loads on the components. Best results are obtained by filling epoxy resins, such as Armstrong C7, with hollow glass spheres, e.g., Eccospheres 30 to 300 microns in diameter. Apart from their low density, such fillers tend to increase the compressive yield strength at some expense of the ultimate compressive strength.

Polyesters are too subject to shrinking and cracking in the present application. Acid catalysts are to be avoided because water, produced during curing of phenolics, causes severe corrosion. Silicones and urethanes lack sufficient strength. Other desirable properties, especially for encapsulating transistors, are low conductivity, high compressive modulus, good elasticity, low viscosity (less than 15,000 centipoise at 70°F), and low cure temperature (less than 200°F). However, the last requirement is subject to certain conditions as outlined below.

Curing agents giving maximum compressive yield strength at room temperature are desirable, but this requirement is counter to the desirably high ultimate strength associated with high-temperature cures. Furthermore, the strength of the potted telemeter increases with age because curing continues for weeks at room temperature. However, long gel times usually require higher temperature cures. Also, low gel temperature creates molecules with steric hindrances or some degree of asymmetry. Whereas aromatic amines are unsatisfactory, amines as a group are desirable and aliphatic polyamines are the best curing agents because of their relatively high strength and low curing temperature.

5.5 Electronics for Telemetry

The range tank, like any closed metal container, functions as a resonant cavity at certain critical frequencies. Thus, the telemetry transmission frequency must be compatible with the physical dimensions, notably the diameter, of the range tank.

The range tank, a circular cylinder, is crudely equivalent to a wave guide of similar shape and dimensions, and can be analyzed and operated in the most fundamental mode, viz., the 0, 1 type of transverse magnetic mode. The cutoff wavelength in that case is theoretically 1.31 diameters (reference 16). The corresponding cutoff frequency, that frequency below which no transmission is possible, is 75 Mc for the present 10-foot-diameter range tank, and is 125 Mc for the 6-foot range tank used at AEDC. The practical cutoff frequency of the AEDC tank is found by experiment to be equal to the cited theoretical value (reference 12), which lends confidence to the present analysis.

Whereas the cutoff frequency for an assumed mode depends only on the tank diameter, the frequency actually propagated within the hypothesized circular wave guide depends on the dielectric constant of the medium therein. Specifically, the frequency of propagation in a medium of relative dielectric constant ϵ (relative to the permittivity in vacuo) within a wave guide is (reference 16):

$$f_g = f_o \sqrt{\epsilon - (f_c/f_o)^2}$$

where f_o is the frequency that would be transmitted in vacuo, and f_c is the cutoff frequency. Transmission can occur only when $f_g \geq f_c$ or, from the above relation, when $f_o \geq \sqrt{2/\epsilon}\, f_c$. The relative dielectric constant ϵ of air, or of other likely test media, at pressures and temperatures of interest is approximately unity. Thus, the minimum transmitting frequency of practical value for the 10-foot tank is about 106 Mc.

Although signal attenuation decreases as the frequency increases, this effect is weak and may be neglected in the present problem. On the other hand, many practical considerations tend to impose upper limits on the frequencies to be investigated. Therefore, the objective of current circuit development is to build and test oscillators which transmit frequencies safely above the estimated minimum, 106 Mc, but no higher than necessitated by the tank characteristics. One imponderable in the foregoing analysis is the influence on the transmission characteristics of auxiliary, e.g., optical, hardware within the range tank.

Several oscillator circuits are being developed with the aforementioned considerations in mind; all are scaled for a package 0.5-inch diameter by 1.1-inches long. Two of these, patterned after circuits used at AEDC and CARDE, can be adjusted to span a frequency range from 40 to 160 Mc; they are represented in figure 19. Both have good electronic stability and contain what is considered to be a minimum number of components. Circuit A has been made to oscillate from 40 to 60 Mc; however, changes in the components can produce frequencies to 200 Mc. Circuit B has been made to oscillate from 60 to 160 Mc; its frequency is likewise strongly affected by changes in the components. Equipment and materials for potting such circuits, according to procedures discussed in section 5.4, are on order.

Systems for telemetry data acquisition are also being studied, including FM receivers with ranges from 50 to 200 Mc, tunable discriminators, and magnetic tape recorders. Models containing accelerometers, as well as models containing pressure transducers, and their circuitry, are under investigation.

6. REFERENCES

1. Seiff, A., The Use of Gun-Launched Models for Experimental Research at Hypersonic Speeds, AGARD Report No. 138, July 1957.

2. Charters, A. C., B. P. Denardo, and V. J. Rossow, Development of a Piston-Compressed Type Light-Gas Gun for the Launching of Free-Flight Models at High Velocity, NACA TN 4143, November 1957.

3. Lord, M. E., Performance of a 40 MM Combustion-Heated Light Gas Gun Launcher, AEDC-TN-60-176, October, 1960.

4. Stephenson, W. B., Theoretical Light-Gas Gun Performance, AEDC-TR-61-1, May 1961.

5. Glass, I. I. and J. G. Hall, Handbook of Supersonic Aerodynamics, Section 18, Shock Tubes, NAVORD Report 1488, Vol. 6, December 1959.

6. Neice, S. E., J. O. Carson, and B. E. Cunningham, Experimental Investigation of the Simulation of Atmospheric Entry of Ballistic Missiles, NACA RM A5726, December 1957.

7. Charters, A. C., The Free-Flight Range: A Tool for Research in the Physics of High-Speed Flight, ARS 1984-61, March 16, 1961.

8. Seiff, A., A Free-Flight Wind Tunnel for Aerodynamic Testing at Hypersonic Speeds, NACA Report 1222, 1955.

9. Kingery, M. K., Preliminary Development of Telemetry for Aeroballistic Ranges, AEDC-TN-59-7, February 1959.

10. Letarte, M., A Miniaturized Telemetry System for Guns and Rocket Firing Status Progress, CARDE Technical Memorandum 255/59, July 1959.

11. Waldron, H. F., Free Flight Facilities and Aerodynamic Studies at Canadian Armament Research and Development Establishment, IAS Paper No. 60-90, July 1960.

12. Kingery, M. K., Progress Report on Development of Telemetry for a Hypervelocity Range, AEDC-TN-60-214, December 1960.

13. Kingery, M. K., An Assessment of Readout Errors Encountered in Radio Telemetry for Gun-Launched Hypervelocity Projectiles, AEDC-TN-61-58, May 1961.

14. Young, R. P., Packaging of Hypervelocity Radio Telemeter to Withstand High Impulse Accelerations, AEDC-TN-61-119, October 1961.

15. Young, R. P., An Examination of Epoxy Systems Useful in Packaging 'High G' Radio Telemeters, AEDC-TDR-62-58, March 1962.

16. Reference Data for Radio Engineers, Fourth Edition, Federal Telephone and Radio Corporation, 1956.

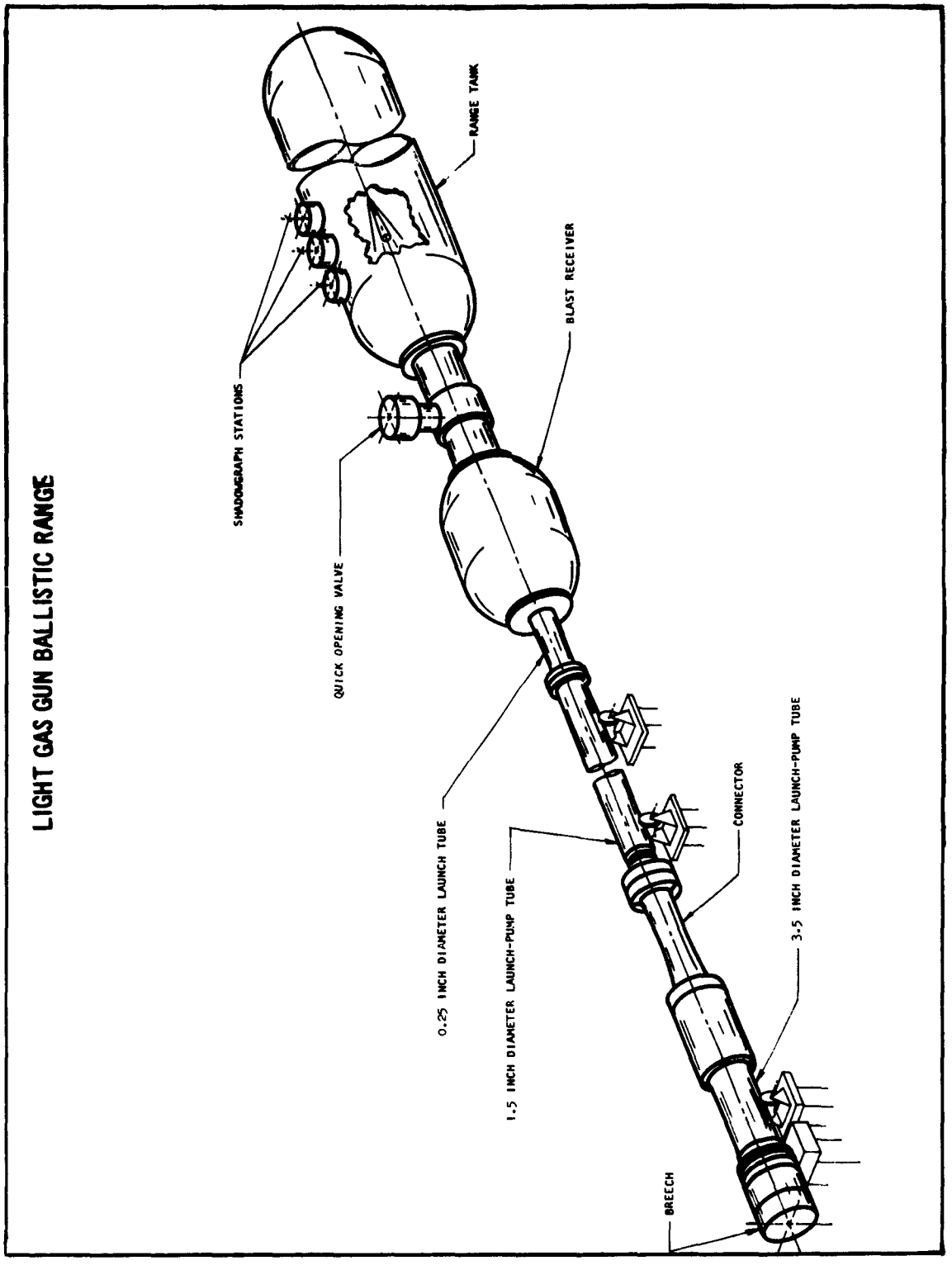
LIGHT GAS GUN BALLISTIC RANGE
SHADOWGRAPH STATIONS
QUICK OPENING VALVE
RANGE TANK
BLAST RECEIVER
0.25 INCH DIAMETER LAUNCH TUBE
1.5 INCH DIAMETER LAUNCH-PUMP TUBE
CONNECTOR
3.5 INCH DIAMETER LAUNCH-PUMP TUBE
BREECH

FIGURE 1A

DOUGLAS AEROPHYSICS LABORATORY LIGHT-GAS GUN AND BALLISTIC RANGE

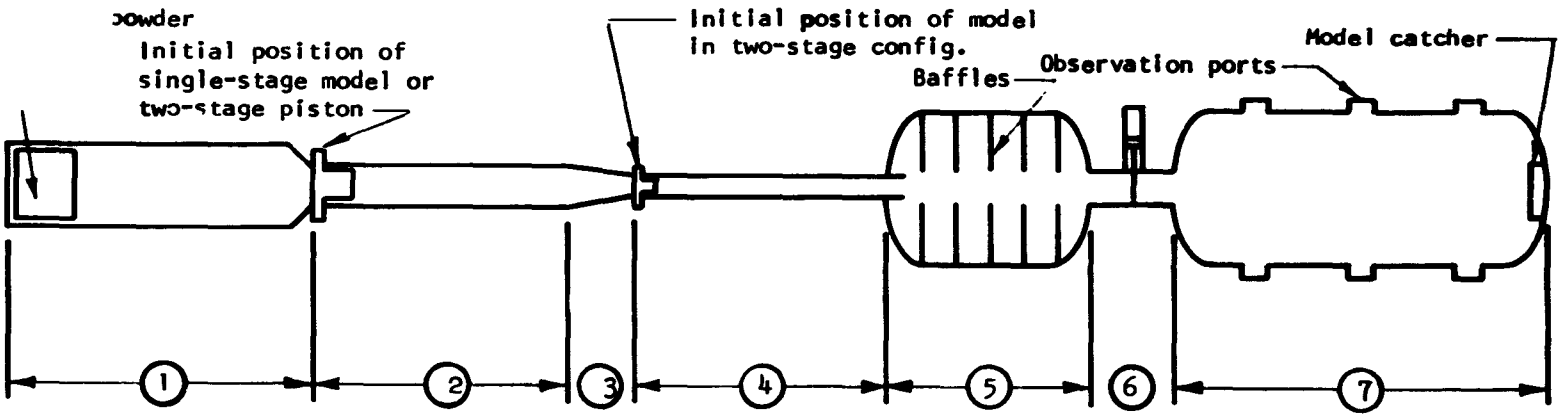

1. PUMP TUBE 3.5 inch ID x 15 feet long; prepressurized typically to 800 psia with helium or hydrogen; designed for 38,000 psia operation.
2. FIRST STAGE LAUNCH TUBE 1.5 inch ID x 26.3 feet long; pre-evacuated in single-stage operation to 100 mm Hg or prepressurized to 200 psia with helium or hydrogen in two-stage operation.
3. CONVERGENT SECTION Taper converging from 1.5 inch ID to 0.25 inch ID in 11.5 inch (7° whole angle) terminating in a break valve; installed only for two-stage operation.
4. SECOND STAGE LAUNCH TUBE 0.25 inch ID x 50 inches long; pre-evacuated to 100 mm Hg.
5. BLAST RECEIVER 8 feet diameter x 15 feet long contains seven baffles pre-evacuated to 100 mm Hg.
6. QUICK OPENING VALVE Separates atmospheres in two tanks. opens in 0.005 second, closes in 0.2 second.
7. RANGE TANK 10 feet diameter x 100 feet long prepressurized to 10 atm or pre-evacuated to 0.01 atm; contains 6 vertical and 6 horizontal shadowgraphs.

FIGURE 1B

HELIUM CONDITIONS GENERATED IN THE PUMP TUBE AS A RESULT OF COMBUSTION OF NITROCELLULOSE GUN POWDER

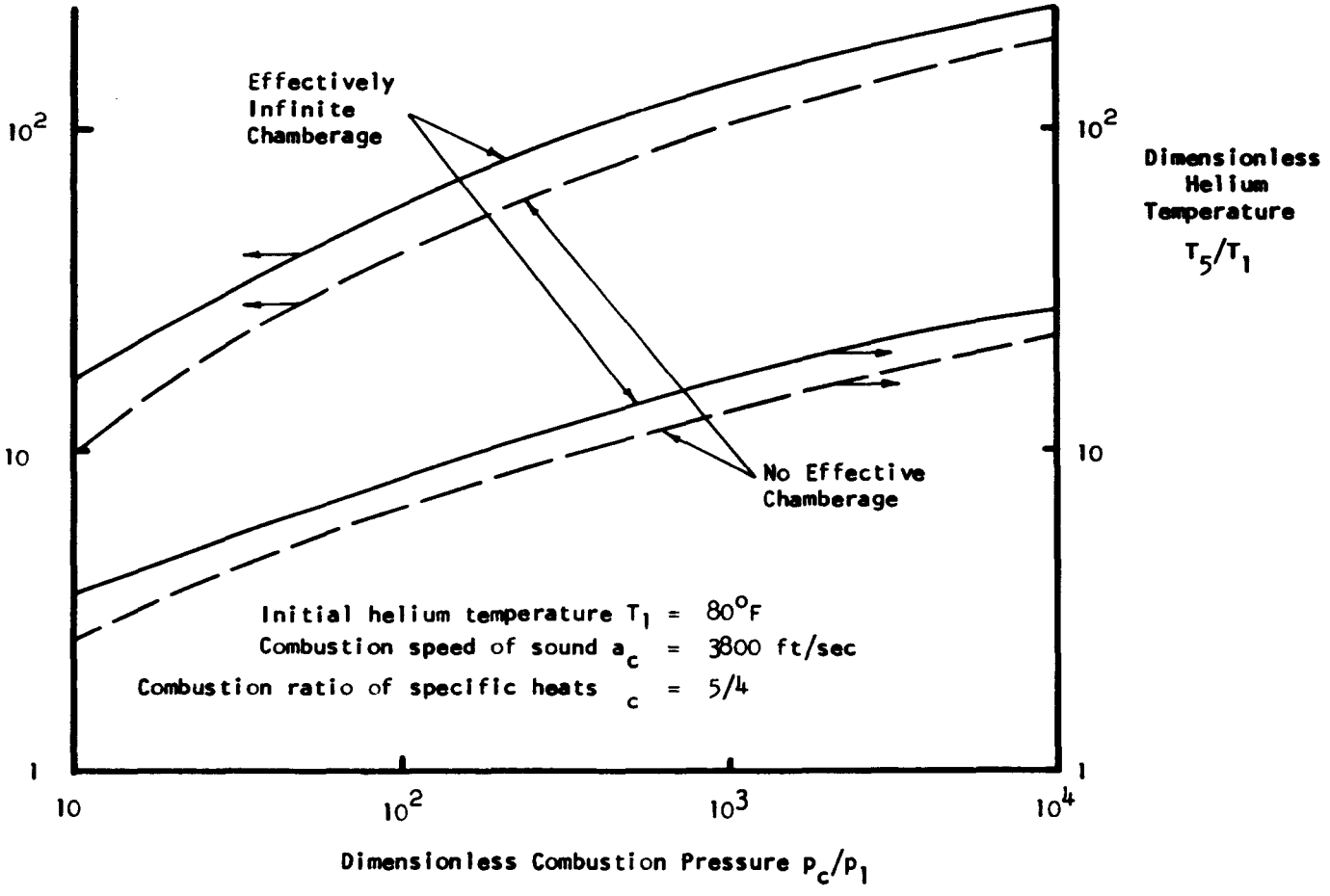

FIGURE 2

PERFORMANCE OF THE PUMP TUBE AT THE DESIGNED PRESSURE LIMIT, 38,000 PSIA

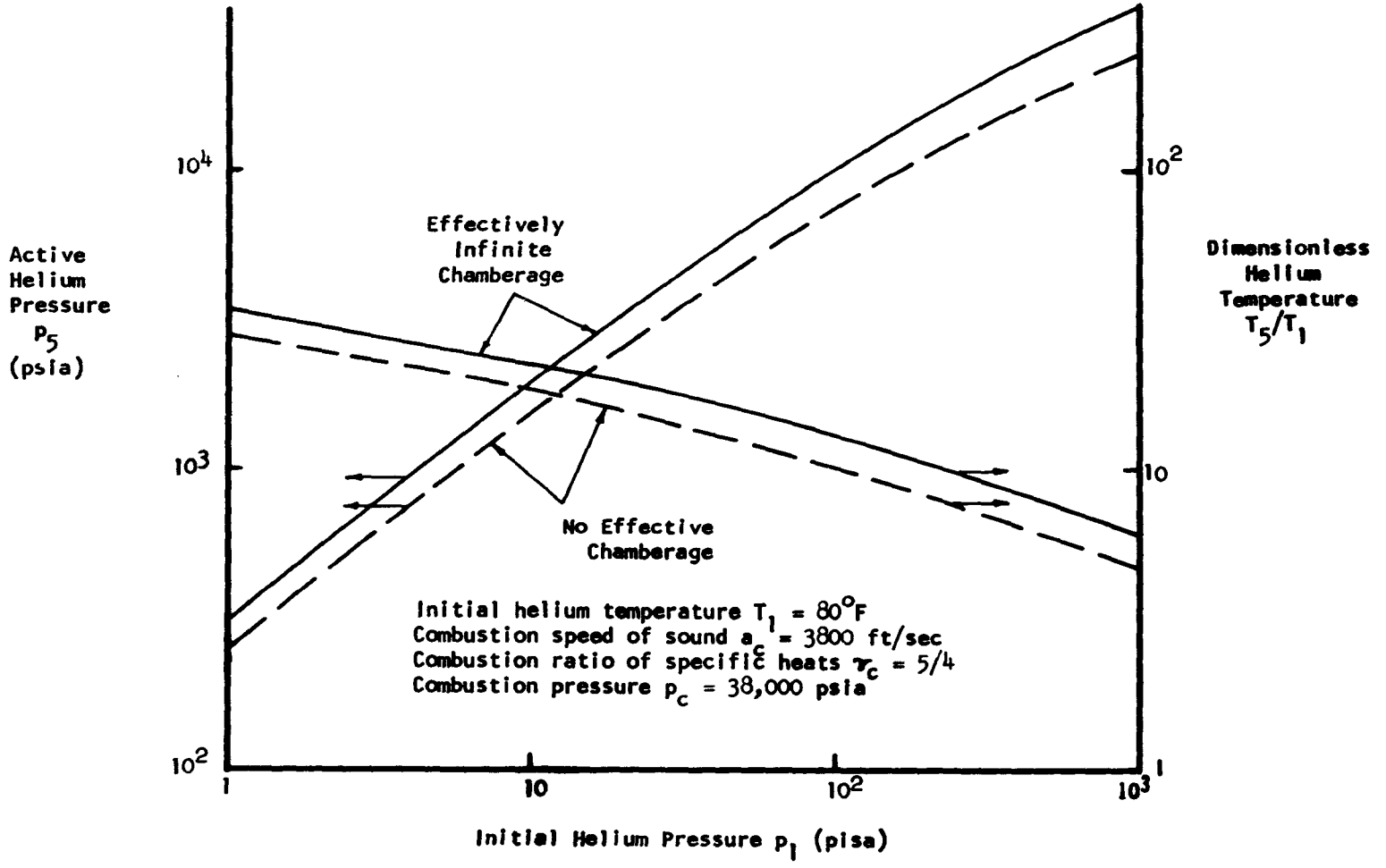

FIGURE 3

PERFORMANCE OF THE 1.5 - INCH SINGLE STAGE LAUNCH TUBE ASSUMING EFFECTIVELY INFINITE CHAMBERAGE

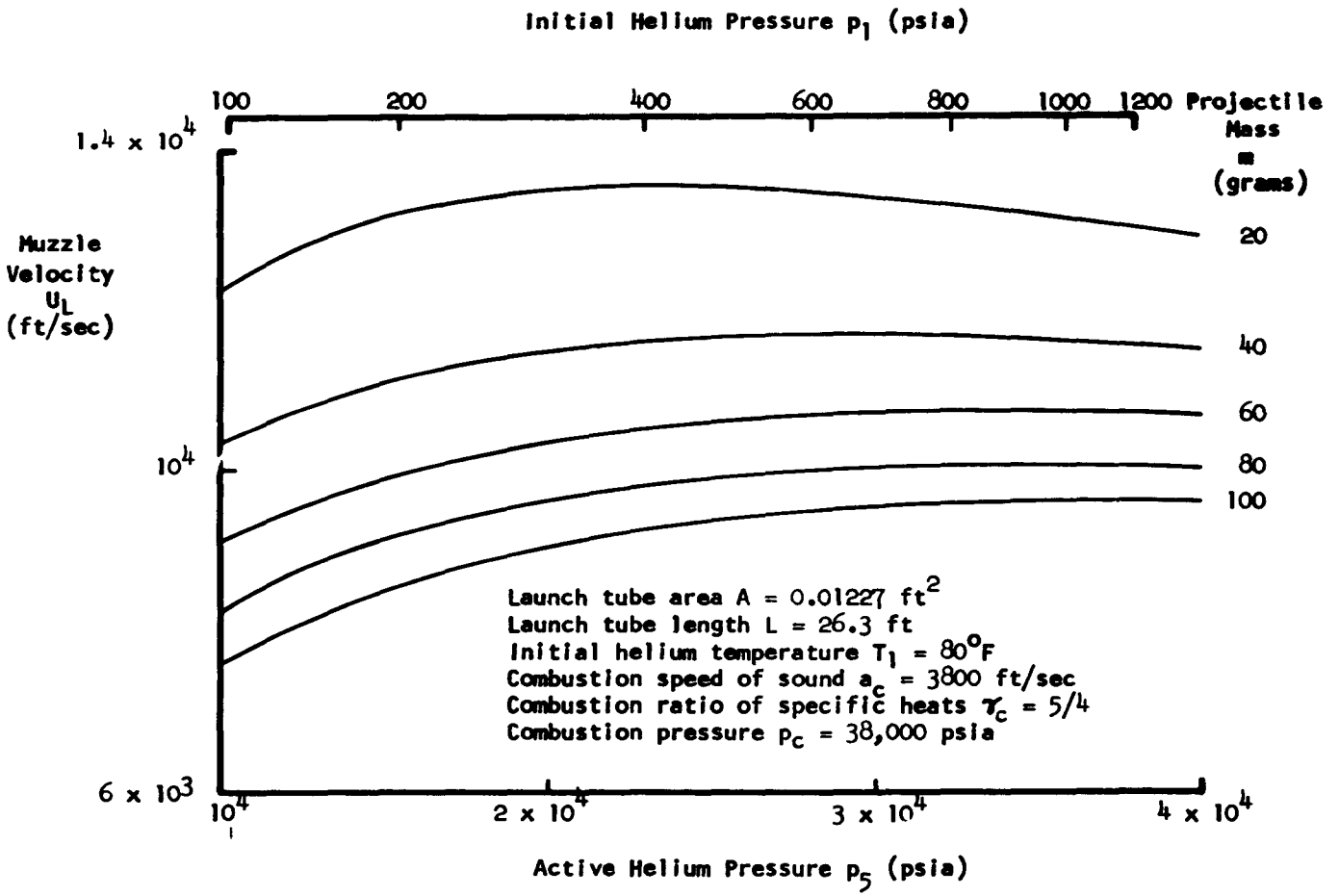

FIGURE 4

PERFORMANCE OF THE 0.25-INCH TWO-STAGE LAUNCH TUBE ASSUMING CONSTANT BASE PRESSURE

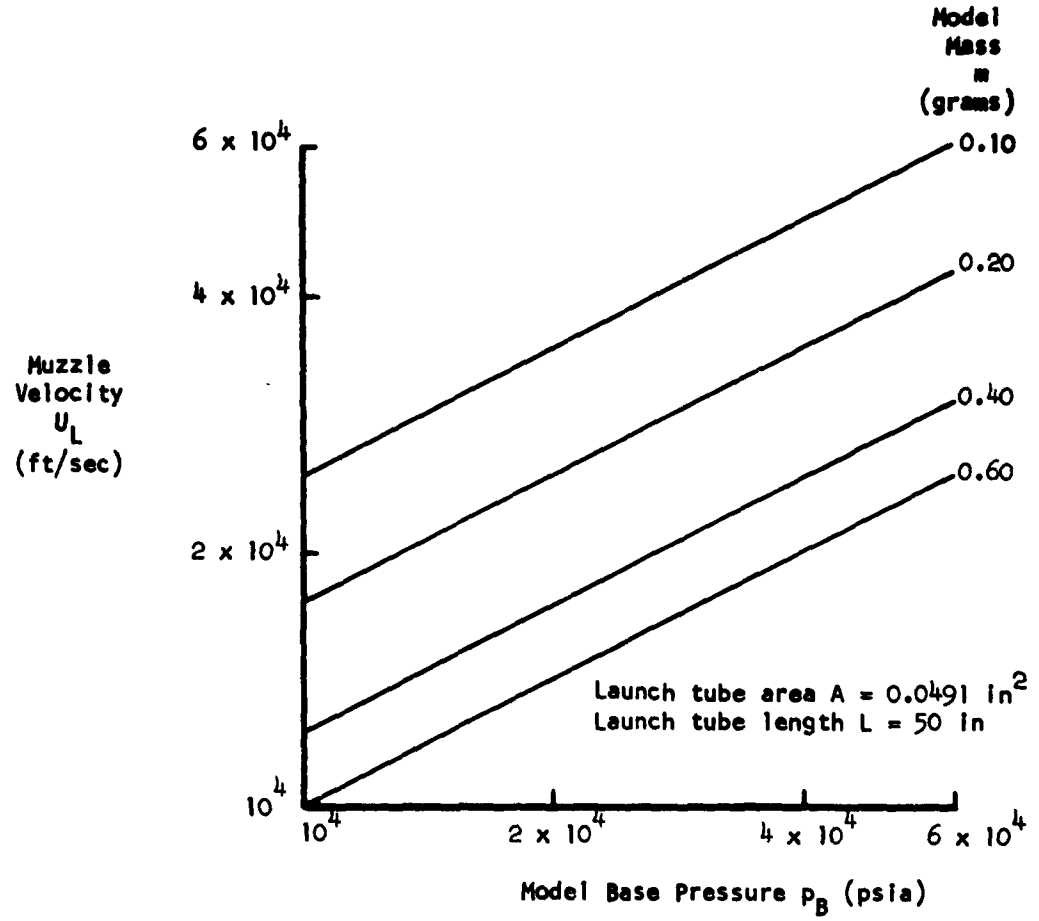

FIGURE 5

MEASURED PRESSURE MAXIMA OF CLOSED-BOMB TESTS AND SINGLE STAGE LAUNCHES

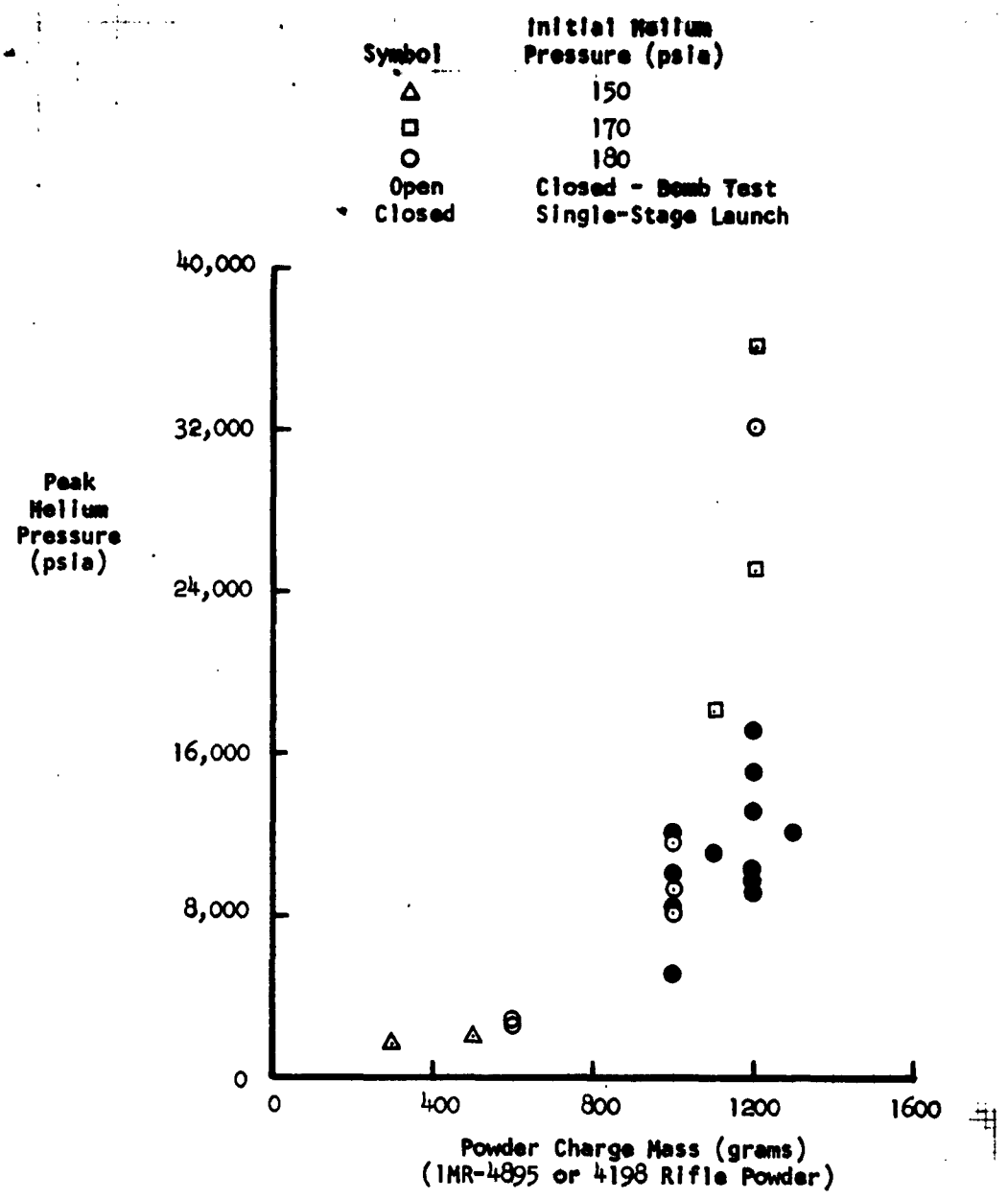

FIGURE 6

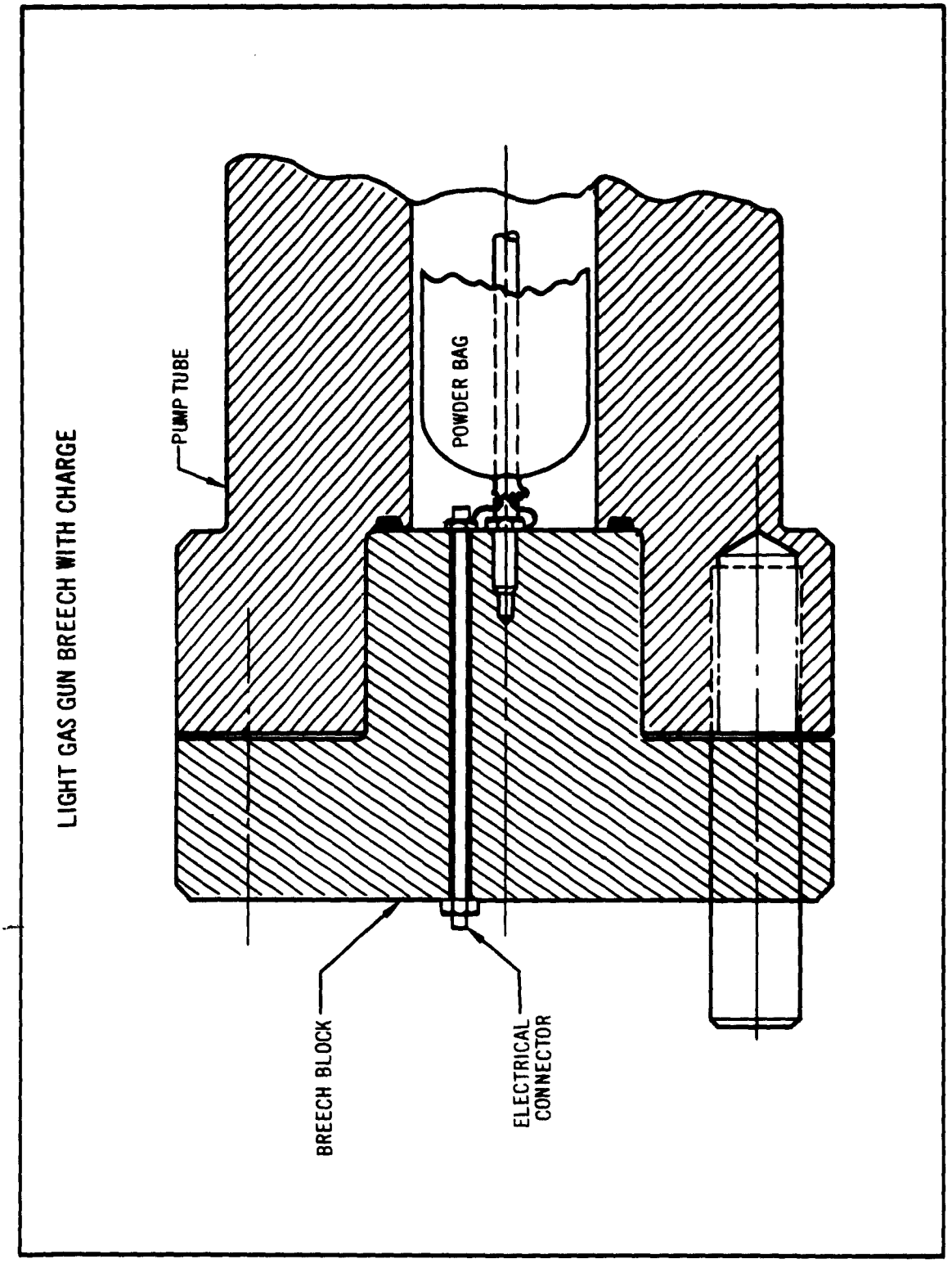
LIGHT GAS GUN BREECH WITH CHARGE
PUMP TUBE
POWDER BAG
BREECH BLOCK
ELECTRICAL CONNECTOR

FIGURE 7

METHODS OF MODEL RELEASE IN THE SINGLE STAGE CONFIGURATION

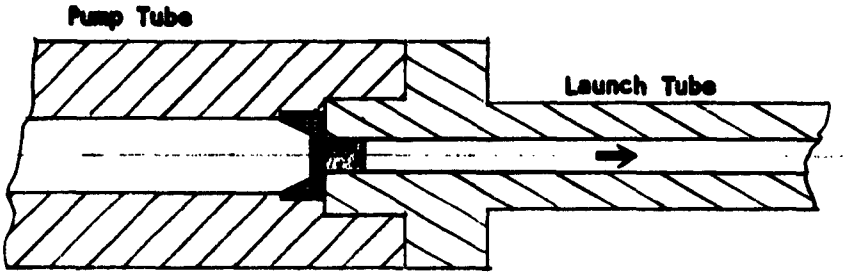

Flared Base Model

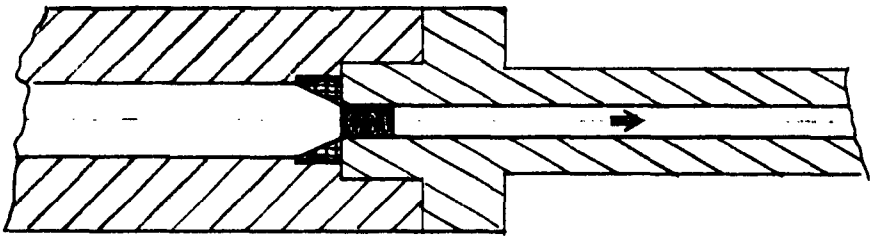

Drive Fit Model

FIGURE 8

MODEL VELOCITY AT TWENTY FEET DOWNSTREAM OF THE MUZZLE
OF THE SINGLE-STAGE LAUNCH TUBE

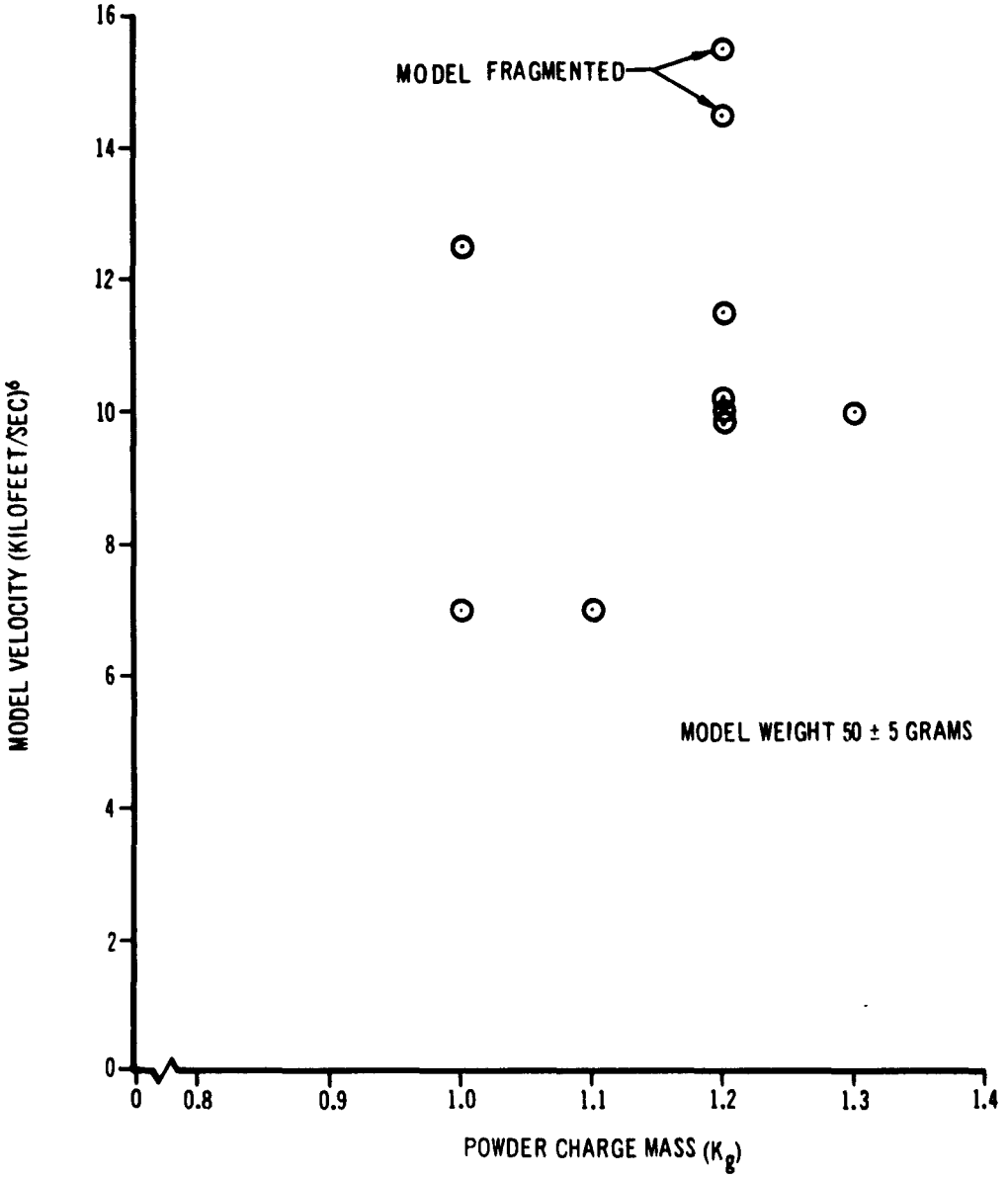

FIGURE 9

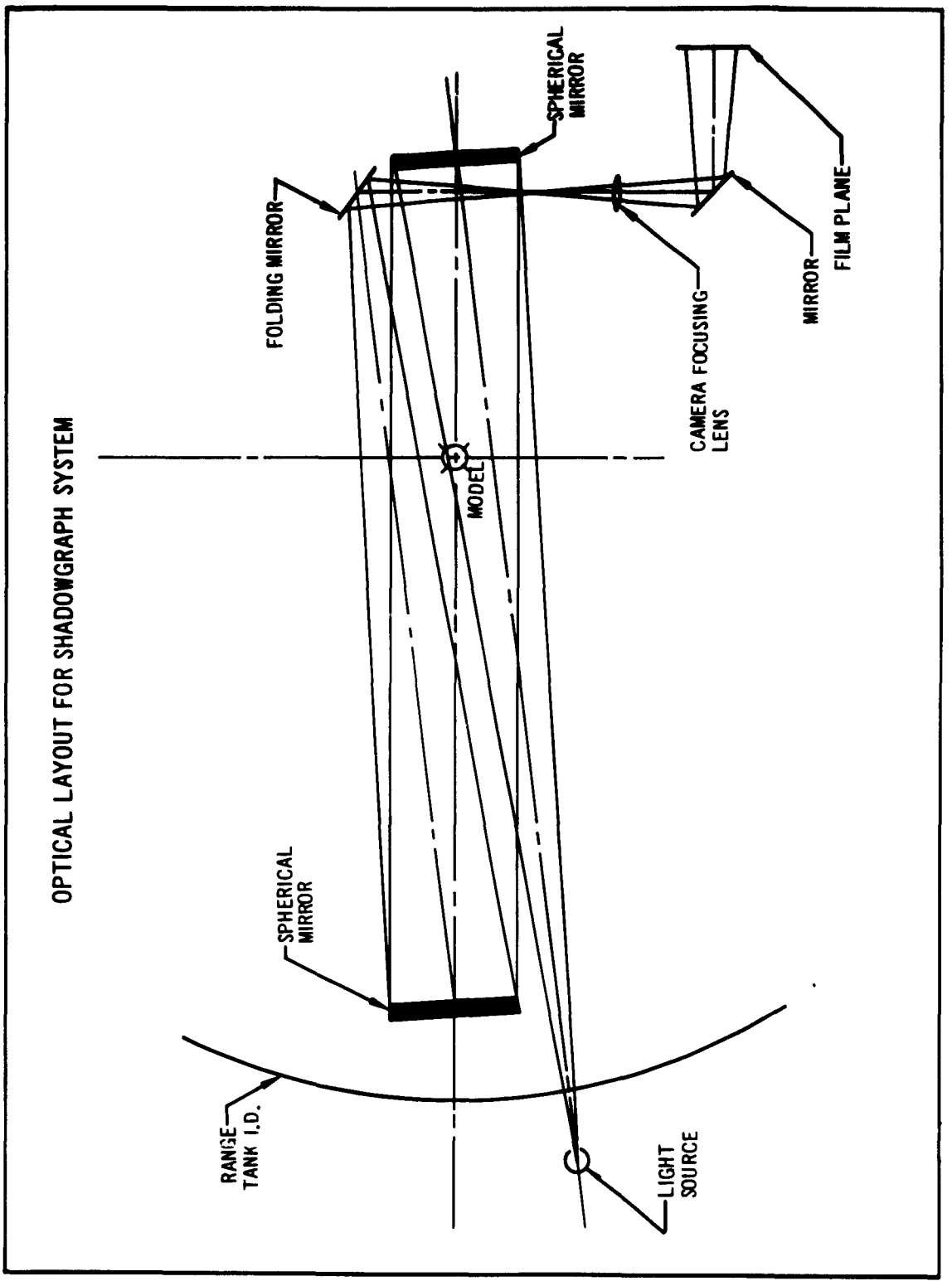
OPTICAL LAYOUT FOR SHADOWGRAPH SYSTEM
SPHERICAL MIRROR
FOLDING MIRROR
CAMERA FOCUSING LENS
MIRROR
FILM PLANE
MODEL
SPHERICAL MIRROR
RANGE TANK I.D.
LIGHT SOURCE

FIGURE 10

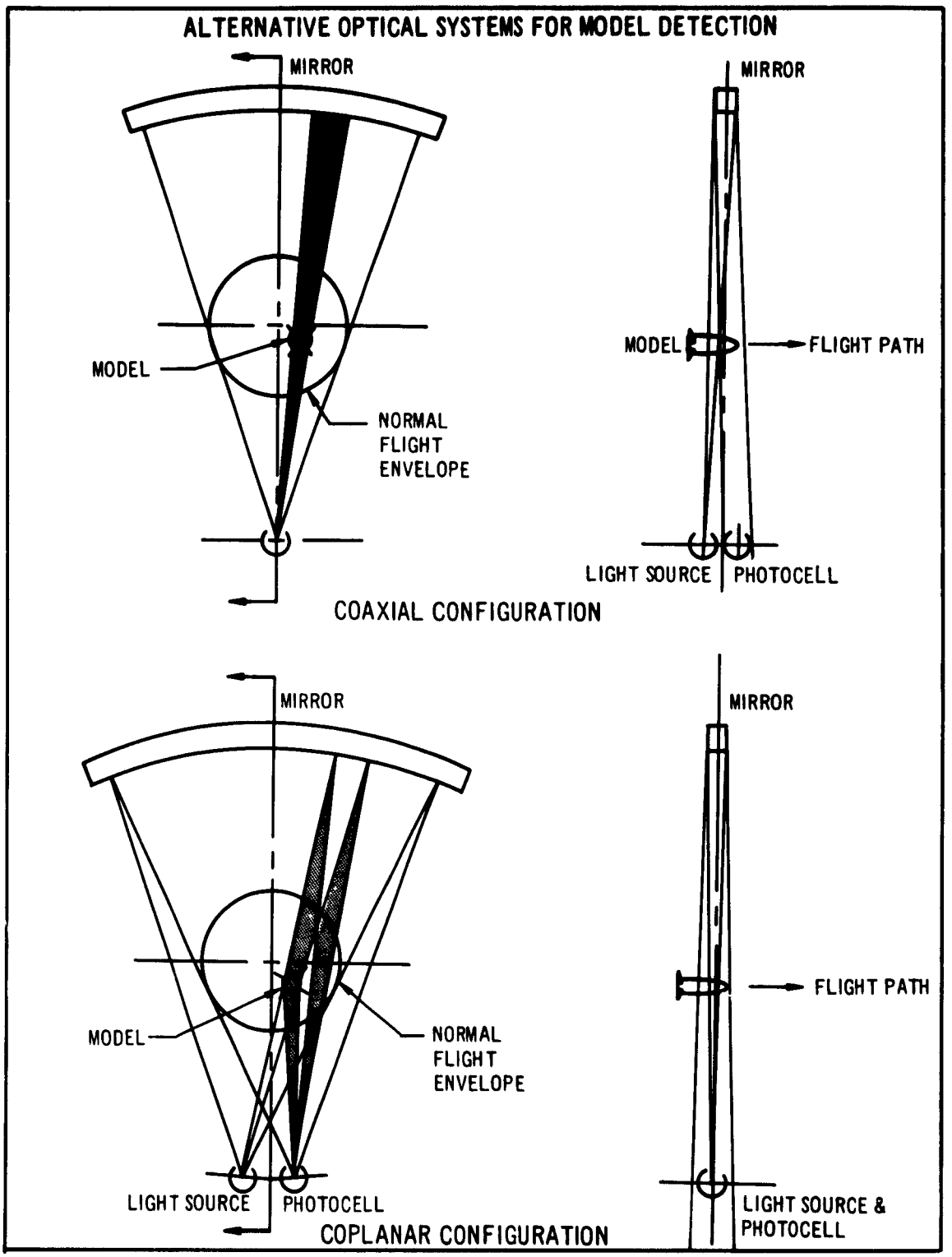
ALTERNATIVE OPTICAL SYSTEMS FOR MODEL DETECTION
MIRROR
MODEL
NORMAL
FLIGHT
ENVELOPE
MIRROR
MODEL
FLIGHT PATH
LIGHT SOURCE
PHOTOCELL
COAXIAL CONFIGURATION
MIRROR
MODEL
NORMAL
FLIGHT
ENVELOPE
LIGHT SOURCE
PHOTOCELL
MIRROR
FLIGHT PATH
LIGHT SOURCE &
PHOTOCELL
COPLANAR CONFIGURATION

FIGURE 11

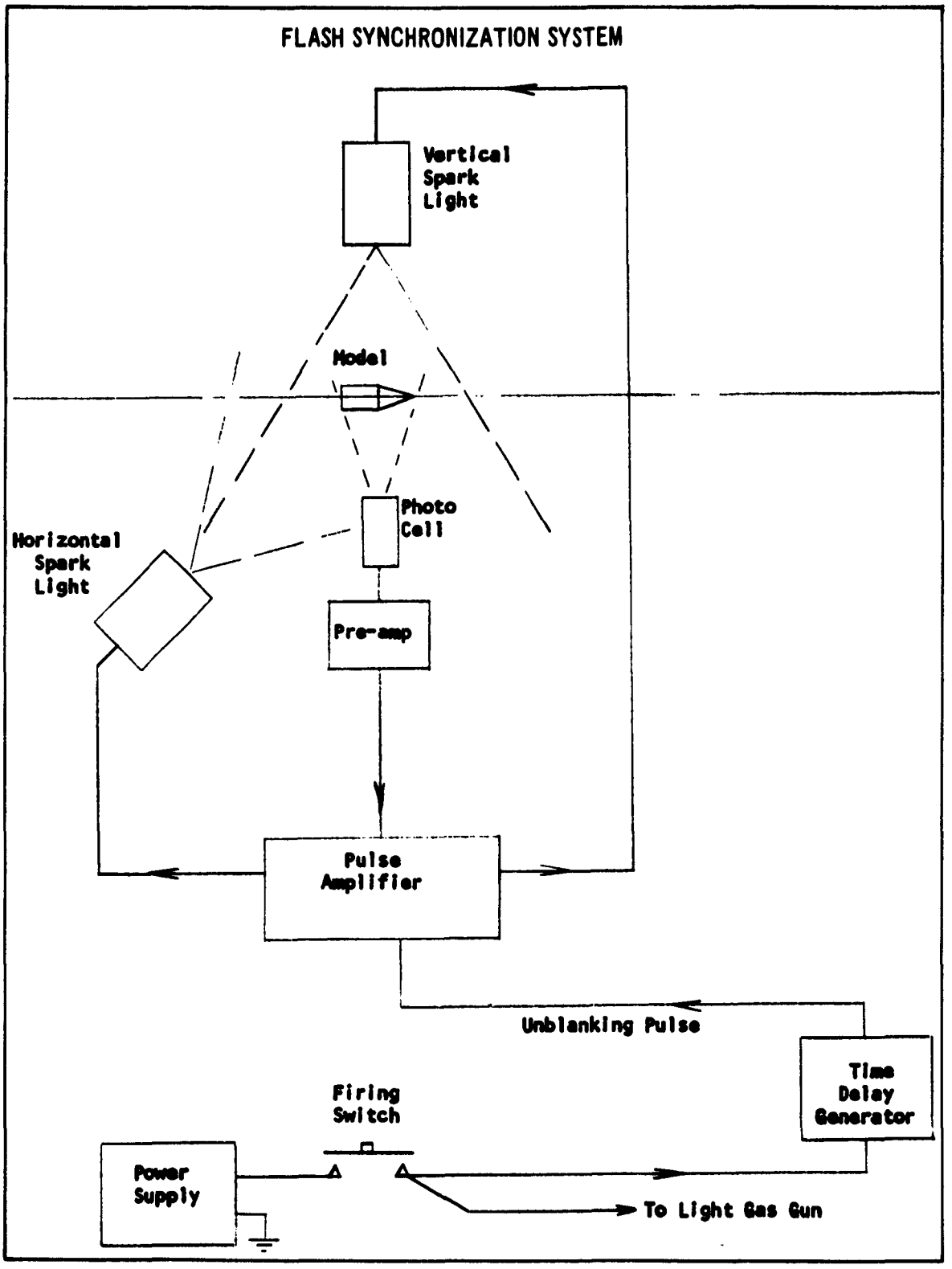
FLASH SYNCHRONIZATION SYSTEM
Vertical Spark Light
Model
Photo Cell
Horizontal Spark Light
Pre-amp
Pulse Amplifier
Unblanking Pulse
Time Delay Generator
Firing Switch
Power Supply
To Light Gas Gun

FIGURE 12

PHOTOCELL AND PREAMP CIRCUIT FOR MODEL DETECTION

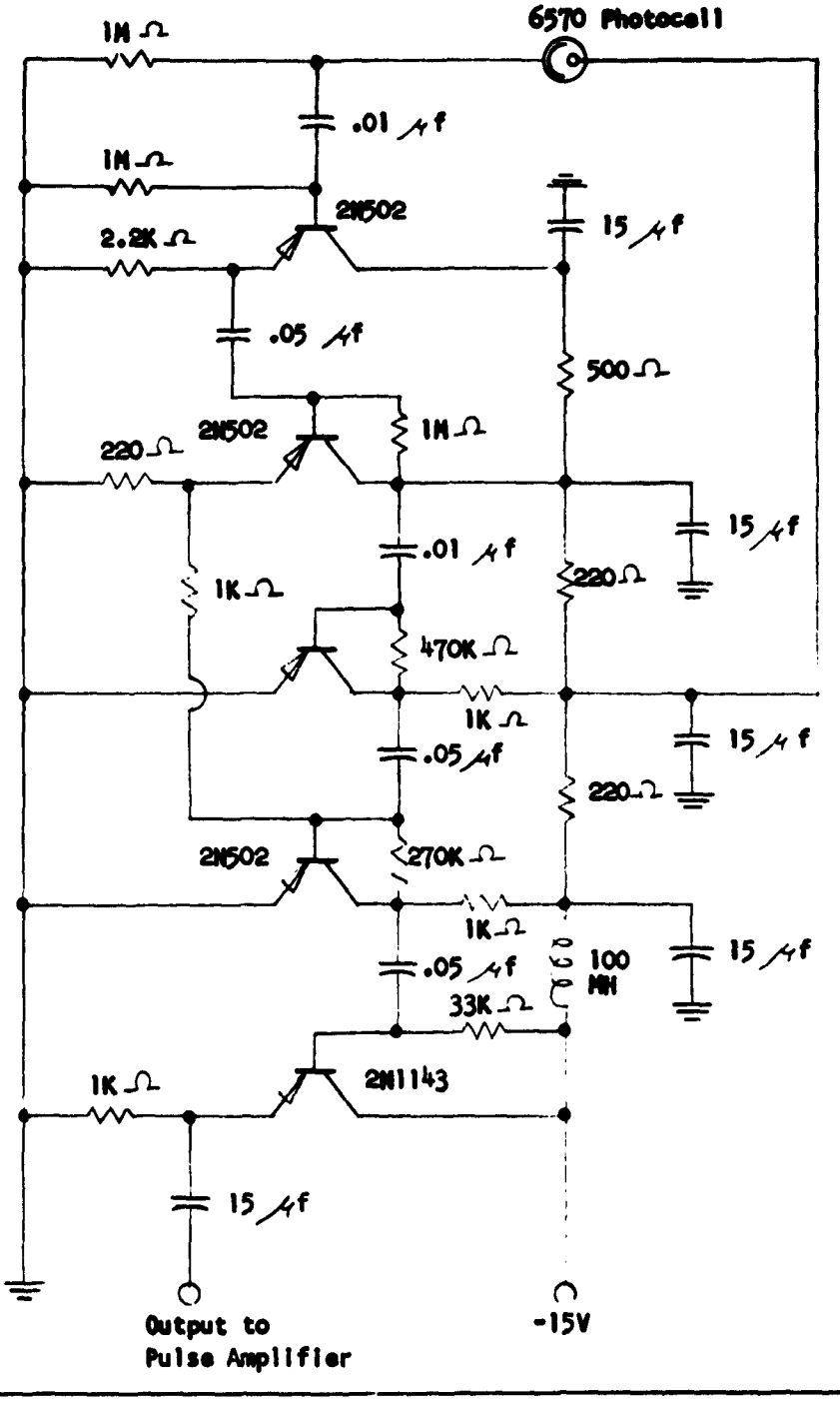

FIGURE 13

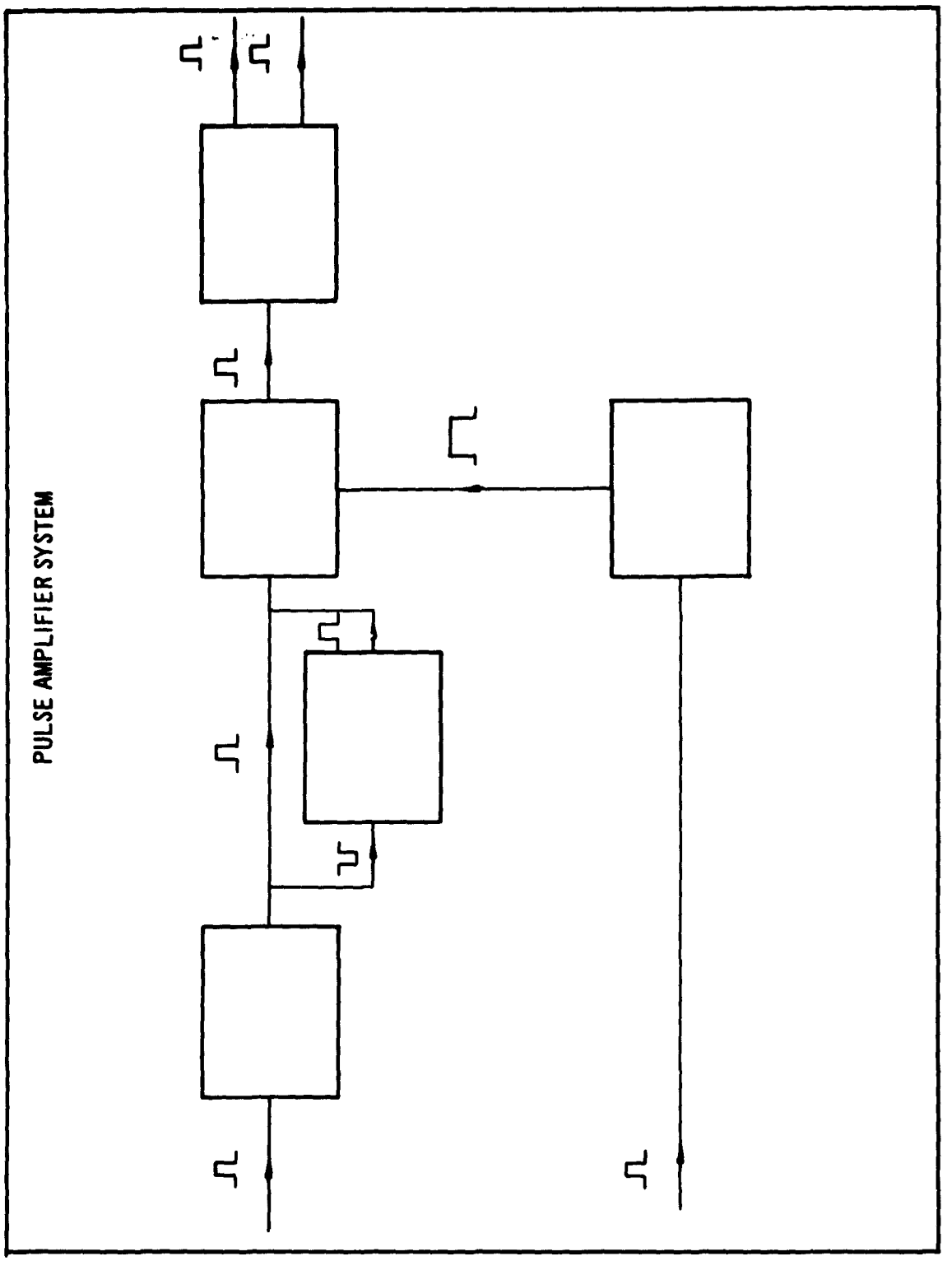

FIGURE 14

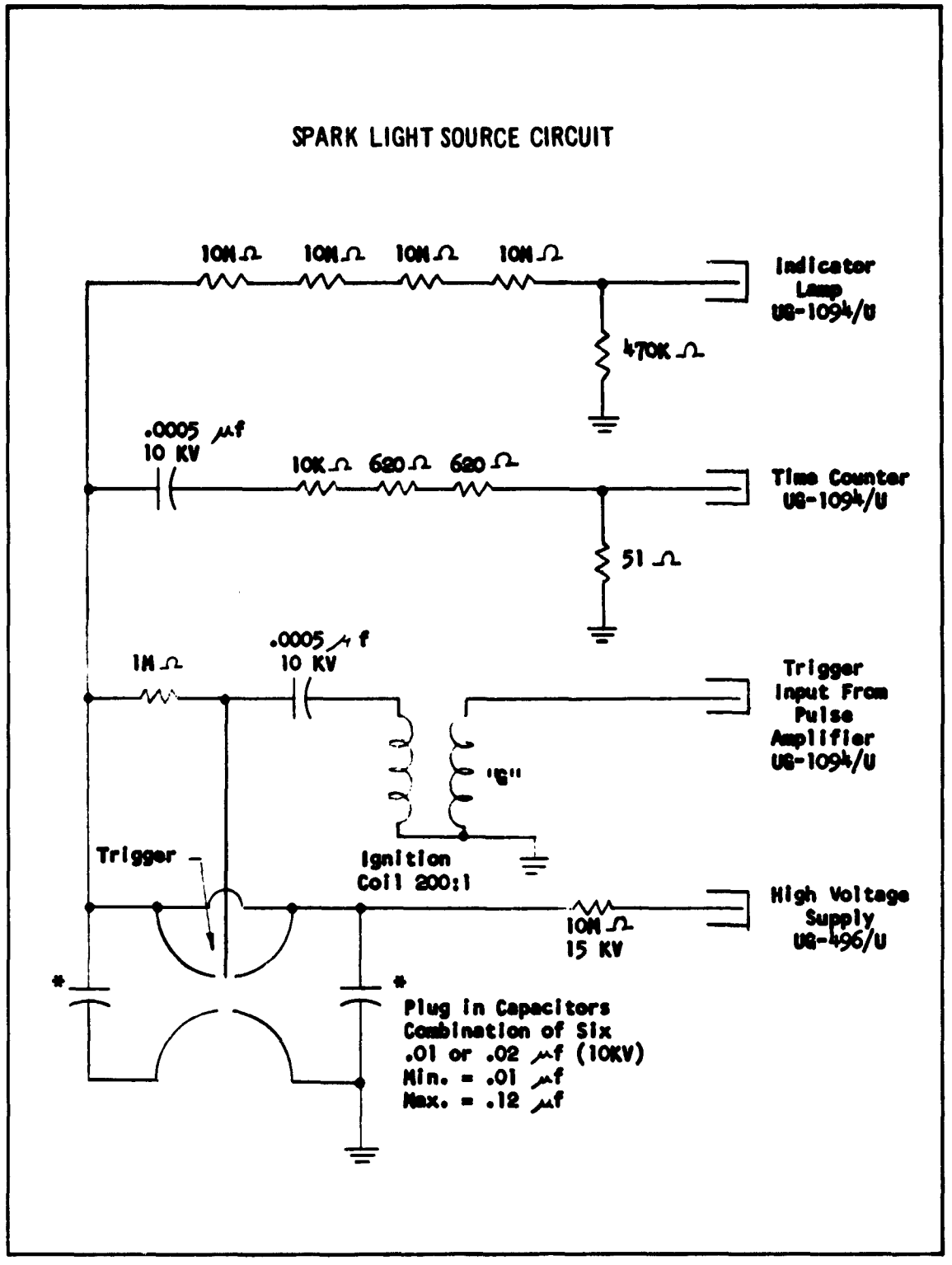
SPARK LIGHT SOURCE CIRCUIT
10MΩ
10MΩ
10MΩ
10MΩ
Indicator Lamp UG-1094/U
470KΩ
.0005 μf
10 KV
10KΩ
620Ω
620Ω
Time Counter UG-1094/U
51Ω
1MΩ
.0005 μf
10 KV
Trigger Input From Pulse Amplifier UG-1094/U
"G"
Trigger
Ignition Coil 200:1
10MΩ
15 KV
High Voltage Supply UG-496/U
*
*
Plug in Capacitors
Combination of Six
.01 or .02 μf (10KV)
Min. = .01 μf
Max. = .12 μf

FIGURE 15

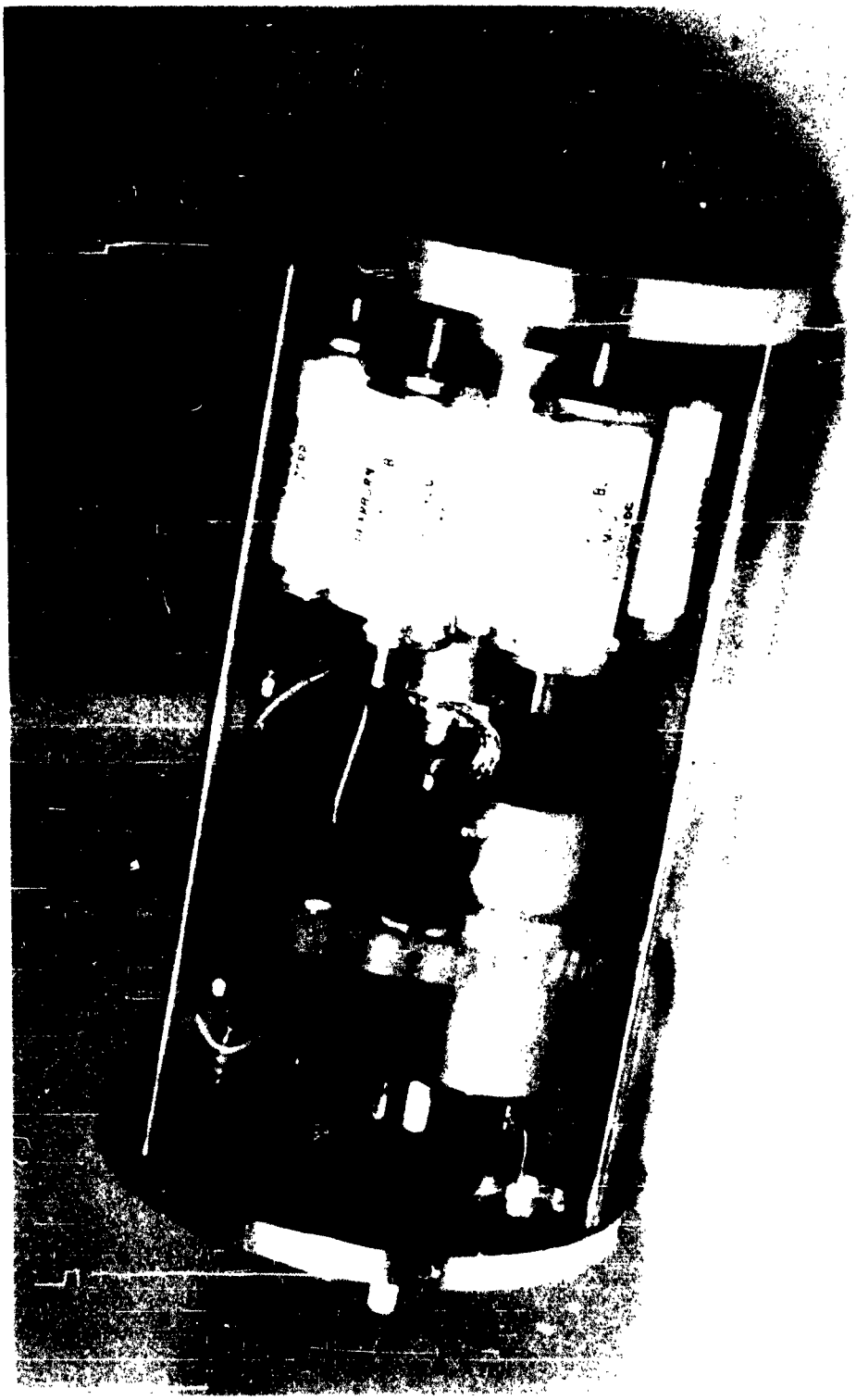

SPARK LIGHT SOURCE ASSEMBLY

FIGURE 16

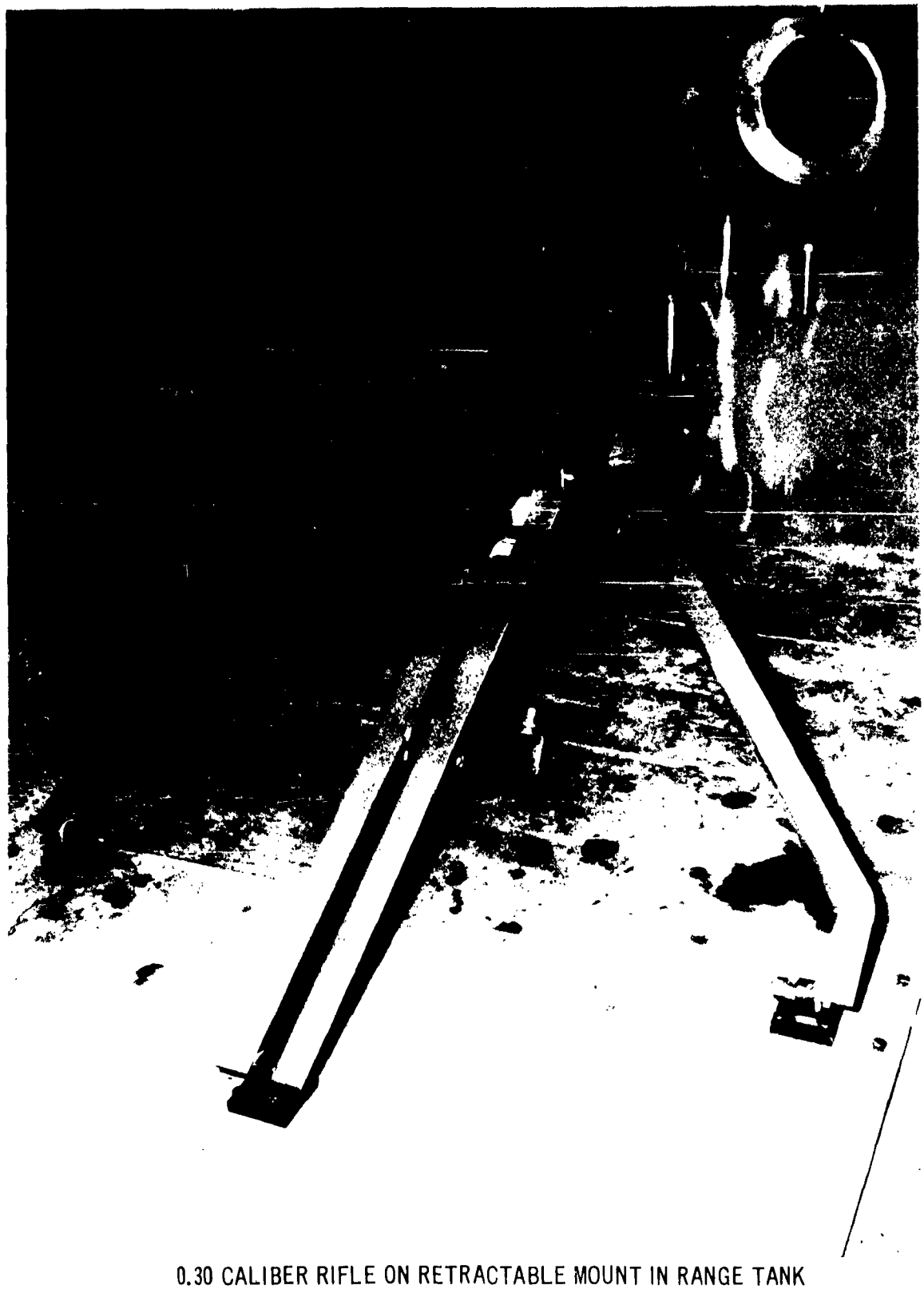

0.30 CALIBER RIFLE ON RETRACTABLE MOUNT IN RANGE TANK

FIGURE 17

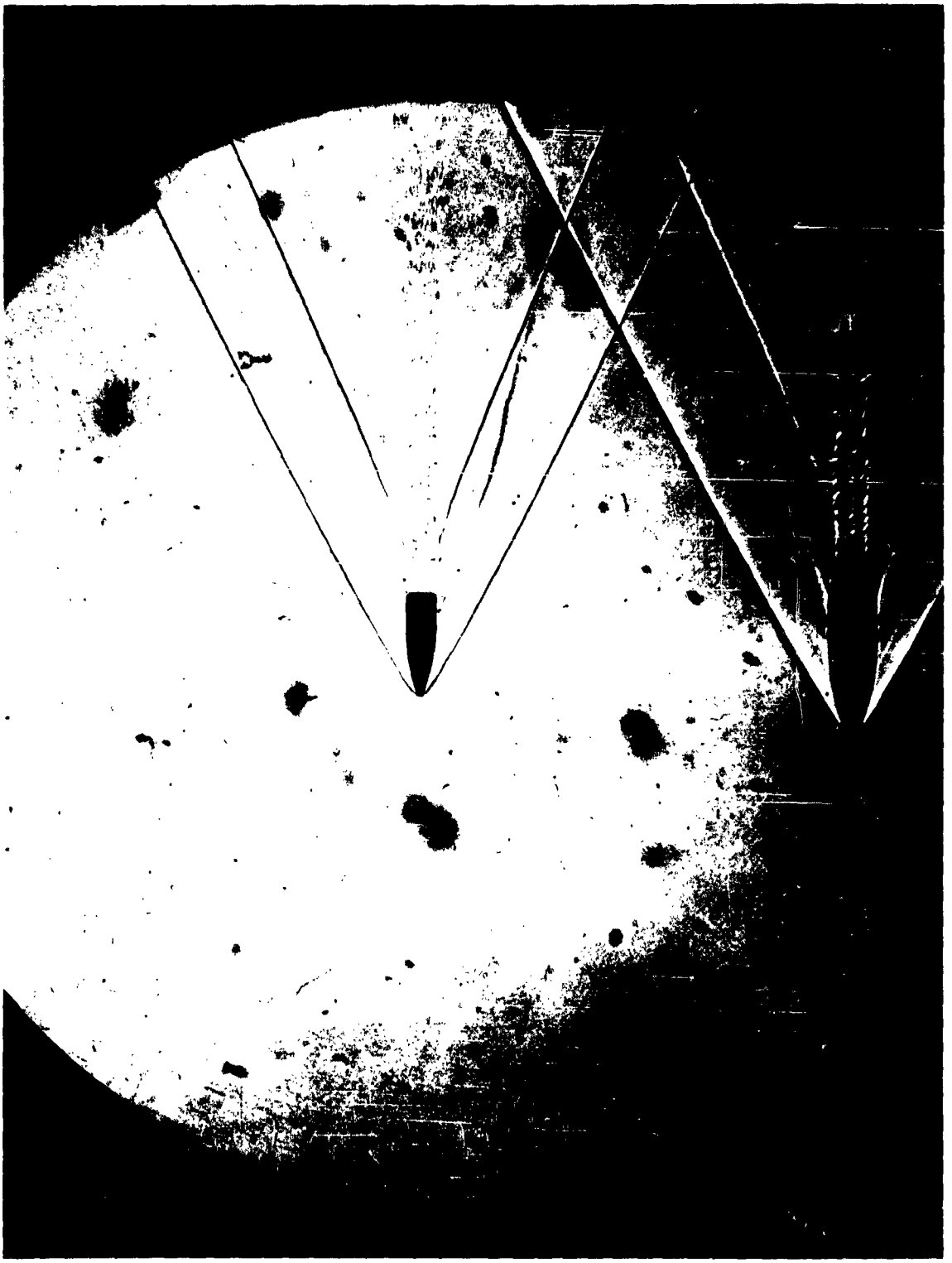

PRINCIPLE (CENTER) AND SUBSIDIARY (LOWER) IMAGES OF 0.30 CALIBER PROJECTILE IN MOTION

FIGURE 18

OSCILLATOR CIRCUITS

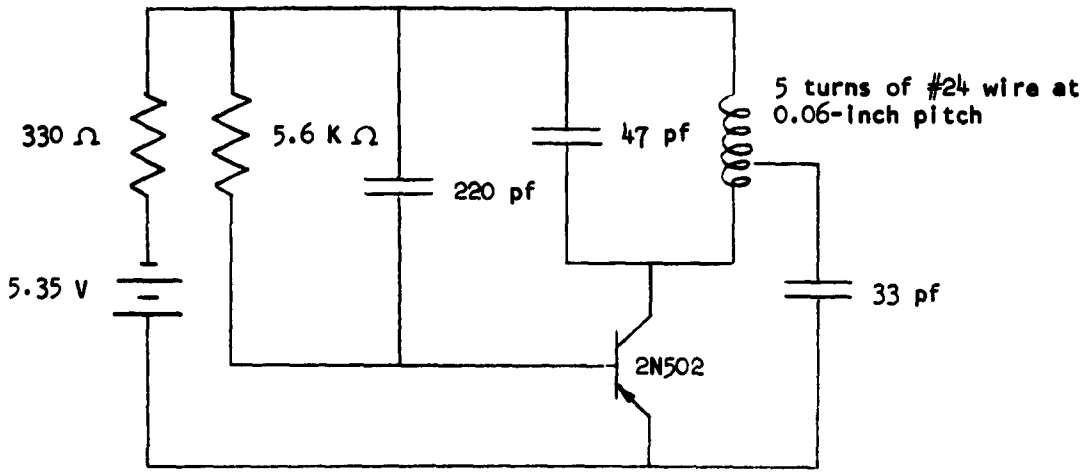

Telemetry Circuit A (typical frequency 55 Mc)

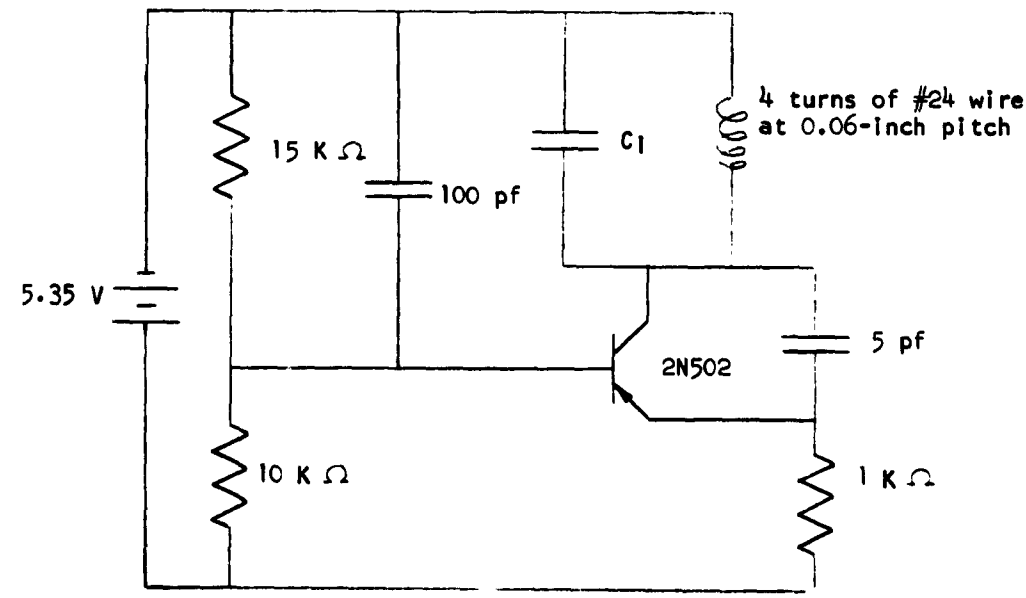

Telemetry Circuit B
(typical frequencies 90 Mc with C_1 = 33 pf and
160 Mc with C_1 = 5 pf)

FIGURE 19

Section 5
Transonic Test Section Studies

J.F.L. Aldrich

January 1, 1963

Report Number SM-41379-5

Sales Order: 81280-287
Engineering Work Order: 51903
Job Work Order: 0001

SUMMARY

The Trisonic Four-Foot Wind Tunnel acquired a transonic testing capability during FY 1962. Whereas the supersonic test section provides for Mach 1.4 to 5, the transonic test section provides for Mach 0.2 to 1.3. An IR&D study of the transonic flow was initiated and completed during this year, primarily to examine flow quality and to calibrate the test section for Mach number distribution and flow inclination. Results are reported in detail in references 1 and 2. Across the 54-inch window region, the Mach number varies ±0.0075 at subsonic speeds and ±0.010 at supersonic speeds. Furthermore the average Mach number in this region can be determined within ±0.003 by appropriate reduction of a routine measurement of pitot pressure. The boundary layer displacement thickness on the perforated walls at zero incidence decreases from 0.5 inch at Mach 0.8 to a minimum of 0.17 inch at about Mach 0.95, increases to a maximum of 0.28 inch at Mach 1.1, and decreases at higher speeds. Transonic flow vectors coincide with the centerline but tend to diverge at other locations. For example, the vertical flow divergence one foot above the centerline is 0.5 degree at subsonic speeds and diminishes at supersonic speeds to zero at Mach 1.2. The flow divergence change per unit distance from the tunnel centerline in the horizontal plane is nearly twice that in the vertical plane, probably due to the lateral position of Mach number control valves. The calibration shows in general that acceptable flow properties and uniformity are generated at transonic speeds.

REFERENCES

1. Aldrich, J. F. L., and B. W. Johnson, Trisonic Four-Foot Tunnel Transonic Test Section Calibration of Mach Number, Douglas Aircraft Company, Inc., Santa Monica Report No. SM 41371, August 8, 1962.

2. Johnson, B. W., Trisonic Four-Foot Tunnel Transonic Test Section Calibration of Flow Inclination, Douglas Aircraft Company, Inc., Santa Monica Report No. SM 41372, December 31, 1962

Section 6
Wind Tunnel Investigations Of A 1/16 Scale Model Of The Proposed Annualar Steam Ejector For The Trisonic Four-Foot Wind Tunnel

Ward V. Speaker

Report Number SM-41379-6

January 1, 1963

Sales Order: 81280-287
Engineering Work Order: 51903
Job Work Order: 0002

SUMMARY

An annular steam ejector has been investigated to determine an acceptable configuration for use in a proposed ejector system for the Trisonic Four-Foot Wind Tunnel. Configurations analyzed and tested on 1/16 scale include combinations of two ejector exit areas, eight ratios of mixing tube length-to-diameter, and two contraction geometries within the mixing tube, all in the presence or absence of a scale model of the existing subsonic diffuser of the subject wind tunnel. Mach number in the ejector and stagnation pressure in the ejector and in the wind tunnel were varied. Wind tunnel Mach number was 4.0. Pressure data from all the configurations were reduced and analyzed to determine the effects of ejector and mixing tube geometry on performance of the system. Minimum length/diameter ratios, minimum operating tunnel pressures, and minimum steam mass flows have been determined, and preliminary judgments have been made which would apply also if air were used as the ejector motive medium in place of steam. Reductions of starting and running pressures by factors as great as 3.3 have been achieved experimentally. However, it is concluded that the configuration of the existing subsonic diffuser would be unacceptable as an element of the ultimate mixing tube, and that a contraction downstream of a constant-area mixing tube may be unnecessary in an optimum system.

TABLE OF CONTENTS

LIST OF ILLUSTRATIONS

NOTATION

A_{j_e}	Ejector nozzle exit area, square inches
A_j^*	Ejector nozzle throat area, square inches
A_m	Mixing tube cross-sectional area, square inches
A_{m_c}	Minimum area of mixing-tube contraction section, square inches
A_N	Tunnel test section cross-sectional area, constant at 9.00, square inches
D	Diameter of mixing tube, constant for these tests at 4.912, inches
D_c	Diameter of mixing tube contraction section throat, inches
A_N^*	Tunnel nozzle throat area, square inches
L	Length of mixing tube constant section, inches
L_c	Over-all length of mixing tube contraction section, inches
ℓ_c	Length of throat section of mixing tube contraction section, inches
M_j	Ejector Mach number, a function of $P_{t_j}/\overline{P}_j$
M_m	Mixing tube Mach number, a function of A_m/A_j^*
M_N	Tunnel test section Mach number, a function of P_{t_N}/P_{t_N}'
P_a	Atmospheric pressure, pounds per square inch
P_c	Stagnation pressure at the downstream end of the simulated Four-Foot Tunnel supersonic diffuser, pounds per square inch
P_{D_E}	Static pressure at the downstream end of the pilot tunnel supersonic diffuser, pounds per square inch
P_{EX}	Static pressure, averaged from two or four locations, at the downstream end of the subsonic diffuser, pounds per square inch
$P_{j1...4}$	Ejector nozzle static pressures at locations 1 through 4 spaced at 90° increments around the nozzle circumference and 0.2 inch upstream of nozzle exit, pounds per square inch
P_{j_5}	Ejector nozzle static pressure no. 5, on ejector horizontal centerline and 0.5 inch upstream of nozzle exit, pounds per square inch.
$\overline{P}_j$	Average of P_{j_1} through P_{j_4}, pounds per square inch
P_N	Static pressure in tunnel test section, pounds per square inch

P_{t_J}	Ejector stagnation pressure, pounds per square inch
P_{t_N}	Stagnation pressure in tunnel stilling chamber, pounds per square inch
P'_{t_N}	Stagnation pressure (behind a normal shock) in tunnel test section, pounds per square inch.
T_{t_J}	Steam stagnation temperature, degrees Fahrenheit
T_{t_N}	Air stagnation temperature, degrees Fahrenheit
$\dot{w}_J$	Ejector steam weight flow, pounds per second
$\dot{w}_N$	Tunnel air weight flow, pounds per second
x_J	Ejector throat control distance, inches
γ	Ratio of specific heats

1. INTRODUCTION

The purpose of an ejector system on a blowdown-to-atmosphere facility is to allow operation at subatmospheric static pressures downstream of the test section. In turn, this allows a corresponding reduction in required stagnation pressures. The acquisition of an efficient wind tunnel ejector system results in specific improvements in four critical performance areas:

1. Reduction of starting loads on large-winged models, allowing force measurements that have heretofore been unobtainable.
2. Reduction of starting loads on panel load and control surface models, allowing considerably more accurate measurements through the use of more sensitive strain-gage systems.
3. Ability to conduct power-on or auxiliary airflow testing with reasonable levels of auxiliary supply pressure.
4. Expansion of the over-all operating capabilities of the wind tunnel by allowing increased altitude (lower Reynolds number) simulation.

Simulation of higher altitudes and, possibly, a Mach 6 capability can be provided the Trisonic Four-Foot Wind Tunnel, which exhausts to atmospheric pressure at present, by reducing the back pressure to subatmospheric levels. To this end, an IR&D investigation has been completed during FY 1962 of an annular steam ejector system applied to a 1/16-scale model of the facility. Many problems accruing ultimately to an air ejector system for the actual facility have thereby been resolved. Experimental tests proceeded in three phases during the period October 1961 through June 1962. Steam requirements dictated that the installation be located at the Torrance Facility (Location C-6).

The purpose of testing a model of the proposed ejector system was to develop the most efficient system for use within the space and power limitations of the Aerophysics Laboratory. Steam was considered as the motive source for the ejector because the proposed arc-heated tunnels in the 1963 forecasts required several stages of steam ejection and an existing source would thus be available.

Various mixing tube configurations were investigated during these tests in an effort to obtain the minimum length-to-diameter ratios, minimum tunnel operating pressure, and minimum steam weight flow. The effect of reducing the exit area of the ejector nozzle was also investigated.

2. FACILITY

The Three-inch Pilot Tunnel was constructed specifically for testing the annular ejector system. The tunnel and ejector are shown in figure 1. Air passes into the stilling chamber through the manually-operated valve at the right. The stilling chamber, bellmouth, and nozzle section (shown in figure 2) were scaled from the Trisonic One-Foot Wind Tunnel design drawings, although the constant-area portion (test section) was lengthened to simulate the Four-Foot Tunnel test section. The two-dimensional nozzle consists of two blocks providing a Mach number 4.0 contour. The two-dimensional supersonic diffuser (figure 3) was scaled from settings commonly used during the early stages of testing in the Four-Foot Tunnel. Actually, more recent testing and calculations show better recovery with smaller diffuser throat areas.

At the end of the supersonic diffuser section is the region in which the annular ejector is located (see Ejector Description, Section 3.), followed by a scaled-down version of the Four-Foot Tunnel subsonic diffuser. Beyond the diffuser is a muffler section, which is non-representative.

3. EJECTOR DESCRIPTION

Technically speaking, the term "ejector" refers simply to the device through which the steam is injected into the tunnel airstream. However, this section will also include mixing tube descriptions.

The ejector section consists of a variable-area annulus whose contours were determined based on information from reference 1. Basically, it consists of two nozzle sections as shown in figure 4. The internal portion of the nozzle section on the left is a transition from the rectangular cross-section at the end of the tunnel supersonic diffuser to a circular section through which the tunnel air passes into the mixing tube. The external portion serves as the inner contour of the steam ejector. The nozzle section shown on the right side of figure 4 provides the outer contour of the steam ejector. The outer portions of the two nozzle sections form the walls of the steam plenum chamber. Note that the outside of the left section and the inside of the right section are threaded, allowing the outer contour to move horizontally with respect to the inner contour, and thus providing variable ejector Mach number M_j. The equations and techniques of reference 1 provide contours for $1.7 < M_j < 3.5$, with theoretically excellent flow qualities. Ejector Mach numbers outside this range are, of course, also obtainable, but with some loss in flow quality. Calibrations of the ejector Mach number as a function of the ejector throat control distance x_j are shown in figure 5. The dashed line in figure 5 represents data that were taken during a time when the seal from the main steam valve became lodged in the ejector, unknown to the operating personnel.

Prior to the last test phase, the ejector exit area was reduced by approximately 25%. This was accomplished by electroplating the ejector inner contours with nickel. Calibration of the reduced-area ejector is also shown in figure 5.

Mixing tube configuration was an important variable during the test. The various configurations tested are shown in figure 6. Diffuser M_1 is the scaled-down subsonic diffuser of the Four-Foot Tunnel. Diffuser M_2 was constructed to replace the M_1 diffuser and could be tested either with or without the 15-inch-long constant-diameter portion which immediately follows the contraction section. Five different constant-area sections S_x were tested by combining the one-inch, two-inch, and four-inch lengths. The contraction section M_3 was constructed to be tested with the M_1 diffuser and combinations of the constant area sections S_{L_x}.

4. INSTRUMENTATION

Instrumentation for the various tests of the annular steam ejector consisted of static and total pressures and total temperatures. The air stagnation temperature was sensed in the tunnel stilling chamber by a Marshall temperature gage, accurate to ±5°. The same type gage was used to sense the steam temperature in the ejector plenum.

Stilling chamber stagnation pressure, ejector plenum steam stagnation pressure, and mixing tube total pressure (behind a normal shock) were measured on Duragage diaphragm-type pressure gages which were calibrated prior to the test and found to be repeatable within about ±0.5 psi of the calibrated value.

Pressures sensed on a 50-tube mercury manometer included tunnel test section static and total behind a normal shock, diffuser statics at the minimum-area section and at the downstream end, and pressures in the transition section just upstream of the mixing tube. Ejector nozzle static pressures and static pressures on the mixing tube and subsonic diffuser sidewalls were also obtained from the manometer. A guillotine was located on the top of the manometer, along with a bypass to atmosphere, to prevent steam condensation in the tubes during ejector start and stop.

5. TEST PROGRAMS

125 runs, comprising the first test phase, were performed between October 23 and November 29, 1961, to calibrate the ejector nozzle control position versus Mach number and to obtain static (no tunnel flow) data on mixing tube configurations M_1, M_2, and M_2S_x. Ejector Mach number ranged between 1.4 and 2.86. Tunnel starts could not be achieved during this first phase.

Prior to the second test phase, the M_3 configuration and its associated constant-area sections S_{L_x} were fabricated and a larger steam control valve was installed. The second phase was conducted in the period February 27 through April 9, 1962, during which 325 runs were obtained. Data with and without tunnel flow were taken on various configurations of M_1, $M_1S_{L_x}$, M_1M_3, and $M_1M_3S_{L_x}$ at ejector Mach numbers between 1.4 to 2.85. Ejector steam weight flows higher than anticipated were required for best tunnel performance.

In an attempt to reduce the steam weight flow, the exit area of the ejector was reduced approximately 25% prior to the third test phase. The third (and final) phase of testing took place between June 15 and June 28, 1962. The only configurations tested in the final 91 runs were $M_1S_{L_4}$, $M_1S_{L_6}$, $M_3S_{L_2}$, and $M_3S_{L_4}$ at ejector Mach numbers 2.0 to 2.5.

The method of obtaining static (no tunnel flow) data was to start the steam ejector with the manometer guillotine closed. When the flow was established, the guillotine was opened and the pressures allowed to stabilize; the guillotine was again closed and the ejector stopped. When tunnel flow was desired, a similar procedure was followed. The ejector was started with the guillotine closed. With the guillotine still closed, the tunnel air valve was opened quickly and the approximate starting pressure noted on the Duragage (by the change in sound). After the tunnel was started, the guillotine was opened and the tunnel total pressure was slowly decreased until the tunnel flow was lost; this (minimum operating) pressure likewise was noted. Then the tunnel was restarted and a total pressure slightly above minimum set and manometer pressures allowed to stabilize. The guillotine was closed, tunnel and ejector shut down and the data recorded.

6. DATA REDUCTION

The raw data, recorded manually from gages or the manometer in psig or inches of mercury, were reduced to psia on a desk calculator. The average of the four ejector nozzle static pressures was ratioed to ejector stagnation pressure and values of M_j were taken from a chart of P_t/P versus M for a ratio of specific heats, γ, equal to 1.33 (for steam). For the same γ the area ratio, A_{j_e}/A_j^*, was obtained from another chart of A/A^* versus M. The steam weight flow could then be calculated, again assuming γ = 1.33, from

$$\dot{w}_j = \frac{g\, P_{t_j}\, A_{j_e}}{\left(\frac{A_{j_e}}{A_j^*}\right)\left(1 + \frac{\gamma-1}{2}\right)^{1/(\gamma-1)}\left(1 + \frac{\gamma-1}{2}\right)^{1/2}\left(\frac{R\, T_{t_j}}{\gamma}\right)^{1/2}} \qquad (1)$$

Tunnel Mach number, M_N, was obtained from reference 2 using the usual normal shock relationship, P_{t_1}/P_{t_2} versus M. For the given value of

M_N from reference 2 an area ratio A_N/A_N^* was obtained and the air weight flow calculated from equation (1) for $\gamma = 1.4$, i.e., from

$$\dot{w}_J = \frac{0.5309\ P_{t_N}\ A_N}{(A_N/A_N^*)\ (T_{t_N})^{1/2}} \tag{2}$$

The Mach number in the mixing tube could be obtained in two ways. The first method was to multiply A_{J_e}/A_J^* (obtained earlier) by A_m/A_J (known) to get A_m/A_J^*. Taking this value into the chart of A/A^* and assuming $\gamma = 1.33$ (since most of the fluid is steam), an approximate mixing tube Mach number, M_m, would result. The second method was to record the stagnation pressure (behind a normal shock) in the mixing tube, to ratio this to the ejector stagnation pressure, and to obtain M_m iteratively from the relation

$$\frac{P_{t_m}'}{P_{t_J}} = \left[\frac{(\gamma+1)\ M_m^2}{(\gamma-1)\ M_m^2 + 2}\right]^{\gamma/(\gamma-1)} \left[\frac{\gamma+1}{2\gamma M_m^2 - (\gamma-1)}\right]^{1/(\gamma-1)} \tag{3}$$

This equation assumes that, although adequate mixing of the air and steam has occurred, P_{t_J} is predominant (and unchanged), and the ratio of specific heats can be assumed to be still that of steam. In the final analysis, this equation can only be approximate; but values obtained by the two methods were surprisingly close, on occasion within ± 0.1.

Several of the important pressures were ratioed to P_{EX} and plotted in various combinations (see Discussion, Section 7.). The ratio of the weight flows was also calculated for use in evaluation of the performance of a given configuration.

7. DISCUSSION

The basic objective of the steam ejector study is to obtain the lowest possible tunnel operating pressure for the least amount of steam weight flow, keeping within the space confinements of the existing Trisonic Four-Foot Wind Tunnel. Since the tunnel operating pressure decreases as the downstream pressure is decreased, the original plan of attack was to check the static performance of several configurations and then to take the best of these and determine its tunnel-on performance. Consequently, static performance was obtained in the first test phase for a number of configurations, M_1, M_2, M_2S_1, M_2S_2, etc. The best static performance was obtained from M_2S_2 and M_2S_3 as shown in figure 7. Although the minimum pressure ratio (ejector suction to exhaust) was not as low as theory (figure 8) or similar experience (reference 3) would predict, it was sufficiently low at $M_J = 2.3$* that reductions

*In figure 8 the experimental data show a break in the curve somewhere above $A_m/A_J^* = 3.5$. It is believed that at the higher mixing tube Mach numbers the temperature of the steam is so low that condensation takes place. Instead of pumping a homogeneous gas, the ejector must now pump a mixture of gas and liquid, at a consequent loss of efficiency.

of starting and operating pressures by a factor of 4 or 5 were envisioned. However, tunnel starts were not achieved for any combination of M_1 or M_2S_x, even though a maximum of 100 psia tunnel total pressure was available. (Approximately 165 psia is required to start the tunnel without ejectors at M = 4.0.)

It is obvious, in retrospect, that the contraction ratio of M_2, which is A_m/A_{m_c} = 0.662, is too small. In addition, references 4 and 5 state that mixing tube L/D ratios between 4 and 8 produce the best results. Since L/D = 8 results in a mixing tube length that is greater than the allowable length of the complete ejector system, it was not considered further. However, mixing tube sections with L/D of 2.0 and 4.0 were constructed for use alone or in tandem. Another contraction section with A_m/A_{m_c} = 0.808 (and an additional L/D = 2.19) was constructed for use with the new mixing tubes.

The new mixing tube configurations were tested during the second phase. The static minimum P_c/P_a value at M_j=2.3 was of the same magnitude as those attained during the first phase of testing, although at the other ejector Mach numbers the performance was not as good. The minimum value of P_c/P_a occurred at higher values of P_{t_j}/P_a than in Phase One. The best static performance, shown in figure 9, was achieved with configuration $M_1M_3S_{L_4}$, which has a total mixing tube L/D = 6.19 (including the contraction section, M_3). During this second phase, the tunnel was started for all configurations of $M_1S_{L_x}$ and $M_1M_3S_{L_x}$ for $1.8 < M_j < 2.8$. Tunnel starts were also obtained with configuration M_1M_3 at M_j = 2.8. Unfortunately, it is meaningless to present plots of P_c/P_a versus P_{t_j}/P_a with tunnel flow as was done in reference 3. Whereas in that tunnel the air flow was dumped into a plenum downstream of the supersonic diffuser, where P_c was truly a stagnation pressure, in our case the P_c measurement was made only by a total pressure tube downstream of a number of oblique shocks standing in the supersonic diffuser.

Notwithstanding the lack of a true measurement of stagnation pressure upstream of the ejector, adequate evaluation of the ejector performance can be obtained by studying curves of minimum tunnel operating pressure versus ejector total pressure. Figures 10 and 11 are composite plots showing the effect of mixing tube length on these pressures both with (figure 10) and without (figure 11) mixing tube contraction, M_3. It can be seen that the lowest tunnel total pressure (46 psia) occurs for configurations $M_1S_{L_6}$ (total L/D = 6.0) and $M_1M_3S_{L_4}$ (total L/D = 6.19) at M_j = 2.3. Ejector steam weight flow required is about 4.1 pounds per second. The tunnel starting pressure for these configurations was approximately 55 psia. Because the steam requirements were considered to be too high, investigation of operating pressures at lower weight flows was desired. Figures 12 and 13 show curves of tunnel total pressure vs. ejector steam weight flow for configurations $M_1S_{L_6}$ and $M_1M_3S_{L_4}$, respectively. It is clearly seen

from the slope of the curves in figure 12 that the sacrifice in minimum operating pressure is very great for any appreciable savings in ejector weight flow. In figure 13, however, at M_j = 1.91 there is a minimum point which provides a compromise between weight flow and operating pressure. Tunnel starting pressure was 62 psia with a minimum operating pressure of 54 psia and ejector steam flow 3.7 pounds per second, about 10% reduction in steam weight flow.

The 10% savings in weight flow was deemed to be insufficient, since original cost estimates for the Four-Foot Tunnel modifications were based on a steam power plant providing only about 700 pounds of steam per second (2.7 pounds per second in the 1/16 scale pilot tunnel). Analysis of the problem indicated that reducing the ejector exit area might effect a substantial decrease in steam flow. The most practical method of decreasing the area was by electroplating the existing ejector nozzle (see Ejector Description, Section 3.). The final ejector area amounted to a 26.3% reduction from the original. The static performance of the system was not as good as that of the first two phases. The best static configuration was $M_1M_3S_{L4}$ (total L/D = 6.19); figure 14 illustrates the data obtained. Data from the second test phase are also shown for comparison. Air-off performance notwithstanding, with tunnel flow, lower minimum operating pressures at lesser weight flows were achieved. Figure 15 is a composite plot of all configurations tested in the third phase. It can be seen that the lowest tunnel operating pressure was obtained at P_{t_j} = 118.5 psia, which was the highest attainable steam pressure. A plot of tunnel total pressure versus steam weight flow is shown in figure 16; the ejector weight flow for the lowest tunnel operating pressure, which occurs at M_j = 2.49, is 3.7 pounds per second. The minimum tunnel pressure is now 41 psia, starting pressure 50 psia. Thus, an improvement in performance over phase two tests was attained with the reduced-area ejector, viz. 11% in tunnel operating pressure and 10% in steam weight flow, but it is not as good as expected.

In figure 16, interesting minima are seen in the curves for M_j of 2.02 and 2.22. At M_j = 2.22, minimum P_{t_N} is 45 psia at 3.55 pounds of steam per second (a 14% reduction from phase two weight flows with nearly the same tunnel pressure). At M_j = 2.02, minimum P_{t_N} is 50 psia at 3.4 pounds per second (a 17% reduction but at higher tunnel pressure than phase two). A fairly important disadvantage of the reduced-area ejector that was brought out in these tests is that approximately 25% higher steam stagnation pressures were required to operate than for the original ejector area. This can be seen even in the static performance (figure 14). Reference 6 states that, for a given A_{j_e}/A_j^*, optimum P_{t_j}/P_c increases as A_m/A_j^* is increased. In addition, the effect of changing A_{j_e}/A_j^* (or M_j) is secondary to the change of A_m/A_j^*. This becomes apparent when one considers that the mixing tube acts somewhat as a tunnel and, to start it and maintain supersonic flow, a minimum pressure ratio is required dependent upon mixing tube Mach number (or area ratio). Mixing tube Mach number M_m

during phase two was about 3.0 compared to 3.5 during phase three. This also explains why the best performance in phase three was achieved using the contraction section, whereas in phase two it was not as important. The point above which a diffuser begins to show advantages, efficiency-wise, is usually considered to occur between Mach numbers 2.5 and 3.0.

The next step in the test program called for investigation of additional mixing tube geometrical effects. However, further testing of the steam ejector was denied by two occurrences: first, the cancellation of the proposed arc-heated tunnels which required a steam plant; and secondly, somewhat later, the expiration of the IR&D funds for the project. This cancellation of the arc-heated tunnels and attendant steam plant had the effect of changing the ejector motive source from steam to air. The 1/16-scale pilot tunnel was consequently moved from the Torrance location to DAL, where it could be set up as a part of the Fluid Mechanics Laboratory with 135 psia air available for both the ejector and tunnel supplies. Work was initiated to determine the best ejector and mixing tube geometries to use with an air-driven system and also to determine how much total air would be required, since this would influence the size and cost of the additional air storage reservoirs. In order to optimize run time, which could be limited by either the ejector or the tunnel, some compromise might be needed in tunnel performance. In order to determine which configurations might best be investigated, total weight flow (steam plus air) data from phases two and three were plotted versus tunnel total pressure for the two best mixing tube configurations with the original ejector and the single best configuration with the reduced-area ejector. These cases are shown in figures 17, 18 and 19. Figure 17 shows that, for mixing tube configuration M_1S_{L6}, the sacrifice in tunnel performance is too great to justify any attempt to decrease total weight flow below 4.8 pounds per second. In figure 18, the aforementioned $M_j = 1.91$ tests on configuration $M_1M_3S_{L4}$ could be an acceptable compromise. This same configuration with the reduced-area ejector (shown in figure 19) presently appears to be the best starting point for air investigations because it has several potential compromise points. If lowest operating pressure is desired, regardless of run time, then an M_j of 2.49 (or higher) appears best. If long run time is important, then Mach number 2.02 is better. Of course, replacing steam by air will undoubtedly increase the required mass flow, but it is believed that the shapes of the curves will not change significantly. Before air ejector tests could be made, funds for the project had expired.

Prior to the expiration of the IR&D funds, fabrication had been started on a clustered-nozzle ejector configuration to replace the annular ejector. The purpose of testing such a configuration is that, if it were successful, it would greatly simplify the final Four-Foot Tunnel rework. Fabrication of the clustered-nozzle ejector configuration was halted prior to completion.

8. RESULTS AND CONCLUSIONS

Results of the three test phases of an annular steam ejector study, including the effect of mixing tube geometry, are as follows:

1. The existing Four-Foot Tunnel subsonic diffuser is not an acceptable mixing tube configuration.

2. Contraction downstream of the constant-diameter mixing tube is desirable at mixing tube Mach numbers in excess of 3.0.

3. The amount of contraction may be determined by diffuser theory and has a considerable effect on ejector performance.

4. Mising tube length-to-diameter ratio of approximately six, either with or without contraction, proved best in tests with a large ejector exit area. Reductions of about 3:1 and 2.5:1 from Four-Foot Tunnel starting and running pressures, respectively, were achieved.

5. Mixing tube length-to-diameter ratio of 6.19, including contraction, provided reductions from Four-Foot Tunnel starting and running pressures of about 3.3:1 and 2.8:1 when the ejector exit area was reduced by 25%.

6. Steam weight flows would scale up to 1050 and 950 pounds per second in the Four-Foot Tunnel for items 4 and 5 above, respectively. Sacrifices on the order of 15% in starting and running pressure reductions would lower the steam requirements to 950 and 875 pounds per second.

Results of the tests of the annular steam ejector and several mixing tube configurations gave rise to some conclusions which may be applicable to the design of the ejector system proposed for the Trisonic Four-Foot Wind Tunnel. The fact that air, rather than steam, will probably be the ejector motive source dictates that caution be used in applying these conclusions directly to the ejector design.

1. Mixing tube length-to-diameter ratio should be about six.

2. The contraction section should not be used because of its complexity, and mixing tube Mach number should be less than 3.0.

3. Ejector Mach number should be adjustable, within narrow limits of 2.3 to 2.5, to provide better performance.

4. Mixing tube area should be approximately five times the minimum throat area for best efficiency and lowest weight flows.

9. REFERENCES

1. Murphy, J. S., and H. Buning, Theory and Design of a Variable Mach Number Corner Nozzle; University of Michigan WTM-221, Progress Report No. 1, April-December 1951.

2. Ames Research Staff, Equations, Tables, and Charts for Compressible Flow; NACA Report 1135, 1953.

3. Howell, Robert R., Experimental Operating Performance of a Single-Stage Annular Air Ejector; NASA TN D-23, October 1959.

4. Sheldon, J. A., and R. H. Hunczak, An Analytical and Experimental Evaluation of a Two-Stage Annular Air Ejector for High-Energy, Wind Tunnels; NASA TN D-1215, June 1962

5. McClintock, F. A., and J. H. Hood, "Aircraft Ejector Performance", Jour. Aer. Sci., Volume 13, Number 11, p. 559, November 1946.

6. Barton, D. L., and D. Taylor, An Investigation of Ejectors Without Induced Flow - Phase I; AEDC-TN-59-145, December 1959.

THREE-INCH PILOT TUNNEL AND STEAM EJECTOR SYSTEM

FIGURE 1

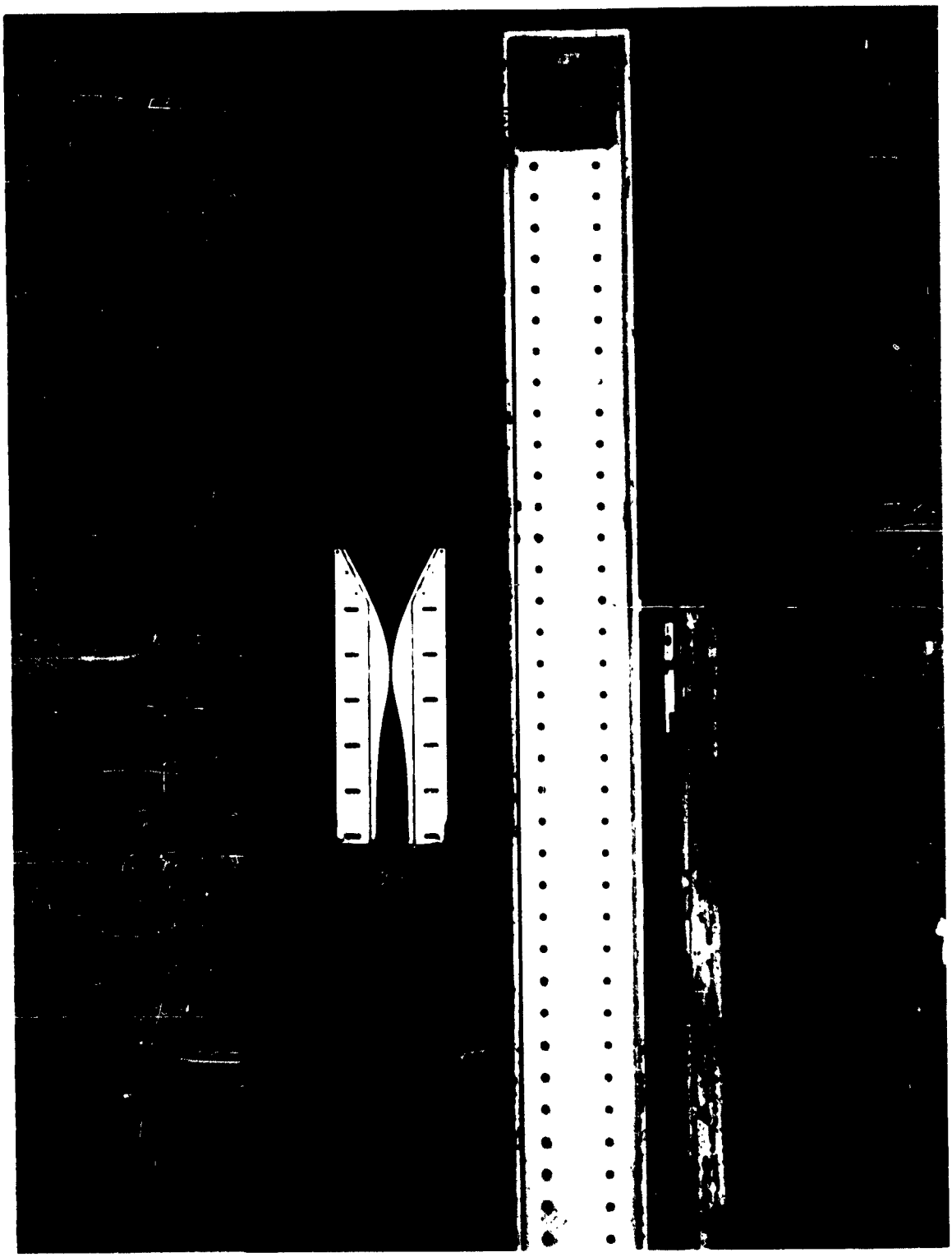

THREE-INCH PILOT TUNNEL DIFFUSER, NOZZLE SECTION, AND STILLING CHAMBER (L TO R)

FIGURE 2

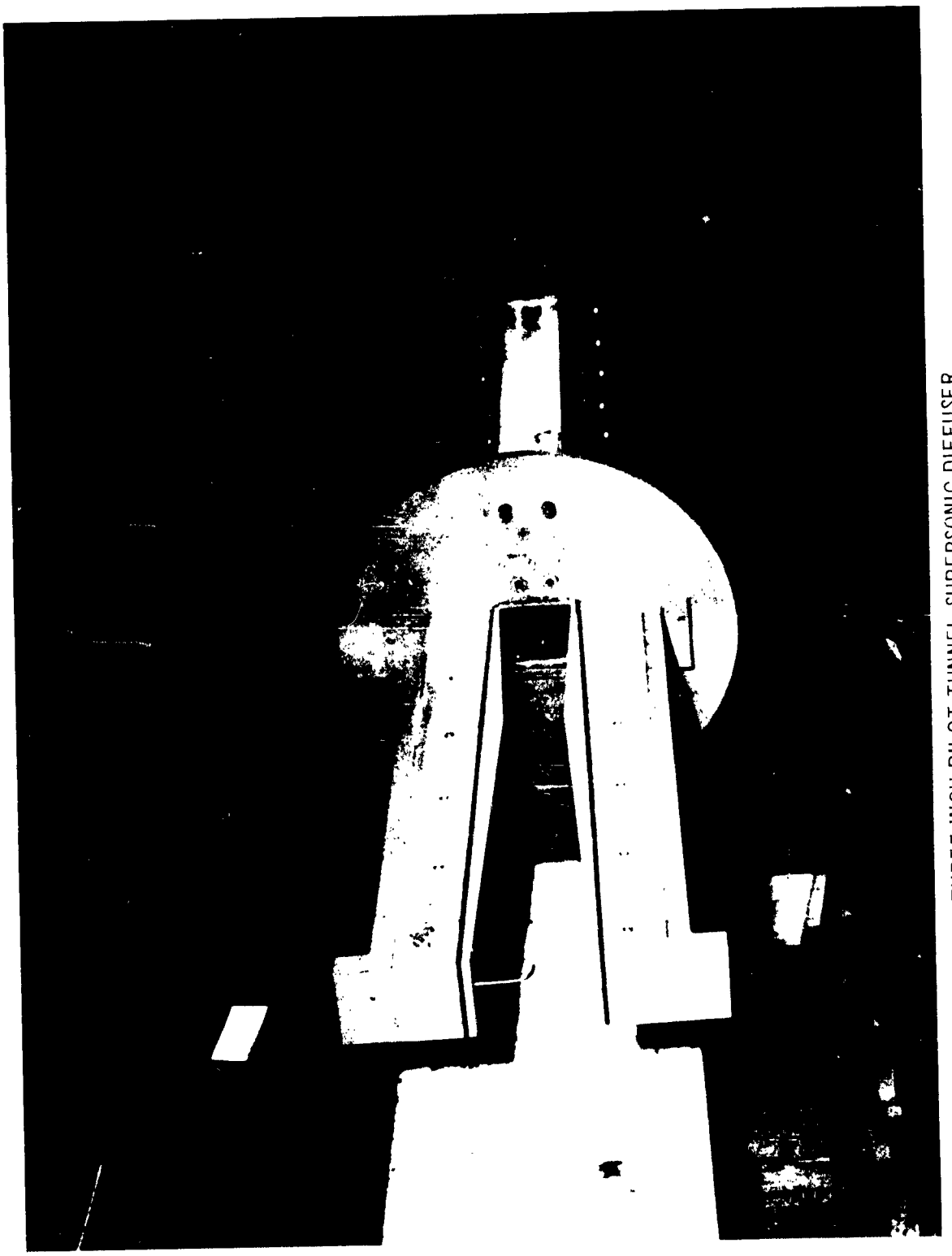

THREE-INCH PILOT TUNNEL SUPERSONIC DIFFUSER

FIGURE 3

STEAM EJECTOR CONTOURED NOZZLE PARTS

FIGURE 4

CALIBRATION OF STEAM EJECTOR MACH NUMBER AS A FUNCTION OF THROAT CONTROL DISTANCE

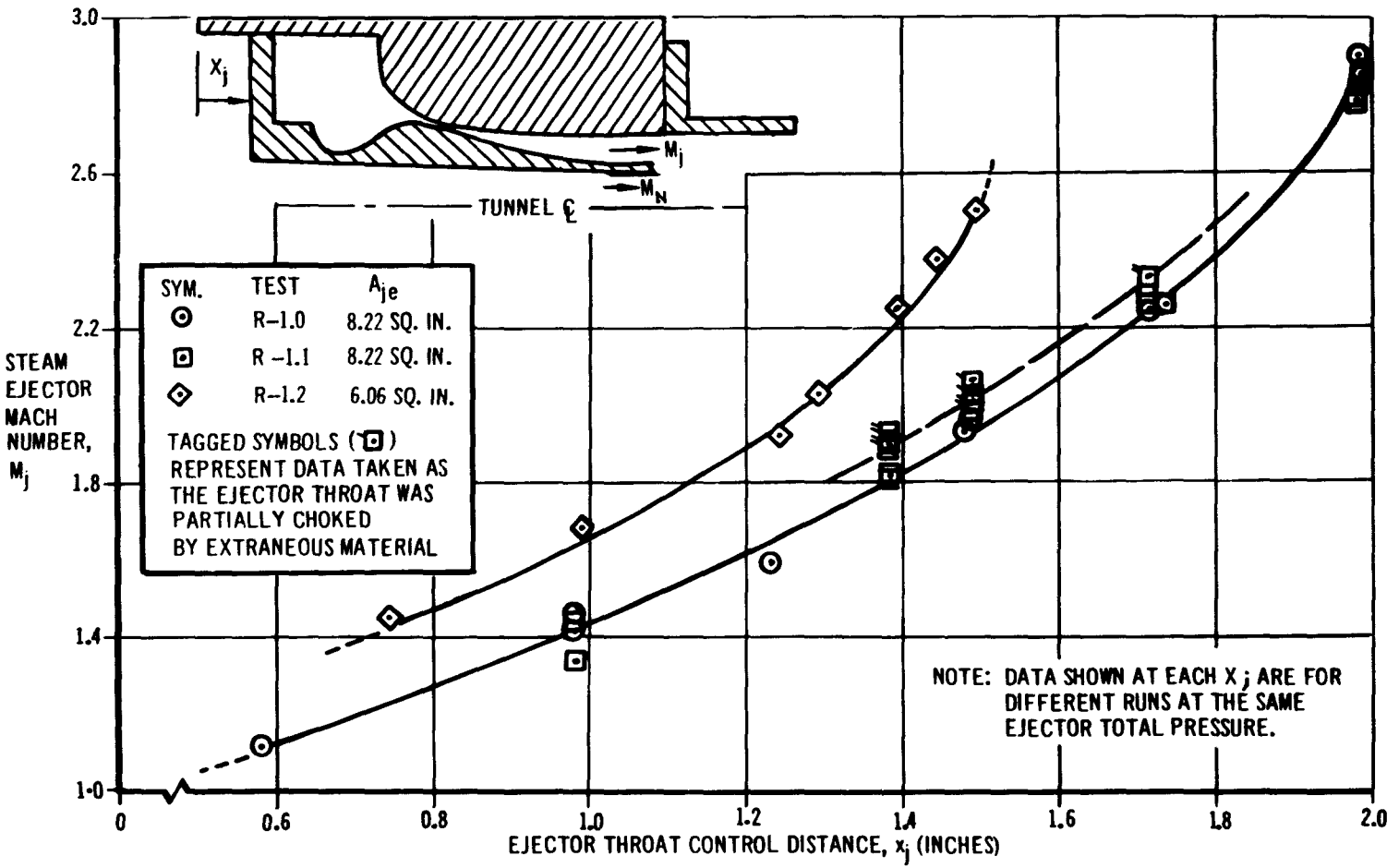

FIGURE 5

MIXING TUBE CONFIGURATIONS

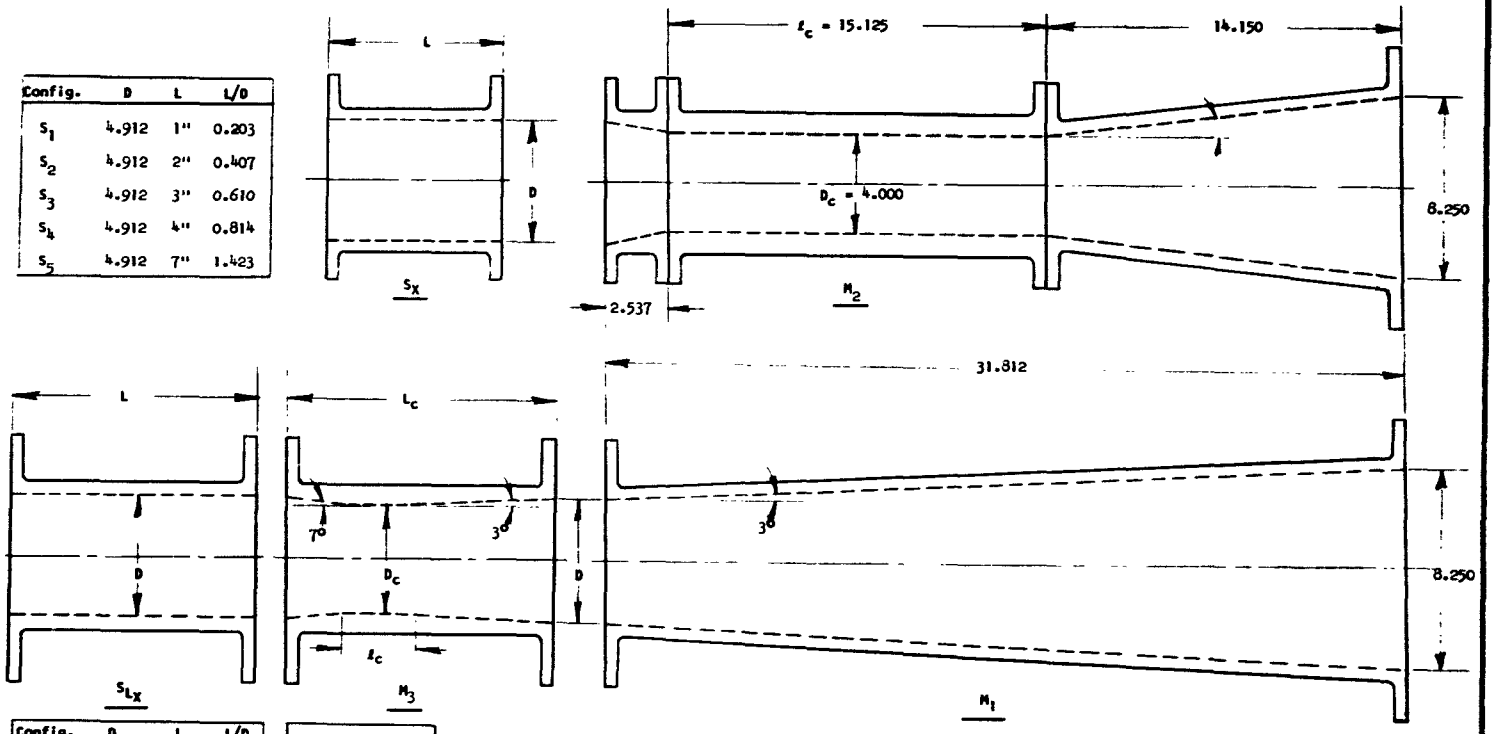

Config.	D	L	L/D
S_1	4.912	1"	0.203
S_2	4.912	2"	0.407
S_3	4.912	3"	0.610
S_4	4.912	4"	0.814
S_5	4.912	7"	1.423

Config.	D	L	L/D
S_{L_2}	4.912	9.812	1.995
S_{L_4}	4.912	19.625	3.998
S_{L_6}	4.912	29.438	5.992

D	= 4.912
D_c	= 4.412
L_c	= 10.75
ℓ_c	= 3.110

Note: All dimensions in inches

FIGURE 6

EFFECT OF EJECTOR MACH NUMBER AND MIXING TUBE LENGTH ON EJECTOR SUCTION PRESSURE VS. EJECTOR TOTAL PRESSURE

(NO TUNNEL FLOW)

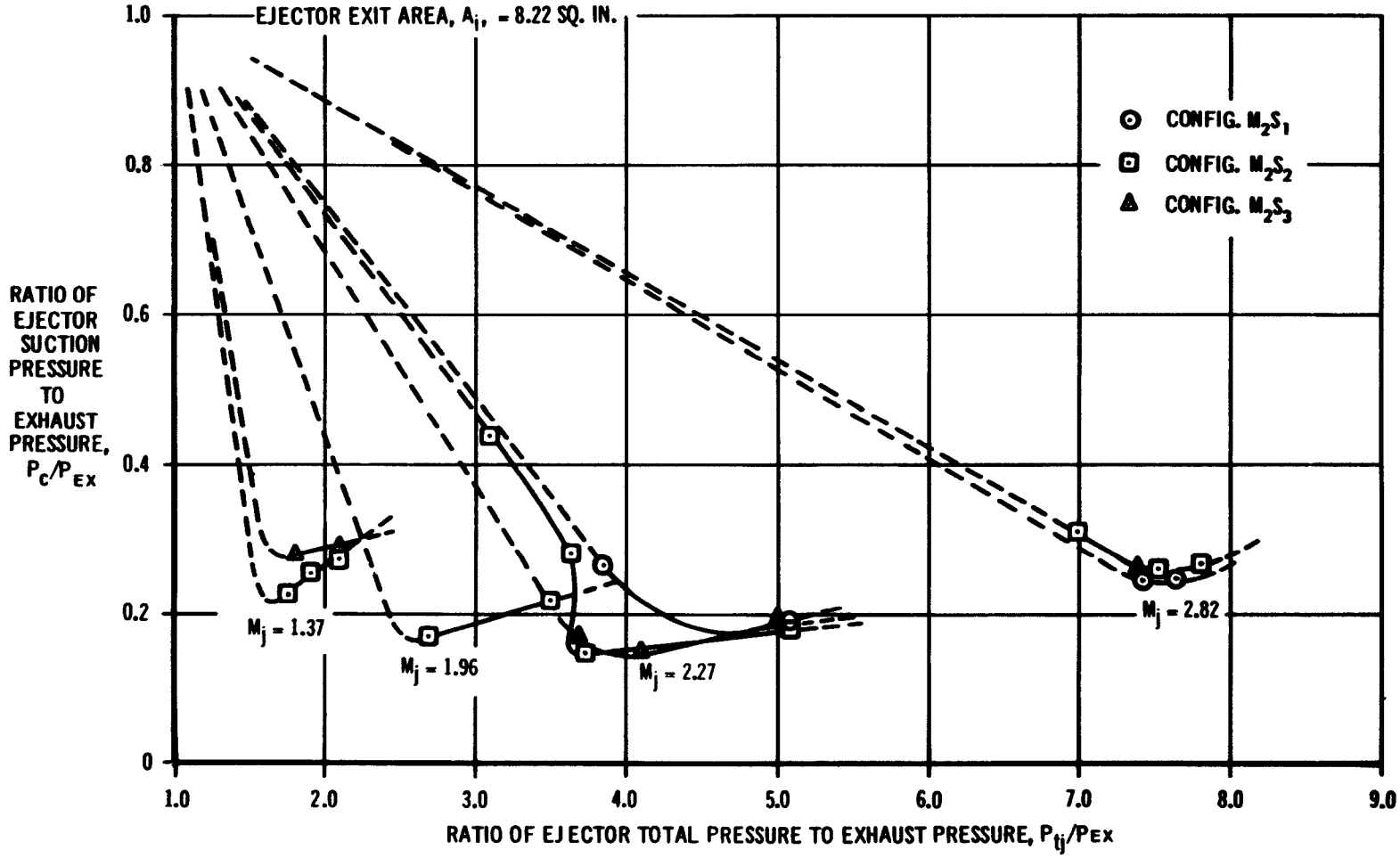

FIGURE 7

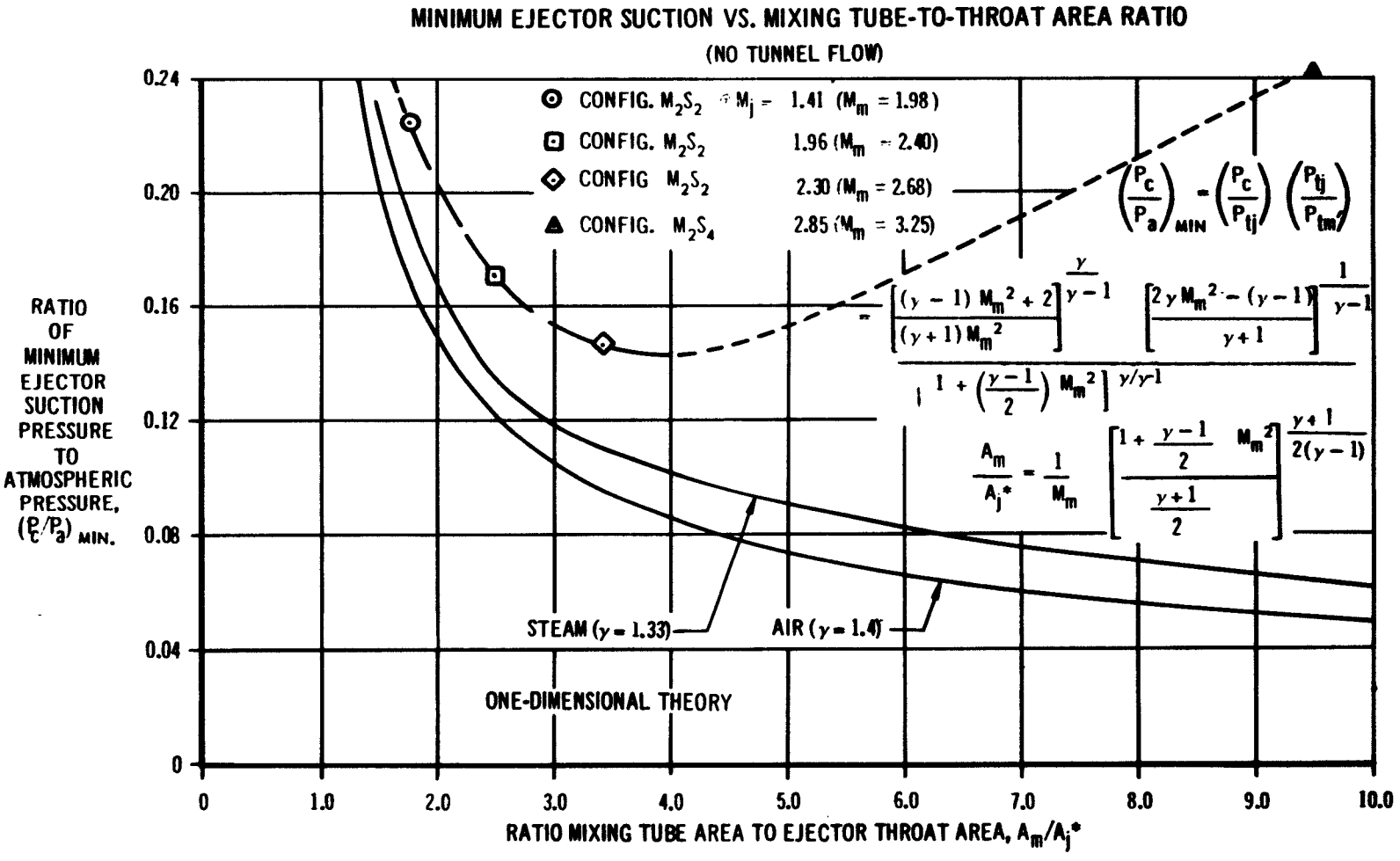
MINIMUM EJECTOR SUCTION VS. MIXING TUBE-TO-THROAT AREA RATIO
(NO TUNNEL FLOW)
CONFIG. M_2S_2 M_j = 1.41 (M_m = 1.98)
CONFIG. M_2S_2 1.96 (M_m = 2.40)
CONFIG M_2S_2 2.30 (M_m = 2.68)
CONFIG. M_2S_4 2.85 (M_m = 3.25)
$\left(\frac{P_c}{P_a}\right)_{MIN} = \left(\frac{P_c}{P_{tj}}\right)\left(\frac{P_{tj}}{P_{tm}}\right)$
$= \frac{\left[\frac{(\gamma-1)M_m^2+2}{(\gamma+1)M_m^2}\right]^{\frac{\gamma}{\gamma-1}} \left[\frac{2\gamma M_m^2-(\gamma-1)}{\gamma+1}\right]^{\frac{1}{\gamma-1}}}{\left[1+\left(\frac{\gamma-1}{2}\right)M_m^2\right]^{\gamma/\gamma-1}}$
$\frac{A_m}{A_j^*} = \frac{1}{M_m}\left[\frac{1+\frac{\gamma-1}{2}M_m^2}{\frac{\gamma+1}{2}}\right]^{\frac{\gamma+1}{2(\gamma-1)}}$
STEAM (γ = 1.33)
AIR (γ = 1.4)
ONE-DIMENSIONAL THEORY
RATIO OF MINIMUM EJECTOR SUCTION PRESSURE TO ATMOSPHERIC PRESSURE, $(P_c/P_a)_{MIN.}$
0.24
0.20
0.16
0.12
0.08
0.04
0
0
1.0
2.0
3.0
4.0
5.0
6.0
7.0
8.0
9.0
10.0
RATIO MIXING TUBE AREA TO EJECTOR THROAT AREA, A_m/A_j^*

FIGURE 8

EJECTOR SUCTION PRESSURE VS. EJECTOR TOTAL PRESSURE

FOR MIXING TUBE CONFIGURATION $M_1M_3S_{L4}$
(NO TUNNEL FLOW)

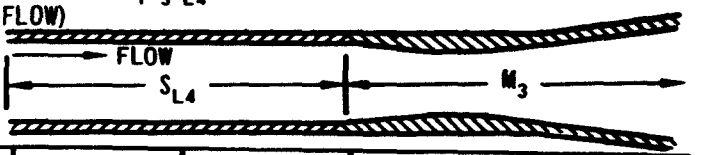

EJECTOR EXIT AREA, A_{je}, = 8.22 SQ. IN.

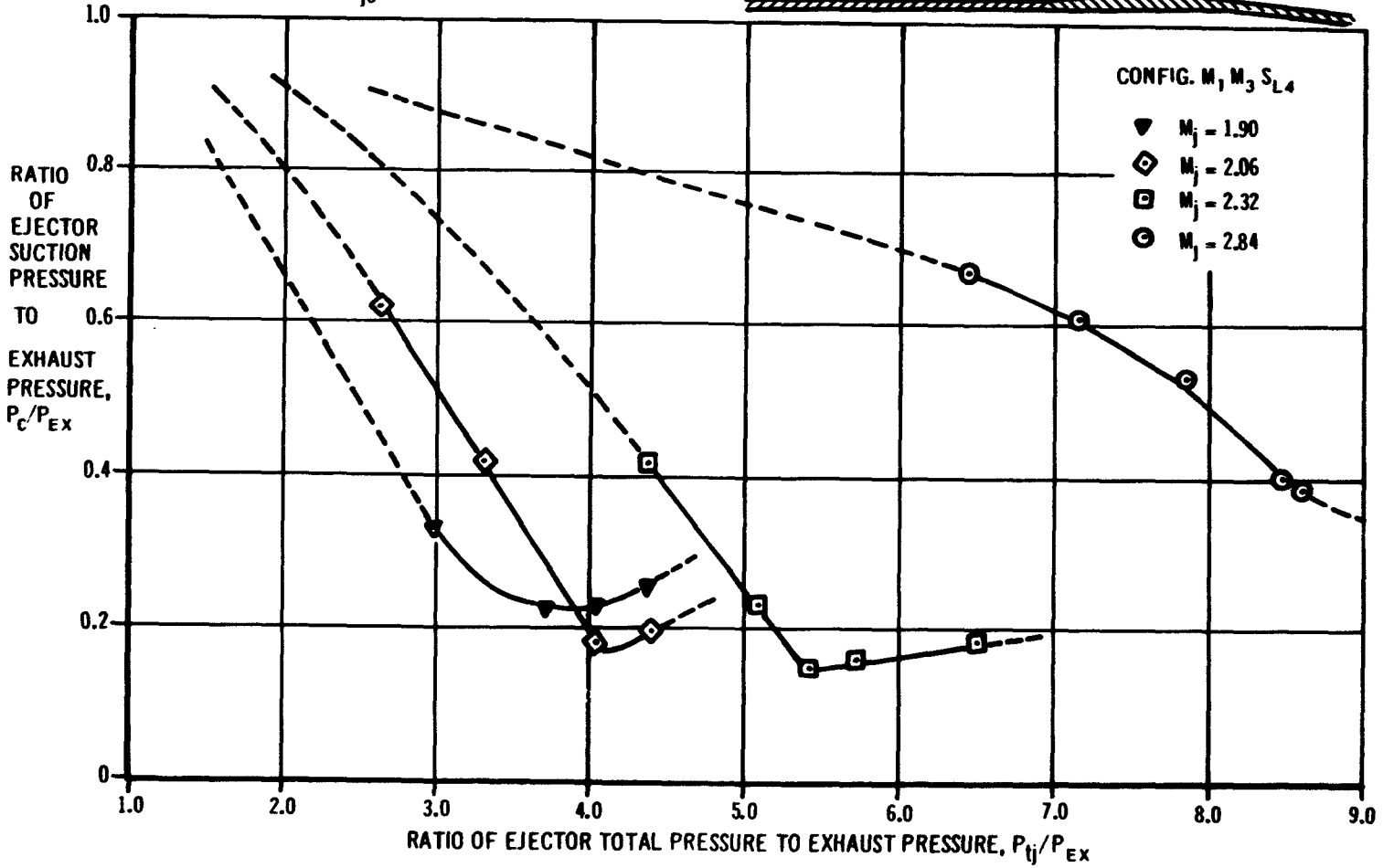

FIGURE 9

EFFECT OF MIXING TUBE LENGHT ON TUNNEL TOTAL PRESSURE VS. EJECTOR TOTAL PRESSURE

FOR VARIOUS EJECTOR MACH NUMBERS
TUNNEL MACH NUMBER - 4.0
(MIXING TUBE CONTRACTION RATIO = : 0.808)

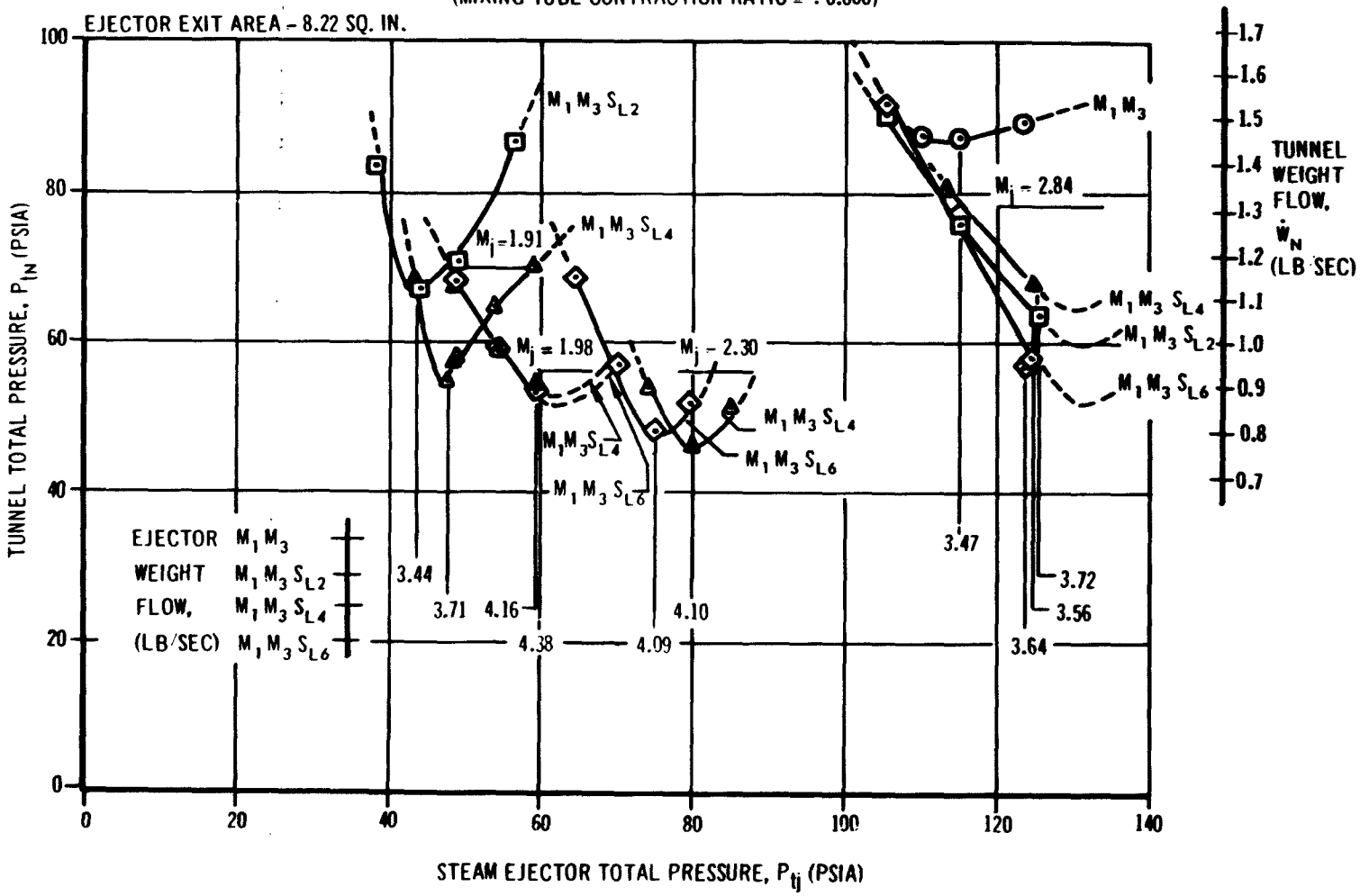

FIGURE 10

EFFECT OF MIXING TUBE LENGTH ON TUNNEL TOTAL PRESSURE VS. EJECTOR TOTAL PRESSURE

FOR VARIOUS EJECTOR MACH NUMBERS
TUNNEL MACH NUMBER – 4.0
EJECTOR EXIT AREA = 8.22 SQ. IN. (NO MIXING TUBE CONTRACTION)

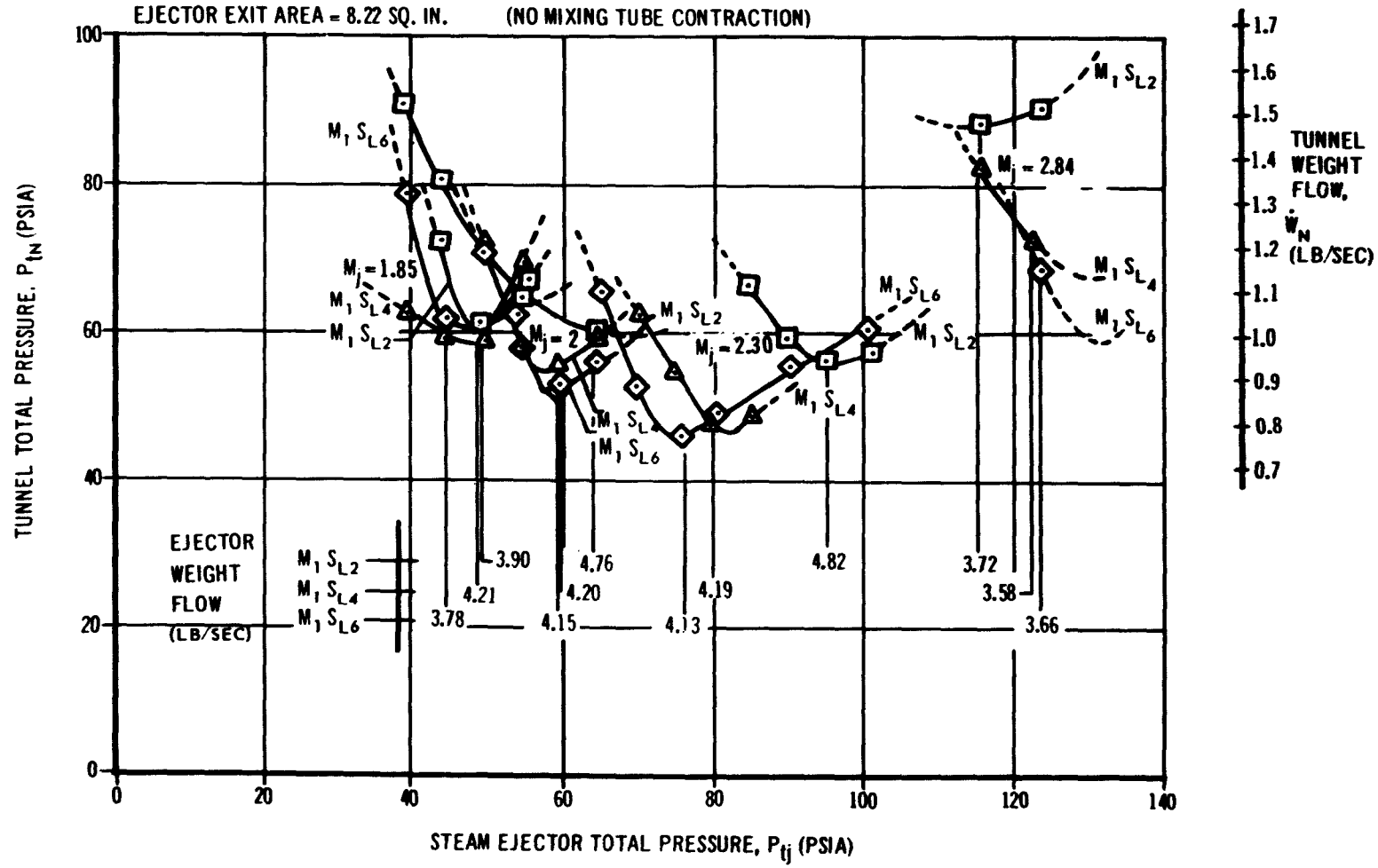

FIGURE 11

EFFECT OF EJECTOR MACH NUMBER ON MINIMUM TUNNEL TOTAL PRESSURE VS. EJECTOR WEIGHT FLOW

FOR MIXING TUBE CONFIGURATION M_1 S_{L_6}

TUNNEL MACH NUMBER = 4.0

EJECTOR E XIT AREA = 8.22 SQ. IN.

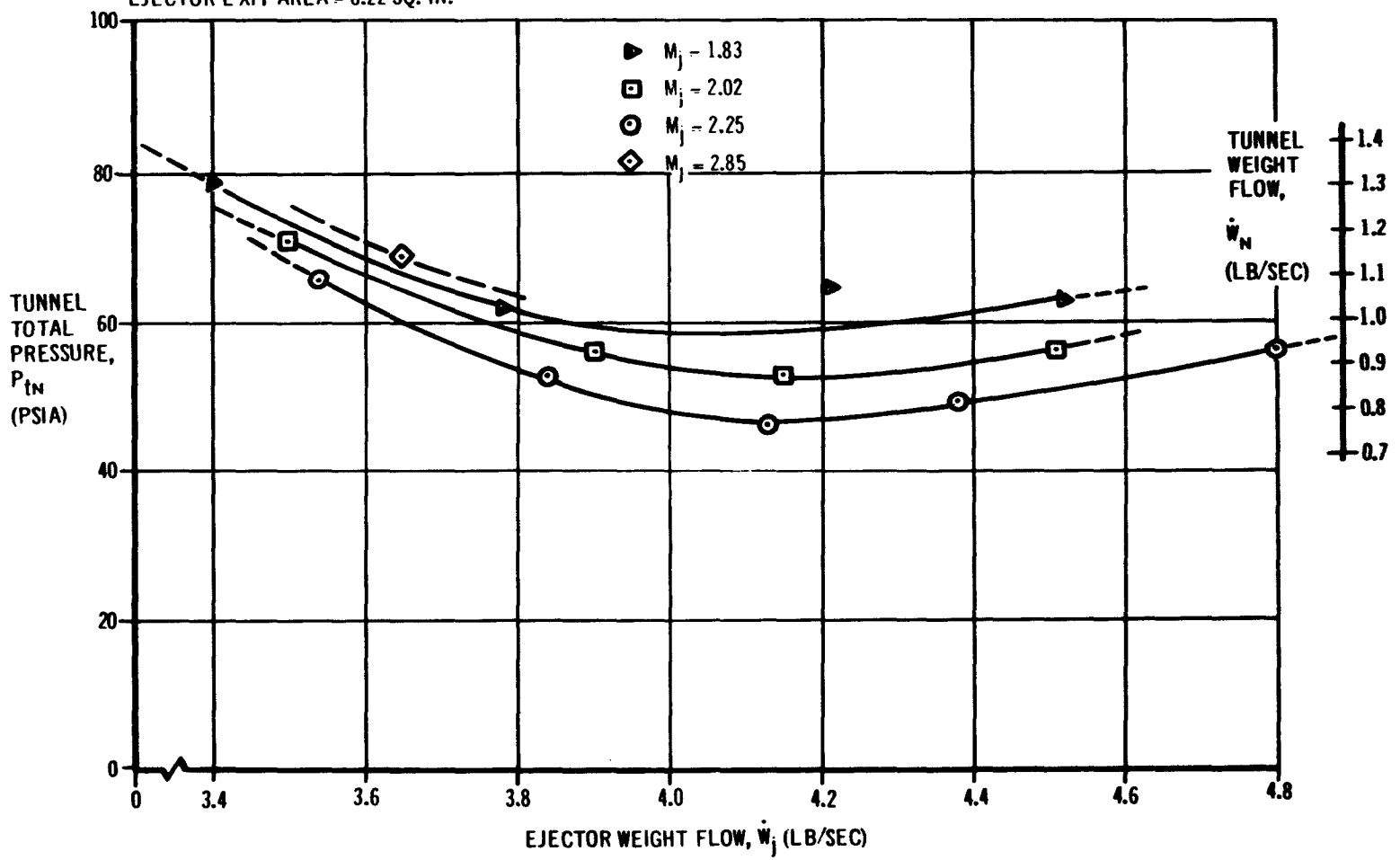

FIGURE 12

EFFECT OF EJECTOR MACH NUMBER ON MINIMUM TUNNEL TOTAL PRESSURE VS. EJECTOR WEIGHT FLOW

FOR MIXING TUBE CONFIGURATION $M_1 M_3 S_{L_4}$
TUNNEL MACH NUMBER = 4.0

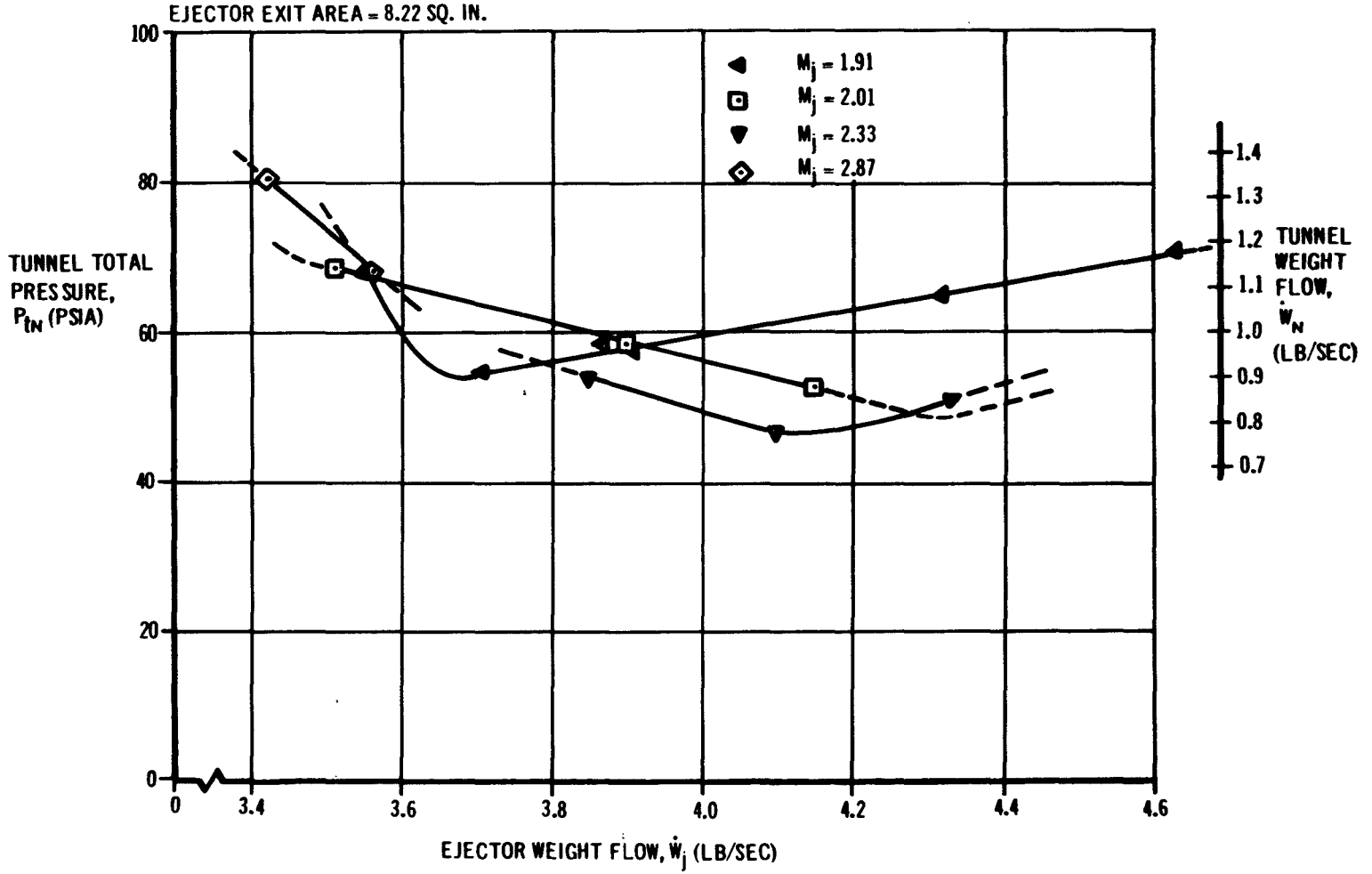

FIGURE 13

EJECTOR SUCTION PRESSURE VS. EJECTOR TOTAL PRESSURE

FOR MIXING TUBE CONFIGURATION $M_1 M_3 S_{L_4}$

(NO TUNNEL FLOW)

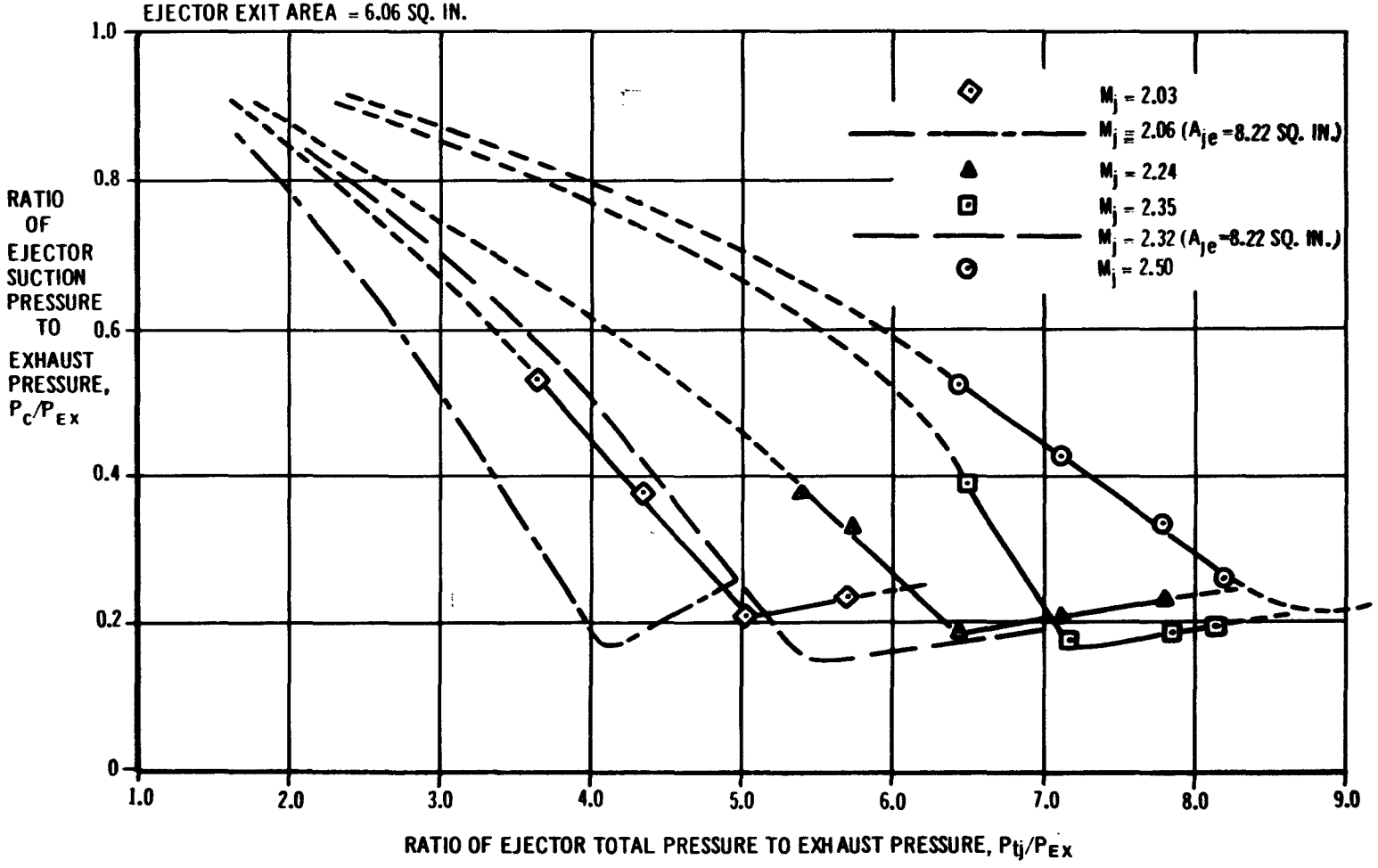

FIGURE 14

EFFECT OF MIXING TUBE LENGTH AND CONTRACTION ON MINIMUM TUNNEL TOTAL PRESSURE VS. EJECTOR TOTAL PRESSURE

FOR VARIOUS EJECTOR MACH NUMBERS

TUNNEL MACH NUMBER = 4.0

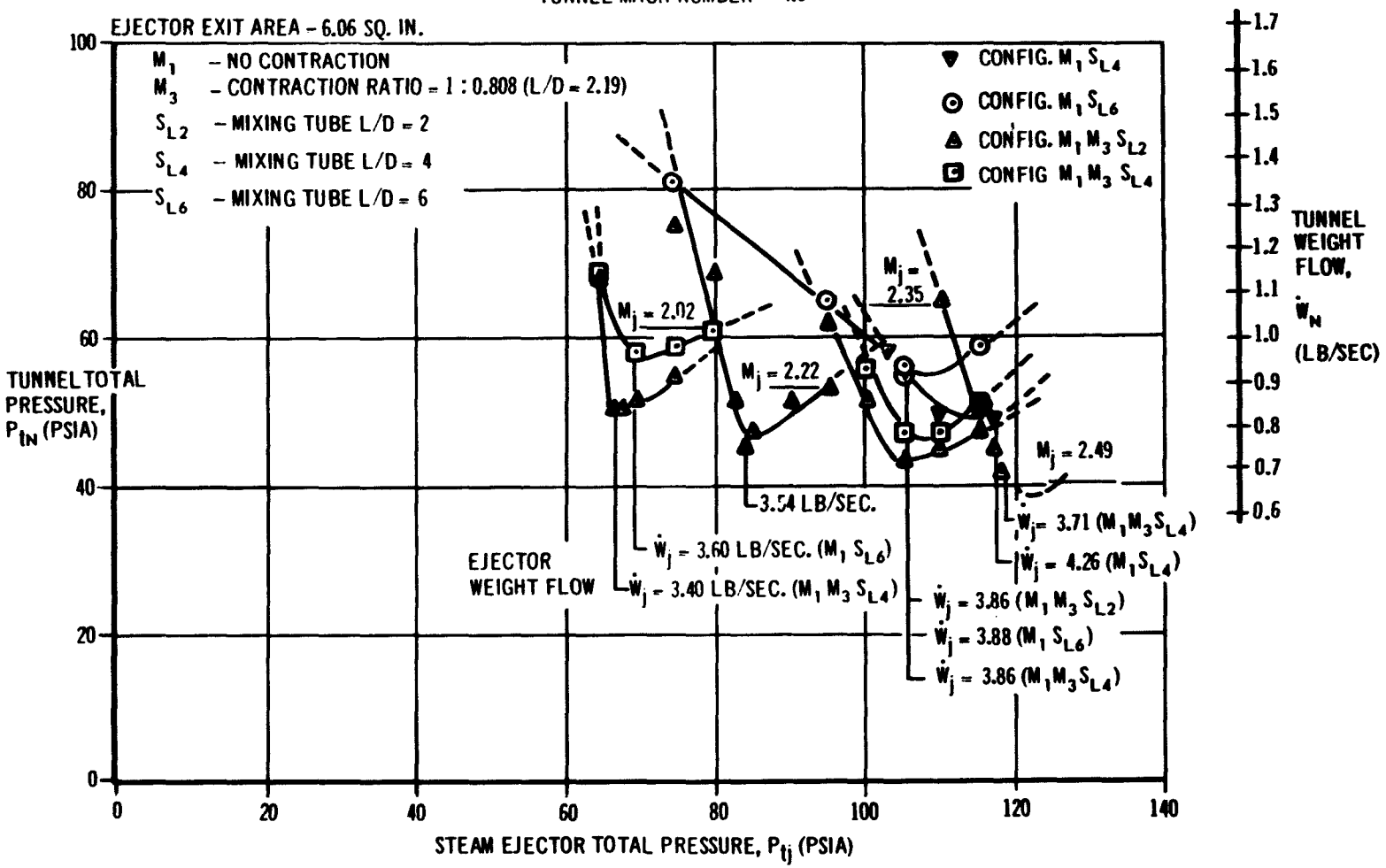

FIGURE 15

EFFECT OF EJECTOR MACH NUMBER ON MINIMUM TUNNEL TOTAL PRESSURE VS EJECTOR WEIGHT FLOW

FOR MIXING TUBE CONFIGURATION $M_1M_3S_{L4}$

TUNNEL MACH NUMBER = 4.0

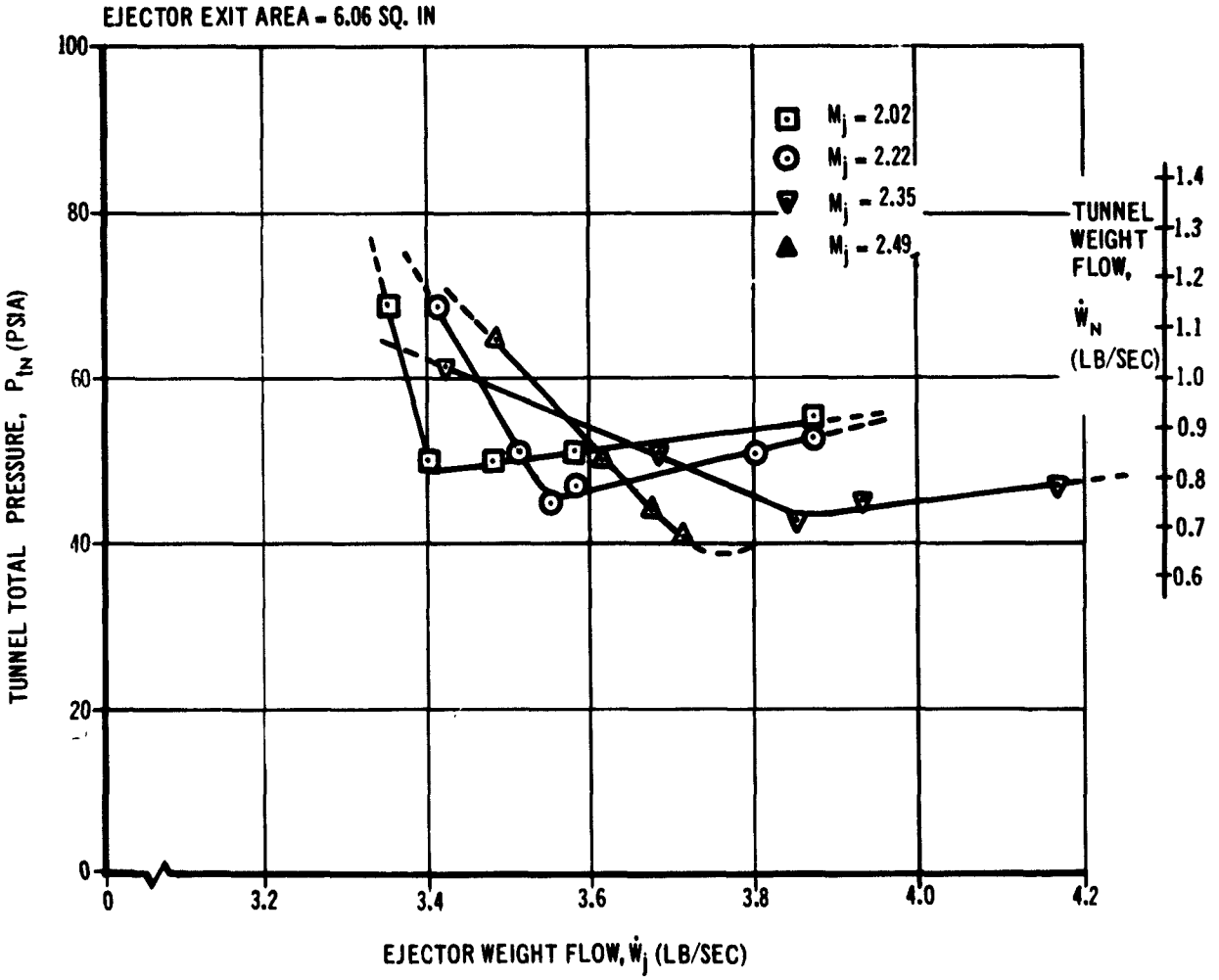

FIGURE 16

EFFECT OF EJECTOR MACH NUMBER ON TOTAL WEIGHT FLOW VS MINIMUM TUNNEL TOTAL PRESSURE

FOR MIXING TUBE CONFIGURATION $M_1 S_{L6}$
TUNNEL MACH NUMBER - 4.0

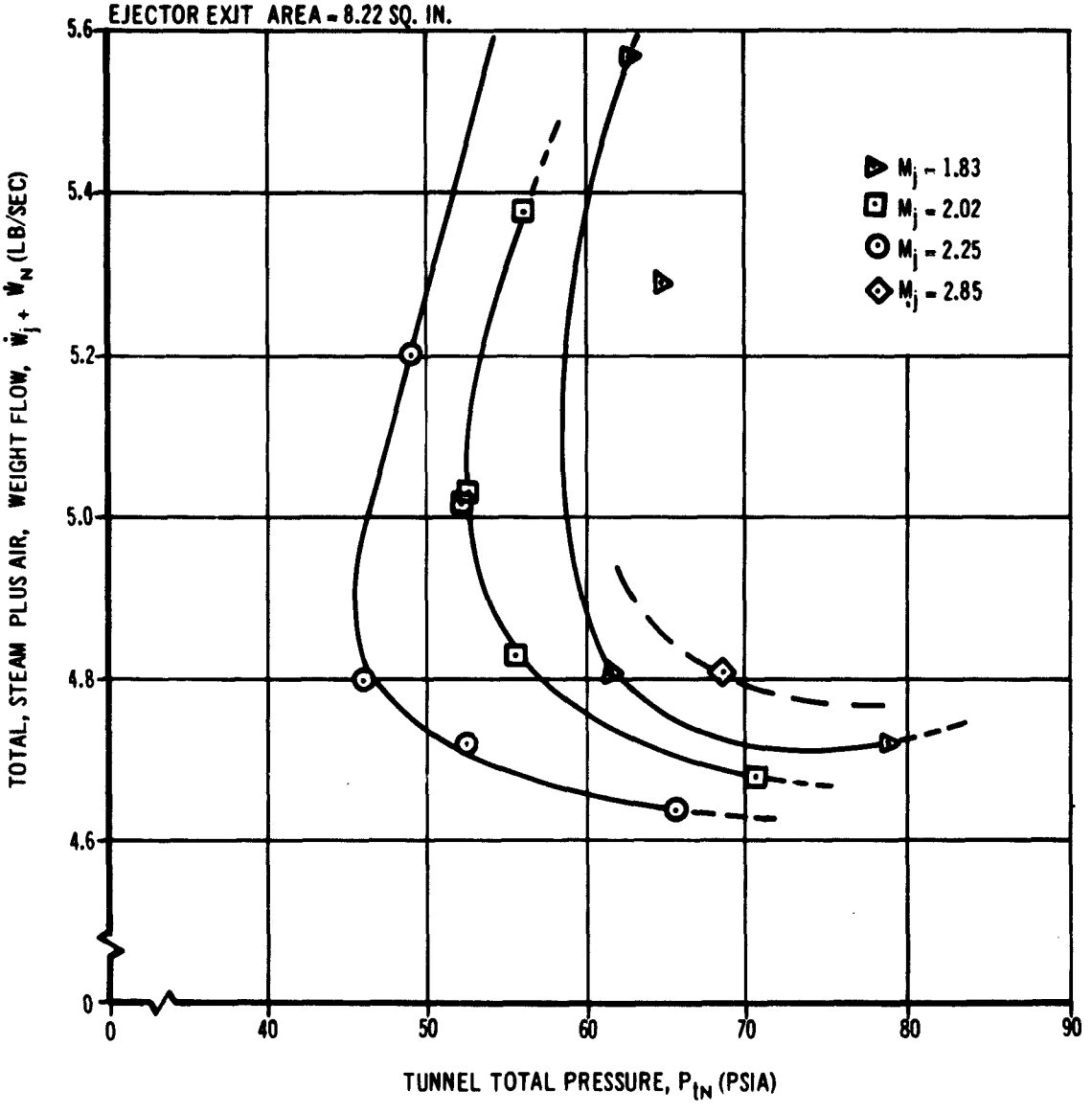

FIGURE 17

EFFECT OF EJECTOR MACH NUMBER ON TOTAL WEIGHT FLOW VS, MINIMUM TUNNEL TOTAL PRESSURE

FOR MIXING TUBE CONFIGURATION $M_1M_3S_{L4}$
TUNNEL MACH NUMBER = 4.0

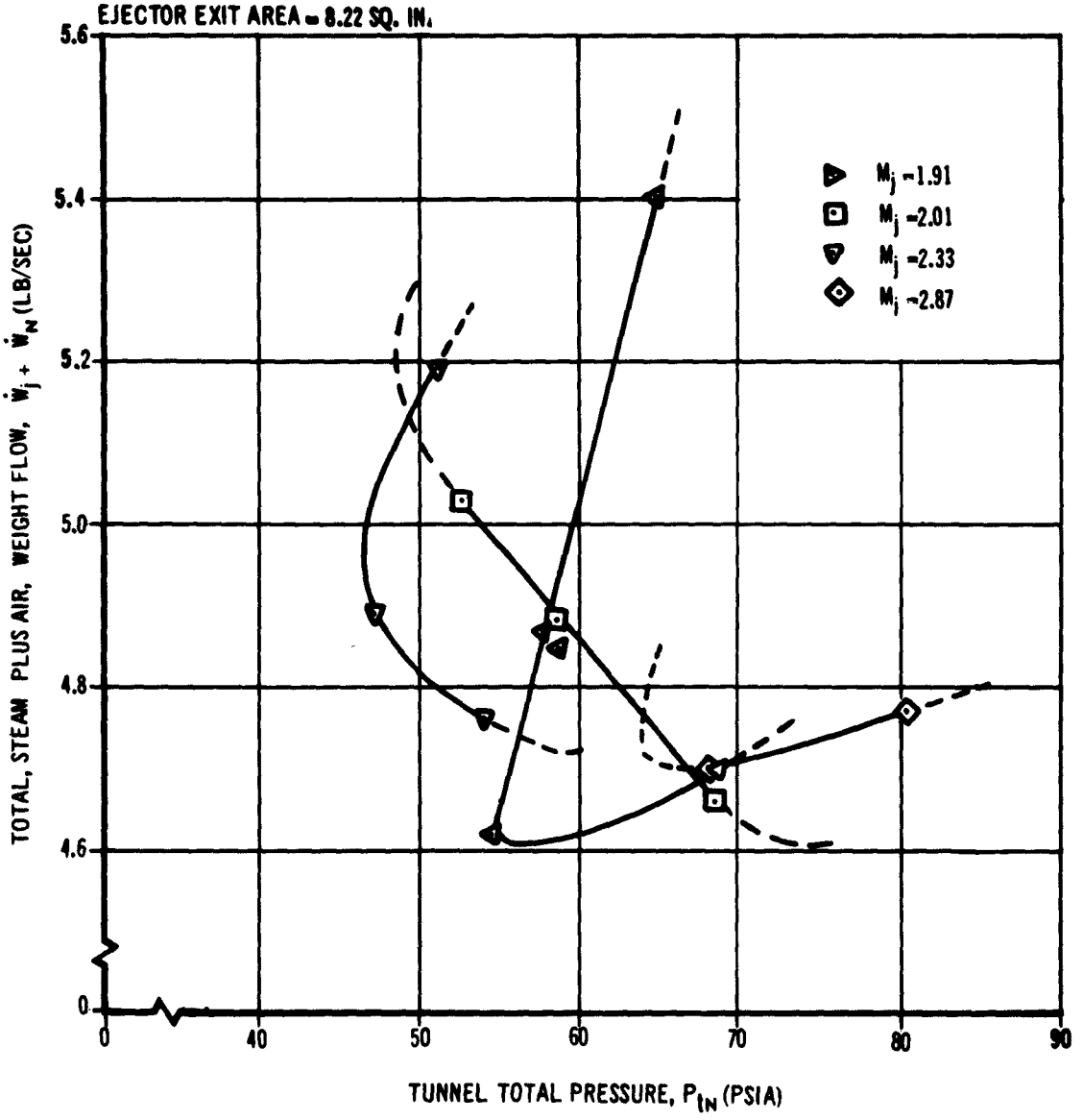

FIGURE 18

EFFECT OF EJECTOR MACH NUMBER ON TOTAL WEIGHT FLOW VS. MINIMUM TUNNEL TOTAL PRESSURE

FOR MIXING TUBE CONFIGURATION $M_1 M_3 S_{L4}$
TUNNEL MACH NUMBER = 4.0

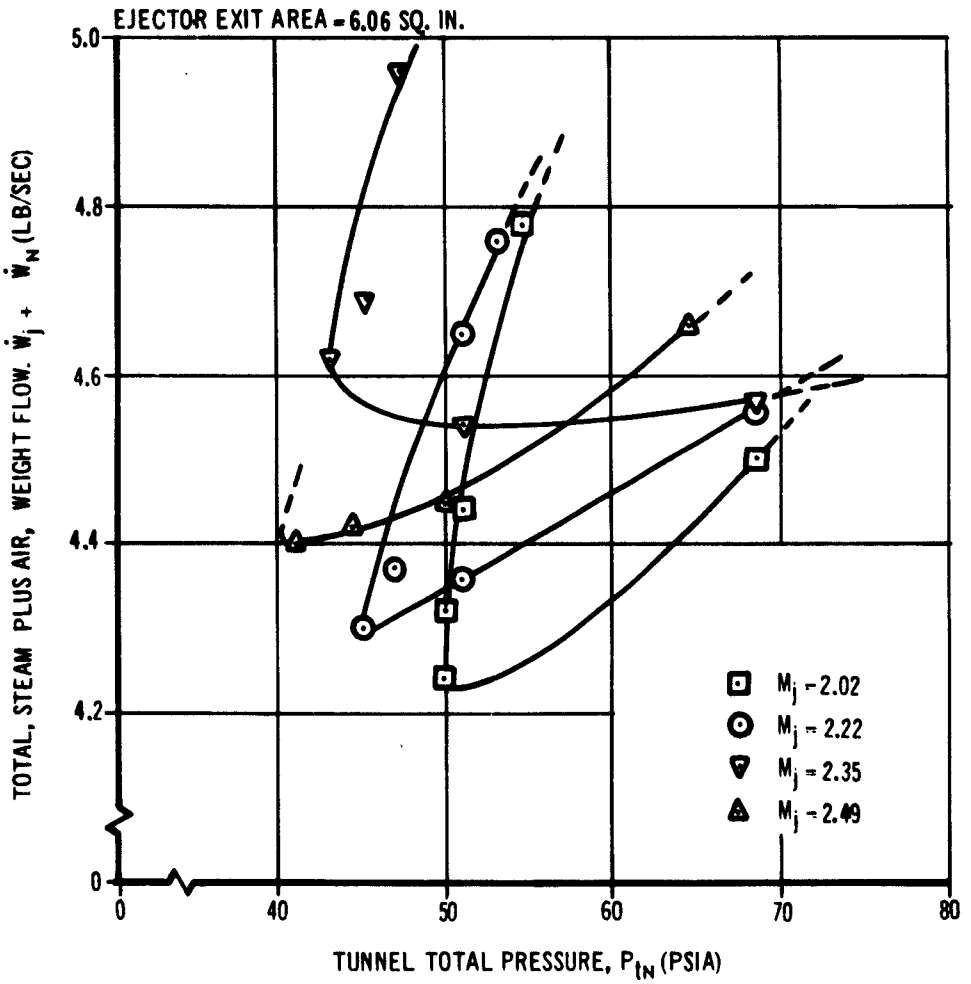

FIGURE 19

Section 7
Hypersonic Wind Tunnel Instrumentation Studies

E.R. Burnop

January 1, 1963

Report Number SM-41379-7

Sales Order: 81280-387
Engineering Work Order: 51904
Job Work Order: 0002

SUMMARY

Five major areas of instrumentation have been investigated, all pertaining especially to the Hypersonic Two-Foot Wind Tunnel but with certain advantages accruing to the entire family of three intermittent wind tunnels at DAL. First, analysis of pressure lag time in capillaries and experience with variable reluctance transducers and with the 160-channel pressure scanner in the trisonic tunnels have led to detailed plans for a system of measuring accurately 70 model pressures at four or more model attitudes at all operable conditions of the Hypersonic Tunnel. Second, electrode materials and configurations have been successfully devised for repeated operation of light sources for shadowgraphs and other optical systems which adhere to the specifications appropriate to Hypersonic Tunnel tests. Third, a reliable six-component strain-gauge balance has been developed and tested in the three wind tunnels to the extent that new balances for special models can now be produced for less than one-third of the cost of commercially-obtainable balances. This device has contributed to the successes of the large number of programs performed in DAL facilities. An acceleration-compensated, three-component balance system also has been developed, which utilizes solid-state strain gauges to realize improvements in sensitivity measured by orders of magnitude. Fourth, high-temperature-measurement procedures, i.e., for temperatures beyond the capabilities of conventional thermocouples, have been studied and operational techniques have benefitted therefrom. Fifth, the precision of the central data-gathering system has been improved so that errors transmitted due to internal noise are limited to 10 microvolts and those due to external electrical fields do not exceed 12 microvolts, satisfactory levels for the foreseeable future.

TABLE OF CONTENTS

1. INTRODUCTION

To progress at all, it is essential that the technology of instrumentation keep pace with new and advanced facilities and with the upgrading of existing facilities. As part of a continuing IR&D study, five major areas of instrumentation have been investigated during FY 1962, all pertaining especially to the Hypersonic Two-Foot Wind Tunnel (reference 1), but with certain advantages accruing to the entire family of three intermittent wind tunnels at DAL. These areas are low-pressure measurement, shadowgraphic flow visualization, force measurement, temperature measurement, and data system accuracy.

2. LOW-PRESSURE MEASUREMENT

Utilization of the Hypersonic Two-Foot Wind Tunnel requires pressure measuring methods which are more sensitive and precise than those used in slower wind tunnels. Following an earlier study (reference 2) of the state of the art, it has been decided to use a differential pressure transducer for all low-pressure measurement, with the reference side of the transducer evacuated to less than 40 microns. The Pace P7D variable reluctance transducer has been selected as best able to satisfy all requirements. During FY 1962 these transducers have been used successfully on tests on the hypersonic wind tunnel at Mach 6 and at Mach 8. Because these transducers are too large for mounting in a model (as are any other transducers which satisfy all other requirements), it is necessary to mount them at the bottom of the strut, where the pressure lag time (time for pressure to stabilize in tubing connecting model to transducer) is tolerable providing the tubing geometry is carefully considered. Space considerations also limit the number of transducers that can be mounted on the bottom of the strut. Consequently, pressure lag and a method of multipressure measurement have been analyzed and are reported in reference 3. From this study and from experience with the 160-channel pressure scanner in the trisonic tunnels, an approach to the problem has been defined which allows 70 model pressures to be measured accurately at several angles of attack and at Mach 6, 8, and 10. This device will be designed and acquired during FY 1963.

3. SHADOWGRAPHIC FLOW VISUALIZATION

A specification for a spark shadowgraph system to serve all wind tunnels has been written and major components have been developed. This system consists of a light source, a high-voltage power supply, a film transport mechanism, a transport mounting frame, and associated controls. It was originally planned to use the spark unit light sources that were developed for the ballistic range. It was soon realized, however, that these spark units had serious shortcomings in more repetitive wind tunnel operations and, hence, an instrumentation development program was started to define the trouble areas and to find solutions that would provide a satisfactory light source. This program has been successfully completed and results are reported in reference 4. The chief results of this investigation consist of finding a successful electrode configuration and finding materials that withstand repeated sparking. Still to be accomplished is the incorporation of the recommended improvements into the final shadowgraph system.

4. FORCE MEASUREMENT

The development of a six-component balance was completed and reported during FY 1961 (reference 5). The success of this work is demonstrated by the large number of tests run in all three wind tunnels during FY 1962, including work on Re-Entry, ASTRO, A4D-6, Supersonic Transport and VAX programs. The overload protection feature was shown dramatically when the half-inch balance 6-500-4 (DAL No. 53) was subjected to an overload greater than 200% without damage to the balance gaging, even though the sting portion of the balance was bent. Results from balances already fabricated and the experience gained enroute have provided the capability of producing new balances as required for wind tunnel model testing at costs of less than one third of those for commercially obtainable balances. During FY 1962 a start was made on balances using solid state strain gages (reference 6). One balance was partially instrumented with these new gages. Preliminary checking has shown a large increase in roll sensitivity. Lack of roll sensitivity had been a very serious limitation in some recent force tests. A new three-component balance using solid state strain gages is under development for use in the Hypervelocity Impulse Tunnel. This balance includes miniature accelerometers to enable electrical cancellation of inertial forces. Piezoelectric crystals will also be studied for future balances for this facility.

It is planned to develop during FY 1963 a procedure to calibrate balances by simultaneously loading all six components. Since this more closely simulates actual loading on a model during a run, it is believed that data validity will thus be improved significantly.

5. TEMPERATURE MEASUREMENT

In most trisonic wind tunnel applications, temperature sensing and measurement by thermocouples is satisfactory. However, the problem of applying thermocouple techniques to measure temperatures about 2700°F as occur in the pebble-bed furnace which preheats air for the Hypersonic Two-Foot Wind Tunnel, has not been satisfactorily resolved. To find a possible answer, high-temperature measurements were studied in a short course at UCLA during FY 1962. The knowledge obtained was used to improve the temperature readout system of the pebble bed heater (reference 7).

6. ACCURACY OF THE CENTRAL DATA-GATHERING SYSTEM

A brief study has been made of the absolute voltage-measuring accuracy of the central data-gathering system during FY 1962. Errors relative to a known voltage source were no greater than 70 microvolts, and in most cases were less than 40 microvolts. After careful adjustment, the deviations were reduced to within 10 microvolts on all 16 recorders. The errors due to noise in the switching system were less than 12 microvolts. These tests showed the central data system to be more accurate than attainable by the present method of using precision shunt resistors as a means to calibrate bridge-type transducers. When self-generating voltage transducers, such as thermocouples, are used, it may be necessary to seek further refinements.

7. REFERENCES

1. Cole, R. M., and G. T. Gibbs, The Hypersonic Two-Foot Tunnel: Description of the Facility and Provisions for Testing, Douglas Aircraft Company, Inc., Report Number SM 41369, dated March 1, 1962.

2. Covey, W. B., Techniques for Measuring Pressures in the Range of 0.03 to 0.1 Psia, Douglas Aircraft Company, Inc., Report Number SM 41368-15, dated December 15, 1961.

3. Aldrich, J. F. L., A Method of Multipressure Measurement in the Hypersonic Wind Tunnel, Douglas Aircraft Company, Inc., Technical Memorandum Number 37, dated August 1, 1962.

4. Bardos, J. A., Investigation of Spark Light Units for Multiple Shadowgraph Usage, Douglas Aircraft Company, Inc., Technical Memorandum GEN-R/AI-L3295, dated November 15, 1962.

5. Crompton, D. D., Internal Strain Gage Balance System Development, Douglas Aircraft Company, Inc., Report Number SM 41368-16, dated December 15, 1961.

6. Burnop, E. R. Seminar on Semi-Conductor Strain Gages, Temperature Sensors, and Transducers, Douglas Aircraft Company, Inc., Memorandum A270-RDS/AL-1M52, dated May 11, 1962.

7. Wright, F. N., The Measurement of High Temperature, Douglas Aircraft Company, Inc., Memorandum A270-RDS/RDL-AL-1M51, dated May 11, 1962.

Section 8
Flow Investigations In The Hypersonic Wind Tunnel

R.M. Cole

January 1, 1963

Report Number SM-41379-8

Sales Order: 81280-387
Engineering Work Order: 51904
Job Work Order: 0003

SUMMARY

Early operation of the Hypersonic Two-Foot Wind Tunnel had been hampered by oblique shock waves which originate at the exit of the contoured nozzle and limit the size of the usable core within the free jet of test air issuing therefrom. Several modifications to the configuration of the scoop which collects this free jet, and to the geometry of strut and pod of the model support system, have been tested. One such configuration produced shock-free flow within the 30-inch window region when the model and pod are translated outside the test section. The greatest improvement, however, results from reducing the wedge angle of the pod, sharpening its leading edge, and properly sealing clearances between strut and scoop. Consequently, configurations for greatly improving test core size and operation have become known.

TABLE OF CONTENTS

LIST OF ILLUSTRATIONS

1. INTRODUCTION

The DAL Hypersonic Two-Foot Wind Tunnel (figures 1 and 2) is a blowdown-to-vacuum facility designed to operate in the Mach 5 to 10 range (see reference 1). Models are tested in the free jet issuing from an appropriate axisymmetric contoured nozzle into a large, evacuated plenum. All of the test flow must circumfuse the model, sting, pod, and strut, and must enter a scoop and diffuser unimpeded if an adequate core of uniform flow is to be maintained. However, early operation had been hampered by oblique or conical shock waves originating in the vicinity of the contoured nozzle exit, diminishing the usable test core and generating high-pressure fields downstream. These high pressures propagate upstream through wakes and boundary layers to distort base flow conditions and to interfere with model force balances and boundary layer transition. These boundary shock waves arise from blockage by the model-strut system, from incomplete swallowing of the jet by the scoop, from separation of the boundary layer from the interior surface of the scoop, and from inefficient diffusion.

An IR&D investigation has been initiated and completed during FY 1962 to optimize tunnel configurations and to maximize the shock-free test core. Several convergent-divergent conical inserts within the lips of the scoop, as well as fairings on pod and strut leading edges, were tested at Mach 8. As a result, configurations which improve the size of the test core have been found.

Figure 3 is submitted to represent the flow mechanism. The strut and pod, located within the scoop, are principal contributors to blockage of the flow. They cause a system of relatively strong shock waves which increase the static pressure downstream of the strut. The adverse pressure gradient causes the flow to separate along the interior surface of the 32-inch-diameter scoop. Flow separation permits establishment of a feedback mechanism which pumps air into the plenum surrounding the test section. (The adverse pressure gradient causes a similar feedback along the sting which adversely affects flow near the model base, not illustrated in figure 3.) This action supports a high plenum pressure and strengthens the oblique shock waves which limit the test core. Meanwhile, the flow separation decreases the effective flow area at the strut and sets up separation shocks. These further increase the downstream pressure. This process continues until an equilibrium condition is reached. Measures which have been taken to improve conditions in the test core are discussed here.

The present tests were preceded by similar flow studies conducted as part of the calibration of the facility at Mach 6 and 8; see reference 2. At that time, the internal contour of the scoop was successfully modified so as virtually to eliminate the shock waves from the test section. However, this modification, in the form of an insert located forward of the strut, requires that the slots which exist in the scoop to admit the strut be sealed along the surface of the insert. This seal would limit

strut travel and would prevent operation of the gimbal which pitches the strut (and model). Such an insert would be impractical during most force tests, for example.

Subsequent analysis suggested several possible solutions to the problems set forth above. The most successful configurations (to date) are described in section 2 and the corresponding test results are summarized in section 3.

2. MODEL AND TUNNEL CONFIGURATIONS

The four models tested, three sharp winged cones and one blunt cone, are shown in figure 4. The M19 models are approximately 10 inches long; their base cone diameters are 3 or 4.5 inches, and their base wing spans are 4 or 6 inches. Model M140-1 is 10.8 inches long and 2.2 inches in base diameter. Six components of forces and moments acting on the model were sensed by an internal strain-gage balance. Model base pressure also was measured.

Three similar inserts, differing in size and ramp angle, were tested in the scoop. Figure 5 shows insert C installed at the leading edge of the scoop forward of the (hidden) strut, with the slot for the strut sealed along the cylindrical scoop surface. Any of the inserts could be installed forward or aft of the strut and the strut slots could be sealed either along the surface of the scoop or along the surface of the insert. The distribution of static pressure was measured along the seal.

A fairing for the leading surfaces of the pod was also tested. The original pod, shown in its retracted position in figure 6, is primarily a blunt wedge of 23-degree half angle and 6-inch base. The pod fairing, shown in figure 7, retains the base thickness but decreases the half angle to 12 degrees and sharpens the leading edge.

3. TEST RESULTS

The results of the first eight runs indicate that any restriction in cross sectional area of the scoop aft of the strut is detrimental to the flow. Each of several combinations of insert configuration and position aft of the strut increased the test section plenum pressure and strengthened the boundary shock waves, relative to the clean configuration.

Four runs (one with each of the models) with insert C at the leading edge of the scoop and with the slot sealed along the contour of the insert produced no improvement. The seal, of course, prevented removal of the pod and model by translating them outside of the scoop during these runs. The next run was made with the same insert and seal, but with pod and model permanently outside of the flow. This configuration produced a pressure in the test section plenum equal to the undisturbed free stream pressure and successfully eliminated the boundary shock wave for the first time. This

run is represented by the point at a pressure ratio of unity in figure 8, which shows typical measurements of the test section plenum pressure as a function of the pod (and model) position. Figure 8 shows how the plenum-to-static pressure ratio normally increased to 4 or more as the pod was translated to the tunnel centerline. Figure 9 gives the position of the conical boundary shock wave that would predictably be observed for this range of pressure ratio. The lowest pressure ratio observed with the pod retracted was about 1.5 prior to the present test.

It is also observed that 20 seconds are required after the flow is started to permit the test section plenum to reach a minimum pressure when the pod is on the tunnel centerline and when an insert is mounted at the leading edge of the scoop and the strut slot is sealed. In the run just discussed and in subsequent runs, this time to establish equilibrium is halved.

The result with pod retracted, described above, suggested the dominant role of the pod geometry relative to the scoop geometry. The next runs showed that sealing along the scoop surface instead of along the insert surfaces, and streamlining the strut, had negligible effect on the flow situation.

Meanwhile, as a result of developing the better understanding of the flow mechanism as described qualitatively in the introduction and in figure 3, the pod configuration was studied. A sharp-edged fairing, described in section 2 and shown in figure 7, was fabricated and installed over the pod. This fairing, tested with no insert on the scoop wall, produced a significant reduction in plenum pressure for all pod positions (except fully retracted), as shown in figure 8. The improved position of the boundary shock angle, as defined in figure 9, is typically 79 degrees.

4. CONCLUSIONS

The tests described herein, and subsequent tests, have indicated the significant influence of certain features of the tunnel configuration. Blockage of the flow by the pod and the shock waves from the pod are primary factors in attaining low pressures in the test section plenum and in establishing shock-free test flows. Streamlining the strut and altering the scoop configuration appear to have secondary influence. The scoop-strut shock system can be weakened, and the feedback-to-plenum mechanism can be subdued, by increasing the scoop cross section in the vicinity of the pod and by decreasing the wedge angle of pod and strut. It is recommended that both approaches be tested further. Advantages already observed are a larger region of uniform flow which allows testing larger models and at larger angles of attack, lower model base pressure and elimination of the problem of pressure feedback along the sting to the model, reduced loads on the model while it is being injected into the stream, lower starting and running pressure ratios for given test conditions, and faster establishment of equilibrium test conditions.

5. REFERENCES

1. Cole, R. M. and G. T. Gibbs, The Hypersonic Two-Foot Tunnel, Description of the Facility and Provisions for Testing. Douglas Aircraft Company, Inc., Santa Monica Report SM 41369, March 1, 1962.

2. Cole, R. M., and G. T. Gibbs, Calibration of the Douglas Hypersonic Two-Foot Wind Tunnel Mach 6 and 8 Nozzles. Douglas Aircraft Company, Inc., Santa Monica Report SM 41368-12, February 1, 1962.

DAL HYPERSONIC TUNNEL DESIGN FEATURES

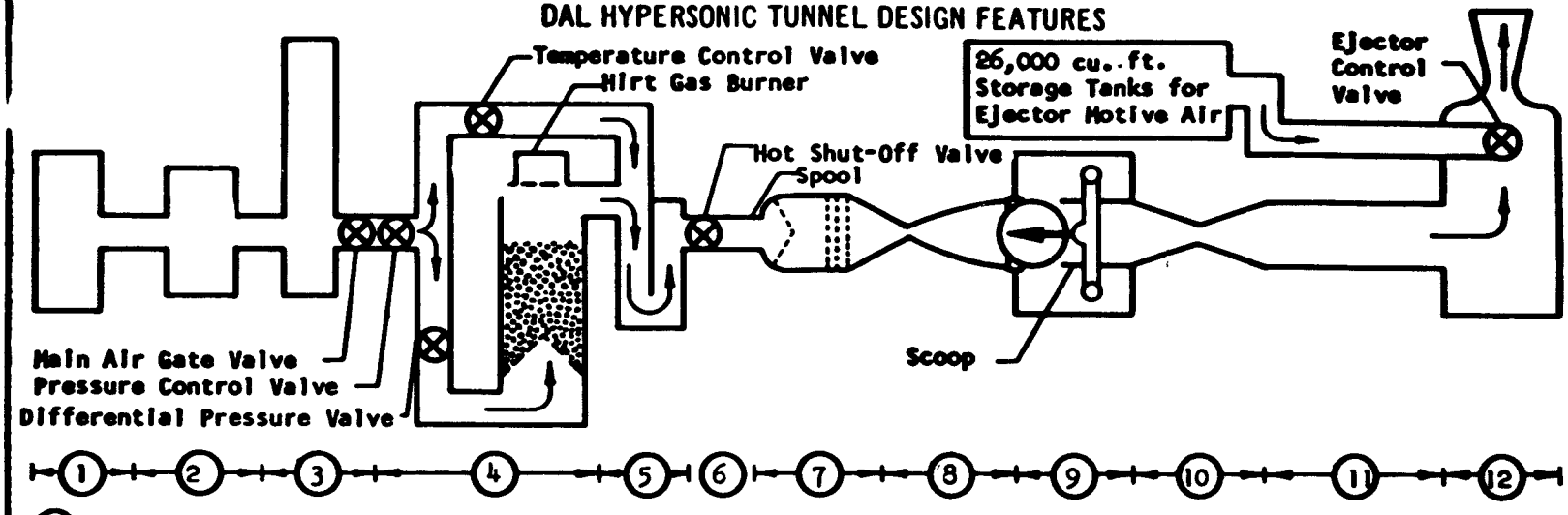

1. COMPRESSOR 6 stage Cooper-Bessemer, non-lubricated, reciprocating compressor with interstage cooling. Intake is 1825 cfm at 14.5 psia and 85°F; exhaust at 3500 psia and 100°F.
2. DRYER Semi-automatic desiccant Pritchard Hydryer dries air to a dewpoint of -50°F or lower.
3. AIR STORAGE TANKS Two vertical cylinders, of 250 ft.^{3} each, store air at 3500 psia and atmospheric temperature.
4. PEBBLE BED HEATER Alumina pebble bed heater regenerated by combustion of natural gas.
5. THERMAL MIXER Mixes hot air from heater and cold air from storage tanks to obtain desired stream temperature.
6. HOT SHUT-OFF VALVE Air-cooled ceramic-lined 12-inch rotovalve, hydraulically actuated between full open and full closed positions.
7. SPOOL & STILLING CHAMBER Removable spools to make up for length of nozzles. 25-inch diameter stilling chamber containing perforated cone and three turbulence screens.
8. NOZZLE Fixed Mach number, axisymmetric nozzles for Mach 6, 8, and 10. Exit diameter approximately 26 inches.
9. PLENUM & TEST SECTION Free jet surrounded by plenum chamber with 30-inch diameter windows on sidewalls. A scoop captures jet. Model support provides ±30° pitch, ±22 inches vertical translation, and ±200° roll.
10. VARIABLE DIFFUSER Two-dimensional single-peak type with top and bottom walls movable.
11. FIXED DIFFUSER Completes expansion to ejector plenum.
12. EJECTOR & MUFFLER One main and four side ejectors reduce exit pressure to 1 to 3 psia, depending on mass flow.

FIGURE 1

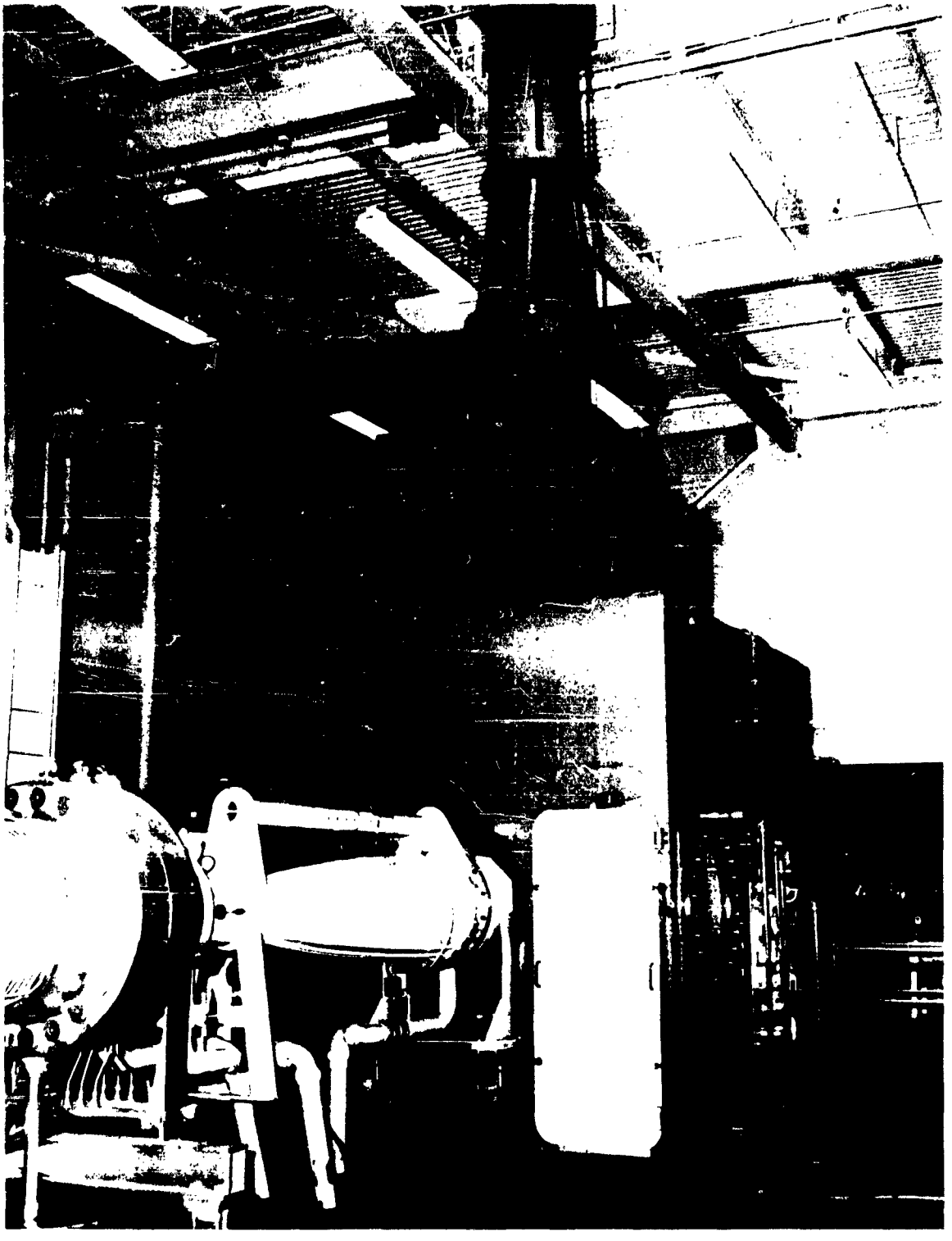

NOZZLE AND TEST SECTION OF THE HYPERSONIC
TWO-FOOT WIND TUNNEL

FIGURE 2

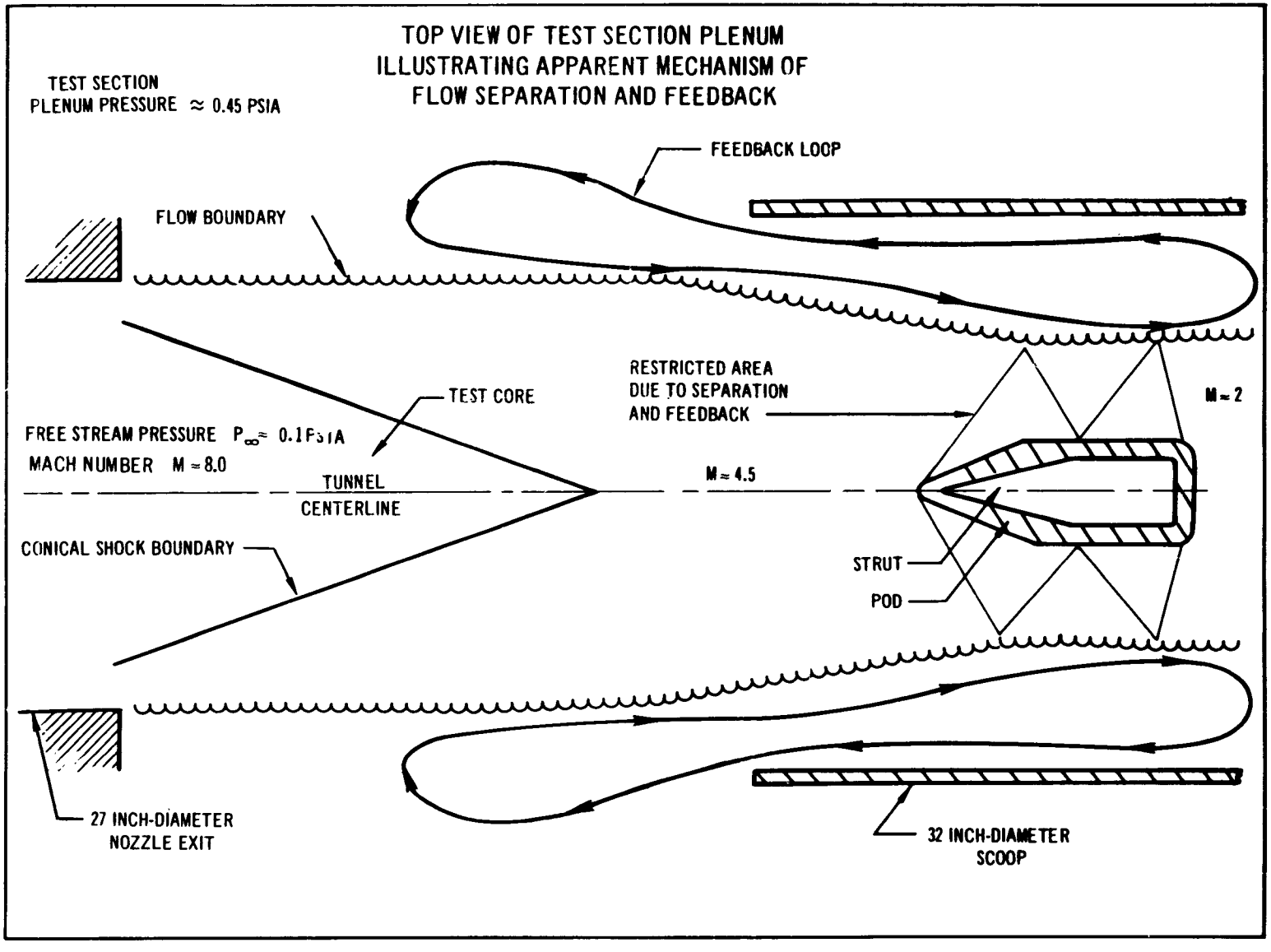
TOP VIEW OF TEST SECTION PLENUM
ILLUSTRATING APPARENT MECHANISM OF
FLOW SEPARATION AND FEEDBACK
TEST SECTION
PLENUM PRESSURE ≈ 0.45 PSIA
FEEDBACK LOOP
FLOW BOUNDARY
RESTRICTED AREA
DUE TO SEPARATION
AND FEEDBACK
M = 2
TEST CORE
FREE STREAM PRESSURE P_∞ ≈ 0.1 PSIA
MACH NUMBER M = 8.0
TUNNEL
CENTERLINE
M = 4.5
CONICAL SHOCK BOUNDARY
STRUT
POD
27 INCH-DIAMETER
NOZZLE EXIT
32 INCH-DIAMETER
SCOOP

FIGURE 3

CONICAL MODELS USED IN TEST HR-5

FIGURE 4

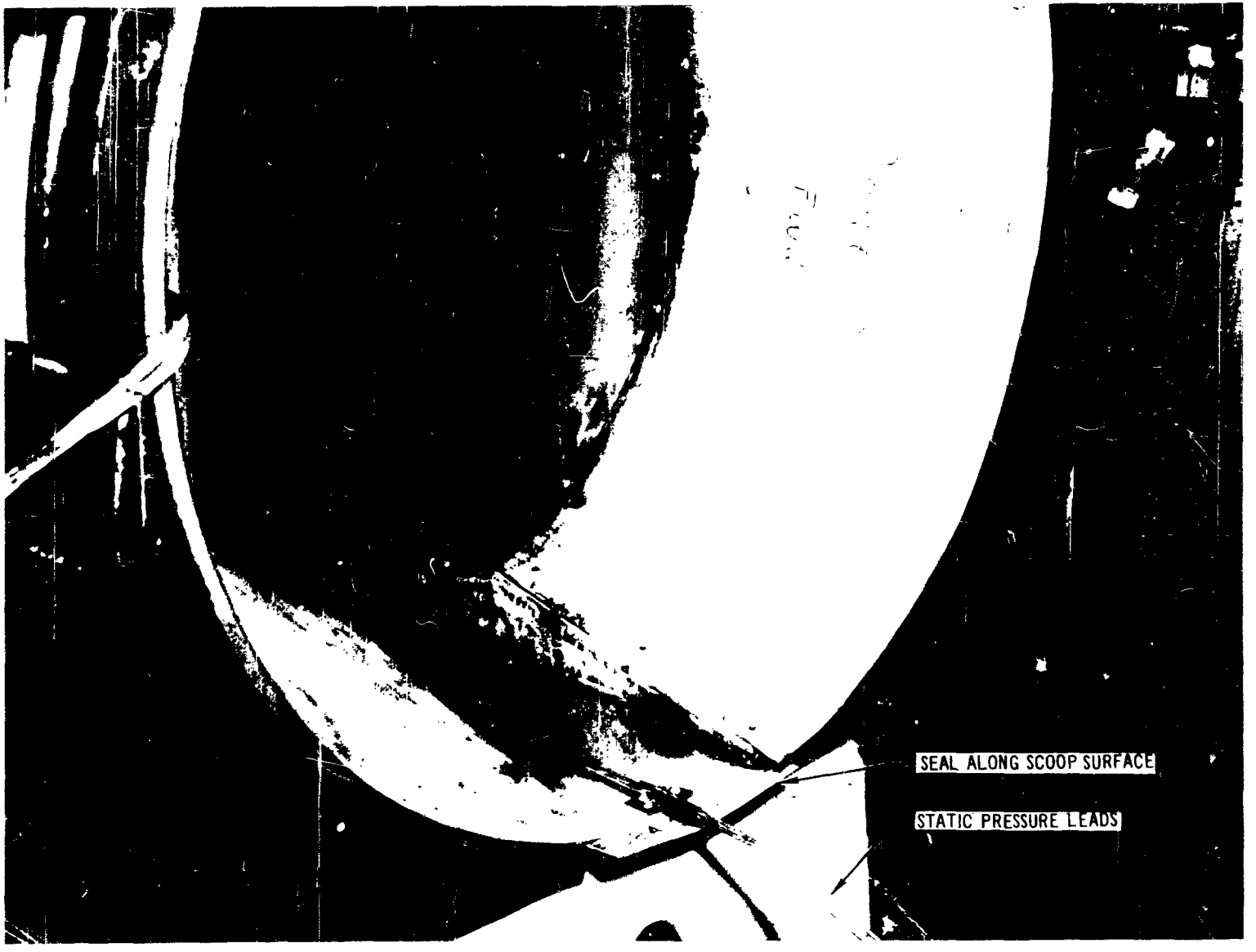

INSERT C INSTALLED AT THE LEADING EDGE
OF THE SCOOP

FIGURE 5

ORIGINAL POD SHOWN RETRACTED BELOW THE FLOOR OF THE SCOOP

FIGURE 6

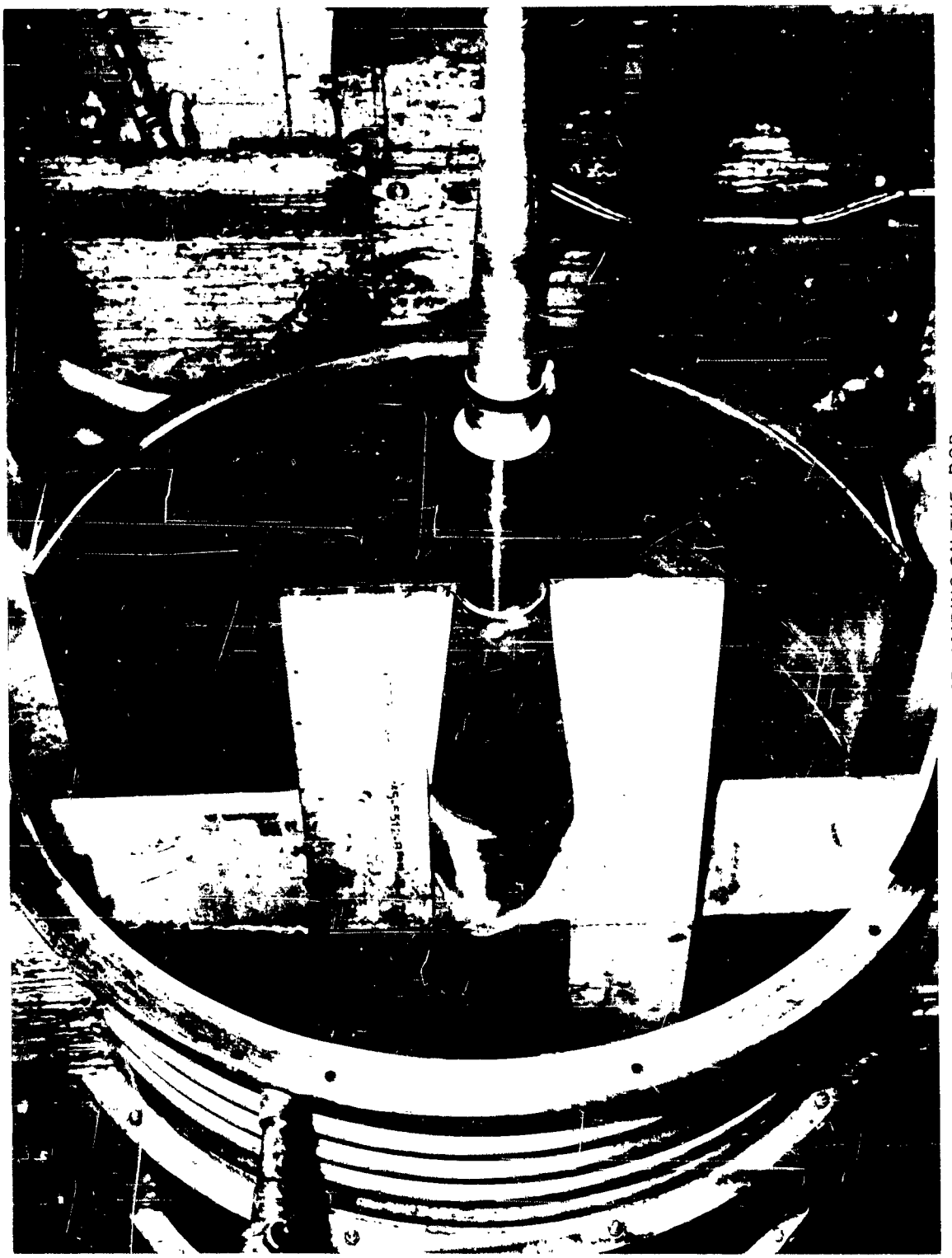

SHARP-EDGED FAIRING ON THE POD

FIGURE 7

DEPENDENCE OF TEST SECTION PLENUM PRESSURE ON POD POSITION FOR SEVERAL TUNNEL CONFIGURATIONS

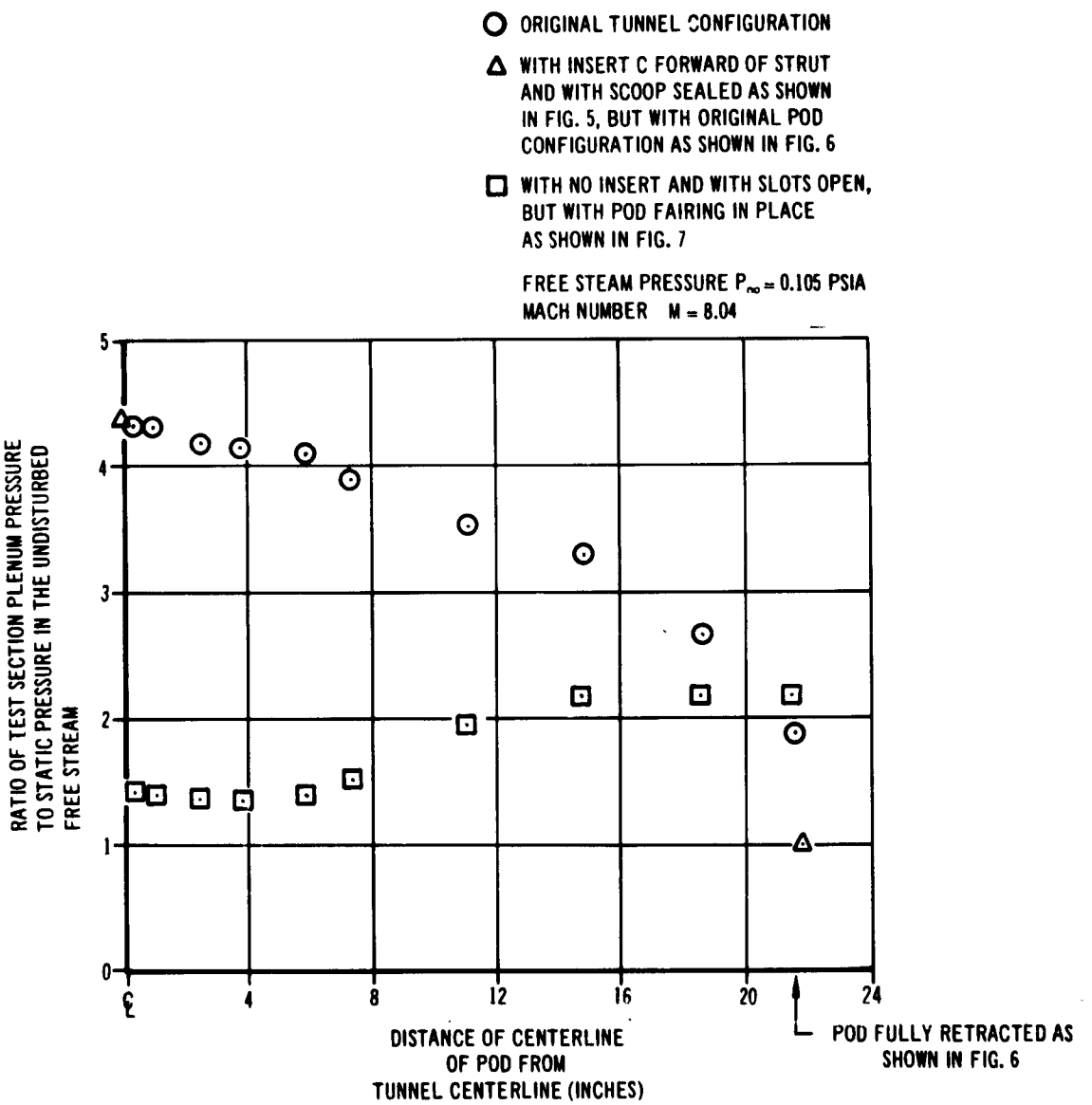

FIGURE 8

POSITION OF BOUNDARY SHOCK WAVE AS A FUNCTION OF TEST SECTION PLENUM PRESSURE

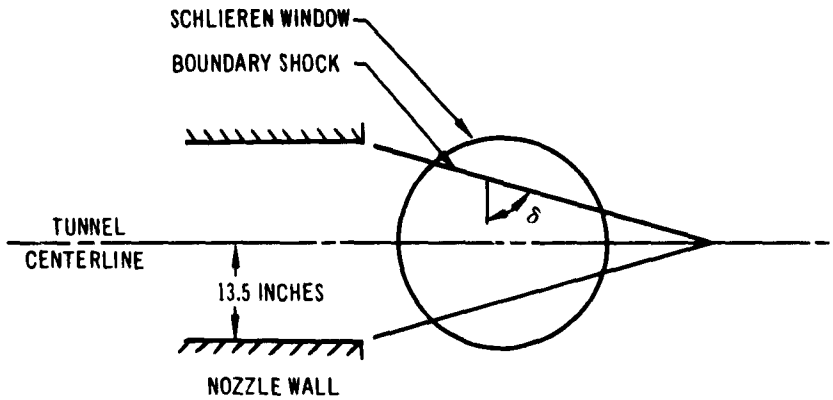

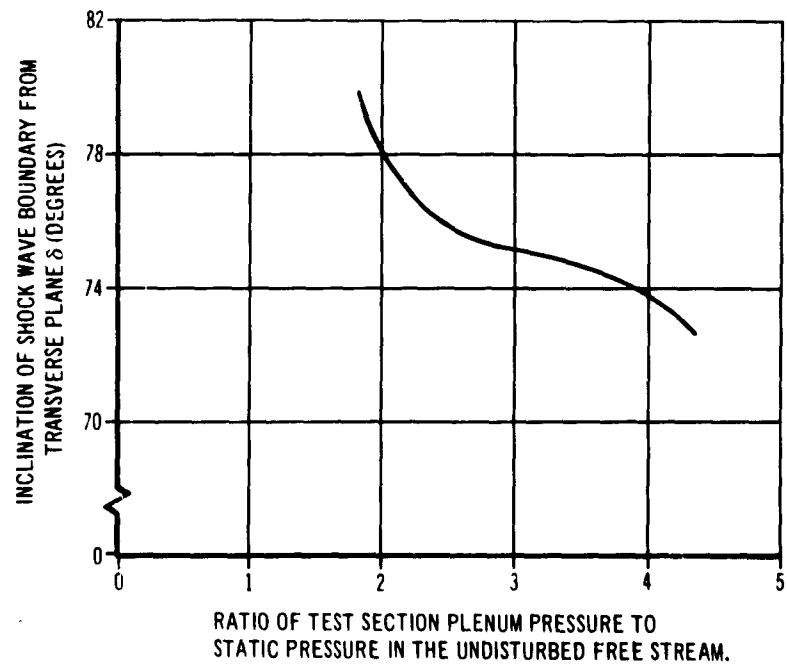

FIGURE 9

Section 9
Optical Flow Visualization Instrumentation

W.A. Stolzenburg

January 1, 1963

Report Number SM-41379-9

Sales Order: 88011-187
Engineering Work Order: 51933
Job Work Order: 0001

SUMMARY

Progress is recorded in three areas of optical flow visualization techniques for intermittent wind tunnels: front lighting, quantitative color schlieren, and glow-discharge visualization. A front lighting system of flashbulbs has been satisfactorily devised whose photographic exposure is well balanced with the existing schlieren system. Substitution of photofloods for the flashbulbs has been less satisfactory from the optical viewpoint. However, this technique can be improved by replacing the predominantly red photoflood with a blue light source to match the blue schlieren light and to adapt to the standard, blue-sensitive film. A satisfactory trichromatic filter for quantitative color schlieren is not yet available, but some success has been achieved with combinations of broad band color filters, which essentially produce a panchromatic image, and with combinations of interference line filters, which essentially produce a trichromatic image. A charged probe has been designed and installed adjacent to a specially-constructed model for glow-discharge visualization in the Hypersonic Two-Foot Wind Tunnel. However, the few tests of this technique have so far been inconclusive.

TABLE OF CONTENTS

LIST OF ILLUSTRATIONS

1. INTRODUCTION

Flow visualization is an indispensable adjunct to wind tunnel operation. The interest in flow visualization techniques has, historically, centered around an appreciation of aerodynamic phenomena associated with flows past complex aerodynamic shapes which do not lend themselves readily to analytical evaluation. As opposed to other types of instrumentation, optical techniques cause no disturbance of the flow field and the entire field of view can be measured simultaneously. Generally, however, optical techniques vary with the speed of the flow and the type of facility in which the flow field is established. As an example, optical techniques for a blowdown type of facility must be quite rapid as opposed to those of a continuously operating facility. Also, transonic and supersonic optical techniques need not be as sensitive as those used at Mach numbers above 6, due to the relatively stronger density gradients at the lower speeds. In general, the object of optical analysis is to analyze the variations imparted to the beam of light in order to find the corresponding changes in density of the fluid which produces such variations.

The purpose of an IR&D investigation begun in FY 1962 is to improve current flow visualization systems and to develop new ones, especially the techniques of front lighting, quantitative color schlieren, and glow discharge. It is felt that increased capabilities in these three areas will provide the most important contributions to the over-all optical data capabilities at DAL.

2. FRONT LIGHTING

Schlieren and shadowgraph methods of flow-field visualization are used extensively at DAL. A typical schlieren photograph of density gradients in the supersonic flow field about a complex model is shown in figure 1. This illustrates the fact that the features of flow around a model more complicated than a body of revolution can be obfuscated by the normal silhouette. Whereas control surfaces, ramps, and similar body features which generate some of the visible schlieren might be illustrated by auxiliary drawings or photographs, a more convenient technique is to employ front lighting. Front lighting technique is to illuminate the model by diffuse reflection of auxiliary light from its surface in such a way as to elaborate the schlieren; for example, see figure 2. This investigation is concerned with techniques of injecting sufficient auxiliary illumination into the schlieren system to provide a suitable reflected image at the photographic plate.

A purpose of the front lighting investigation is to determine what factors influence achievement of good, front-lighted, schlieren and shadowgraph photographs. To be considered, in addition to methods for injecting sufficient auxiliary lighting into the optical system to make the model visible, is the effect of the placement of components of a particular schlieren or shadowgraph system on its front-lighting capability.

An inherent characteristic of this system is that it is difficult to balance the exposure of the single photographic plate in areas illuminated only by the secondary (frontal) light with that in areas illuminated by the primary (e.g., schlieren system) light source. A further complication is that the auxiliary light contributes to exposure in the latter areas. Among the parameters controlling the film exposure, those relating to the primary light are largely fixed by requirements independent of front lighting; likewise inflexible is the light-path length from model to film, a principal factor influencing exposure due to front lighting. Consequently, the parameters influencing exposure to the secondary light are, in practice, its source color and intensity, distance from source to model, its duration, and the efficiency of diffuse reflection from model and background. Since the problem is primarily to maximize exposure in the model area, without obscuring schlieren, these requirements amount to selecting a color spectrum for the secondary source which matches the primary, selecting maximum source intensity, minimizing separation of source from model, maximizing secondary source duration within limitations of model movement or film transport, employing a model surface that is an efficient diffuse reflector, and employing an absorbent (black) background. Additional specifications are that the secondary source must operate with a frequency compatible with the desired framing rate, and that the secondary source must not physically disturb the flow or the primary light path.

One system which meets the foregoing requirements to a slight extent, and which was employed to obtain figure 2, is a multiplicity of flashbulbs. They are available in the spectrum (blue) of the schlieren light and corresponding film sensitivity; they can be arranged to yield high intensity; they are extinguished before their heat can affect the light path, and they are economical. However, they had to be positioned outside the tunnel window, which represents a severe penalty due to reflection at the window surfaces and due to absorption by the glass, and which causes a slight penalty due to light-path length; their duration is limited; and they are not easily adaptable to multiple photographs. This system is far from optimum, therefore, and was tried only as a quick method for gaining experience.

Another system which was tried is a multiplicity of flood lamps. Twelve 375-watt reflectorflood lamps were used around the periphery

of the window outside the Trisonic Four-Foot Wind Tunnel. With respect to the cited criteria, this system is submarginal. The flood lamps do not yield sufficient light itensity in the required spectrum; they must be positioned outside the tunnel window; and their heat distorts the field of view. Advantages of photofloods include their continuous nature and economy. The best photographs obtainable suffered not only from heat distortions, but from inadequate illumination of the model.

An ideal, but expensive, system would use similar lamps for primary and secondary sources, viz., B-H6 mercury vapor lamps. This type of lamp could operate as a flash light source in the schlieren system and, perhaps mounted inside the test-section walls, could operate as a small, intense, continuous secondary source. A synchronized mechanical shutter would control exposure to the secondary, front lighting source. Some auxiliary ventilation would be included to control heat effects of the secondary source.

3. QUANTITATIVE COLOR SCHLIEREN

Color schlieren techniques offer certain advantages over black and white processes and, thus, lend themselves to quantitative analysis of density gradients in flow fields. Colorimetry implies the color specification of light in terms of its classical characteristics, viz., dominant wavelength or color, purity or extent to which the color can be represented quantitatively by a pure spectrum color, and average luminance, transmittance or reflectance, all with reference to a stated or standard illuminant. These physical or objective values are perceived subjectively as sensations of hue, saturation, and lightness or brightness, all subject to physiological and phychological processes. With these concepts in mind, three advantages of color schlieren can be stated. The eye is able to differentiate more easily between hues than between levels of brightness due to monochrome tones, so that the color system is more sensitive for visual observation. Furthermore, the color schlieren picture offers nearly even luminance, so that no region of low apparent brightness can occur which might be obscured by an adjacent region of higher brightness. Finally, opaque bodies appear black and are more readily distinguished from adjacent colored areas of flow than from adjacent gray areas of flow.

These considerations suggest certain refinements of existing color schlieren technology which might provide quantitative gasdynamic data. Specifically, if the photographic film is exposed only to three relatively pure colors, appropriate calibration in terms of the tristimulus values might enhance the ability to analyze density levels in the entire flow field solely by optics.

In current use at DAL is the tricolor optical filter approach to color schlieren, described in reference 1, whereby the knife edge in a conventional schlieren system is replaced by three adjacent coplanar filters (see figure 3). For maximum coverage of the chromaticity (wavelength vs. purity) field, red, green, and blue filters are chosen. Width of the central green filter coincides with the size of the light source image at its sharpest focus. Dimensions of the red and blue filters are sufficient to intercept all possible diffracted light rays.

The first filter assembled and tried at DAL was constructed from three Kodak Wratten filters placed side by side. The transmittance characteristics of the components are shown at the left side of figure 3. Even though a mercury vapor lamp was employed, the wide band passages of the Wratten filters admit a considerable number of the many emitted lines from the light source wherever light diffraction is to be recorded. Thus, although major features of the flow field are colored in a characteristic manner and can be analyzed qualitatively, any observed hue and saturation could be interpreted as the result of any of a number of combinations of source wavelengths and would not be amenable to quantitative analysis. Essentially, this optical system can be designated as panchromatic, or even orthochromatic, but not trichromatic.

The central idea of the current investigation is that the observed color at a localized region of the reproduced flow field can be uniquely correlated as a measurable mixture of only two color sources if a truly trichromatic optical system can be achieved. Interference line filters may have the necessary characteristics of high transmittance of the desired color wavelength and low transmittance of neighboring wavelengths to serve the stated purpose. Consequently three such filters were selected, two to match the strong blue and green lines emitted by the mercury vapor lamp and a third to cover the strongest orange-red lines from this source, and were purchased from Jena Glass Works Schott and Gen., Mainz, West Germany. The transmittance characteristics of the components of the ideal resultant filter are shown at the right side of figure 3. Pacific Optical Corporation, Inglewood, California, contracted to cut and assemble two trichromatic filters from these components. During tests in the Trisonic Four-Foot Wind Tunnel, the image produced by the schlieren system using the resultant filters was greatly distorted, and multiple images occurred, due to the nature of the Schott interference filters. Whereas the Wratten filters discussed previously are very thin and can easily be mounted in the same plane between two glass plates, good coplanar assembly of interference filters is difficult to accomplish. An interference filter is usually composed of a layer of clear glass, a semitransparent silver film, a transparent spacer film one-half wavelength thick, a second semitransparent silver film, another layer of clear glass, and finally a colored glass plate which filters the weak harmonics passed by the basic interference filter and

which generally reinforces the interference filter over a broad band. The total thickness of this sandwich is different for each color. Not only was one exterior surface of the trichromatic filter noncoplanar therefore, but the three transparent spacer films were noncoplanar. The distortion and multiplicity of images was evidently due to either or both of these noncoplanar features.

Measures are now being taken to eliminate the cited problems by improving the construction of a trichromatic filter from three interference filters.

4. GLOW DISCHARGE

Conventional techniques for flow visualization tend to become inadequate in hypervelocity wind tunnels because of the extremely low pressure and density levels. At freestream pressures below about three millimeters of mercury, optical methods, e.g., schlieren and shadowgraph, that depend upon light refraction due to density gradients, become ineffective. It is advisable, therefore, to investigate other methods of flow visualization. Two such methods are absorption techniques, based upon the absorption of characteristic wavelengths of electromagnetic radiation by certain molecular species, and glow discharge techniques, based upon the emission of visible radiation by certain molecular species when electrically excited. Interest at DAL has centered on glow discharge techniques but (instead of adding electrical energy upstream of the model, as suggested in reference 2 for example) applying the electrical field about the model, for example, as described in reference 3. From these prior studies, it appears that emission by electrical stimulation methods, although less sophisticated than absorption methods, may be simpler to produce and interpret and may be more reliable.

A probe and model were designed, constructed, and tested in the Hypersonic Two-Foot Wind Tunnel to investigate the practicability of producing and observing a plasma between the two parallel bodies in high speed, rarefied airflow; see figure 4. The model is a simple cone-cylinder with fins, sting, and pod. Various model nose cone angles are provided to investigate effects of shock impingement aft of the probe nose. The probe is supported by a cylindrical alumina insulator with suitable strength and dielectric properties. Typically, probe and model would be separated by a variable distance, up to eight inches, and would be equidistant from the tunnel centerline. By putting the nose of each body at about the same longitudinal station, an electrical field can be produced near the model but its flow field will be unaffected aerodynamically by the presence of the probe. A d.c. power supply is available to charge the insulated probe negatively to as much as 2500 volts; at this potential, rated current is one ampere.

Results of the only tests so far are negative due to failures in the power supply. In the first trial, a relay in the high voltage circuit failed. In the second trial, the fuse for limiting current load opened at about 1100 volts. Both elements have been repaired and readjusted in preparation for further tests. Thus, at 3 millimeters of mercury ambient pressure and at Mach 8, no plasma has become visible at 1100 volts.

5. CONCLUSIONS

As a result of front lighting studies, it can be concluded that illumination of the model for schlieren or shadowgraph photography in the intermittent wind tunnels at DAL is practicable. The best secondary light source would be located at several stations inside the wind tunnel wall on the camera side of the tunnel. A fast, intense, blue light that can be recycled about every half second, and that would not interfere with the primary light path by blockage or by perturbations due to heating, would be ideal.

The first step toward quantitative color schlieren is within reach, viz., purification of the primary colors and construction of a coplanar trichromatic interference filter. The next step will be to calibrate color schlieren plates in terms of hue, saturation, and brightness, and to correlate these tristimuli with pressure or density variations in the object flow field.

The glow discharge method of flow visualization promises to yield qualitative data at rarefied conditions when proper voltage and separation values are obtained.

6. REFERENCES

1. North, R. J., A Colour Schlieren System Using Multicolour Filters of Simple Construction, National Physical Laboratory, Aero Note 266, August 1954.

2. Evans, R. A., A New Method of Flow-Visualization for Low Density Wind Tunnels, University of California, Institute of Engineering Research Technical Report Number HE-150-119, January 1954.

3. Koester, E. H., J. J. Minich, and R. H. Lee, Comments on 1) The Effects of Wall to Free-Stream Temperature Ratio on Boundary Layer Separation and 2) Use of Ionization for Flow Visualization in the JPL 21-Inch Hypersonic Wind Tunnel, Jet Propulsion Laboratory, California Institute of Technology, Internal Memorandum WT21-T57, September 1962.

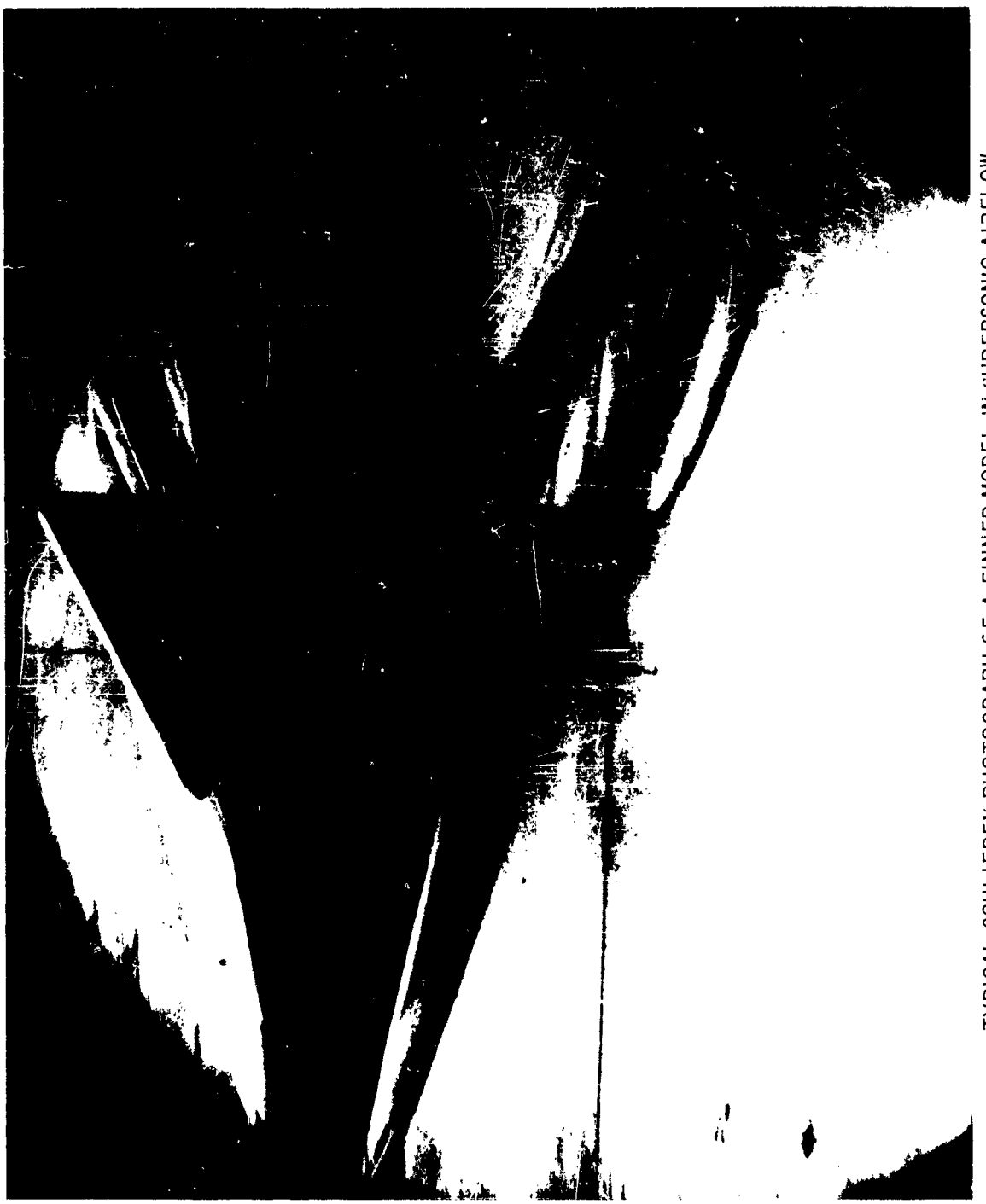

TYPICAL SCHLIEREN PHOTOGRAPH OF A FINNED MODEL IN SUPERSONIC AIRFLOW

FIGURE 1

SCHLIEREN PHOTOGRAPH OF A FINNED MODEL IN SUPERSONIC AIRFLOW
WITH FRONT LIGHTING BY AN ARRAY OF FLASHBULBS

FIGURE 2

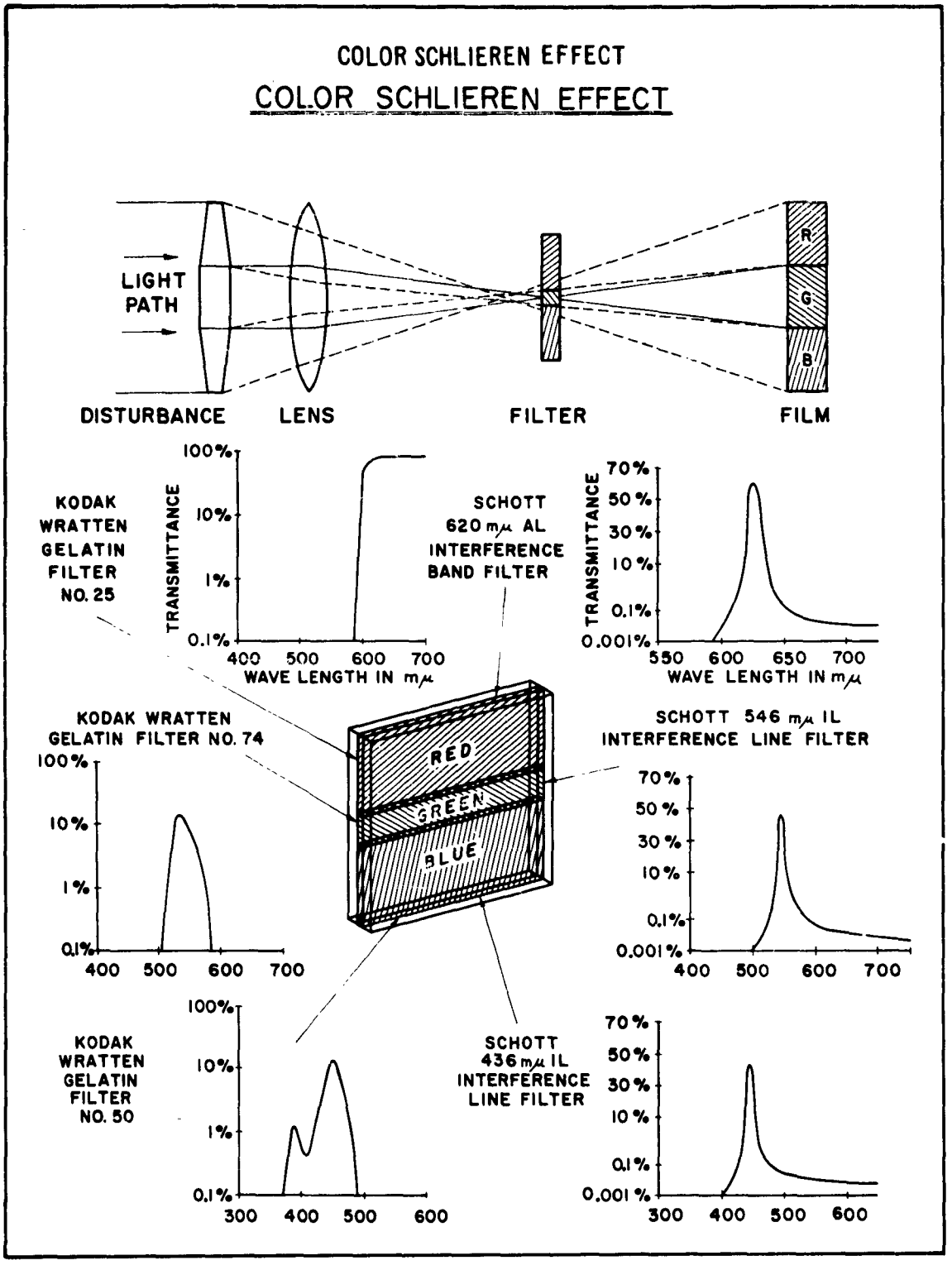
COLOR SCHLIEREN EFFECT
COLOR SCHLIEREN EFFECT
LIGHT PATH
R
G
B
DISTURBANCE
LENS
FILTER
FILM
KODAK WRATTEN GELATIN FILTER NO. 25
TRANSMITTANCE
100%
10%
1%
0.1%
400 500 600 700
WAVE LENGTH IN mμ
SCHOTT 620 mμ AL INTERFERENCE BAND FILTER
70%
50%
30%
10%
0.1%
0.001%
550 600 650 700
WAVE LENGTH IN mμ
KODAK WRATTEN GELATIN FILTER NO. 74
100%
10%
1%
0.1%
400 500 600 700
SCHOTT 546 mμ IL INTERFERENCE LINE FILTER
70%
50%
30%
10%
0.1%
0.001%
400 500 600 700
RED
GREEN
BLUE
KODAK WRATTEN GELATIN FILTER NO. 50
100%
10%
1%
0.1%
300 400 500 600
SCHOTT 436 mμ IL INTERFERENCE LINE FILTER
70%
50%
30%
10%
0.1%
0.001%
300 400 500 600

FIGURE 3

PROBE, MODEL, AND SUPPORT FOR GLOW DISCHARGE EXPERIMENT

FIGURE 4